NTNU

Norwegian University of
Science and Technology

Utmattingsundersøkelser av AA6005

Effekten av forskjellige

Per Fredrik Tunestam

Materials Science and Engineering
Submission date: February 2016
Supervisor: Hans Jørgen Roven, IMTE
Co-supervisor: Trond Furu, IMTE

Norwegian University of Science and Technology
Department of Materials Science and Engineering

Preface

This report is the result of a master's thesis done at the Department of Materials Science and Engineering at the Norwegian University of Technology and Science (NTNU). The aim of this thesis was to investigate the effect of long time storage and heat treatment of AA6005 to the same hardness, but in temper states pre- and post peak hardness. This thesis is a continuation from the specialization project carried out by the author in the spring of 2015. The results from this work is presented in chapter 4 Results and marked with a citation.

First, I would like to thank my supervisor Professor Hans Jørgen Roven for his guidance and help during this work. Further, I would like to thank Pål Christian Skaret for training and assistance in the MTS laboratory, Yingda Yu for training and assistance in the EM-laboratory, and Trygve Lindahl Schanche for his assistance in the heat-, metallographic-, and microscopy laboratories. Additionally, I would like to thank Professor II Trond Furu, my co-supervisor, and Hydro Aluminium for providing the profiles used in this report.

Abstract

The aim of this thesis is to investigate the effect of ageing, both natural and artificial, at room temperature on the fatigue properties of AA6005. Artificial ageing was done to reach a temper state of equal hardness on each side of peak hardness (T6).

Preliminary testing was done on AA6005. These consisted of hardness and electric conductivity measurements after different ageing times from T1 condition and after solution heat treatment. The microstructures of the alloy was investigated by means of optical microscopy and electron microscopy to analyse the primary particles, in all temper states.

The results showed that AA6005 has excellent fatigue resistance in T1 after 12 years in storage, and the fatigue resistance increases in an under-aged temper state while decreases in an over-aged temper state. Also fatigue does not affect the electric conductivity of AA6005.

Sammendrag

Oppgavens formal var å undersøke effekten av elding, både naturlig og kunstig, ved romtemperatur på utmattingsegenskapene ti AA6005. Innherding ble gjort slik at en tilstand med lik hardhet på hver side av maximal hardhet (T6) ble nådd.

Forsøk ble gjort på AA6005. Dette bestod av måling av hardhet og elektrisk ledningsevne etter utherding fra T1 tilstanden og etter innherding. Mikrostrukturen til legeringen ble undersøkt ved lysmikroskopi og elektronmikroskopi for å analysere primær partiklene i alle tilstander.

Resultatene viser at AA6005 har utmerkede utmattingsmotstand i T1 tilstand etter lagrig i 12 år, og utmattingsmotstanden økte i den undereldede tilstanden, mens den minsket i den overeldede tilstanden. Utmatting påvirker ikke den electriske ledningsevnen til AA6005.

Table of Content

Preface i

Abstract ii

Sammendrag iii

Table of Content iv

Abbreviations and Denotations viii

1 Introduction 1

2 Theory 2

2.1 Aluminium 2

2.2 Production and Extrusion 2

2.3 Vickers Hardness 4

2.4 Ageing 4

2.5 Electric Conductivity 7

2.6 The Stress-Strain Curve 8

2.7 Fatigue 10

2.7.1 Stress Cycles 11

2.7.2 SN-curve 12

2.8 Fatigue Fracture 14

2.9 Energy Dispersive Spectroscopy 15

3 Experimental 16

3.1 Delivered Material and Chemical Composition 16

3.1.1 Production Process 17

3.1.2 Definitions of Directions of Extruded Profile 18

3.1.3 Definition of Temper States 19

3.2 Artificial Ageing 20

3.3 Microstructure Examination 21

3.3.1 Primary Particle Optical Microscopy 21

3.3.2 Primary Particle Chemical Composition Analyses 21

3.4 Electrical Conductivity 22

3.5 Tensile Testing 22

3.6 Fatigue Testing 24

3.6.1 The Fatigue Specimen 24

3.6.2 Testing after Cyclic Loading 25

3.7 Fractography 26

4 Results 27

4.1 Micrograph of the Grain Structure 27

4.2 Primary Particles 28

4.2.1 Optical Microscopy Analyses of the T1 Temper State 28

4.2.2 Optical Microscopy Analyses after Solution Heat Treatment 30
4.2.3 Chemical Composition Analyses 34
4.3 Artificial Ageing 40
4.4 Electrical Conductivity 41
4.5 Tensile Testing 43
4.6 Fatigue Testing 48
4.6.1 S-N Curves 48
4.6.2 Hardness after Fatigue testing 52
4.6.3 Electrical Conductivity after Fatigue Testing 55
4.7 Fractography 57
4.7.1 Overview of Examined Specimens 58
4.7.2. Stage II Crack Growth 60
4.7.3. Stage III Crack Growth 70
5 Discussion 72
5.1 The Effect of Artificial and Natural Ageing on AA6005 72
Observed Microstructural and Material Property Changes 72
5.1.2 Hardness 73
5.1.3 Electrical Conductivity 73
5.2 The Effect of Ageing Time on Fatigue Properties 74
5.2.1 Stress Correction 76

5.2.2 Hardness 79

5.2.3 Electrical Conductivity 79

6 Conclusions 80

7 Further Work 81

8 References 82

Appendix A – Artificial Ageing Data 83

Appendix B – Fatigue Data 85

Abbreviations and Denotations

ED	Extrusion direction
TD	Transverse direction
ND	Normal direction
UA	Under-aged condition
OA	Over-aged condition
r	Radius
RO	Run out
RT	Room temperature
R	Stress ratio
ASTM	American Society for Testing and Materials
HV	Vickers Hardness
P	Load [kg]
L	Average length for HV
f	frequency [Hz]
N	Number of cycles
N_f	Number of cycles until fracture
F	Force [N]
σ	Stress [MPa]
ε	Strain [mm/mm]
σ_f	Fracture stress [MPa]
σ_y	Yield stress [MPa]
σ_{UTS}	Ultimate tensile stress [MPa]
SEM	Scaning electron microscope
OP-S	Oxide polishing suspension
DC	Direct chill
ε_f	Fracture strain [%]
ε_u	Uniform strain [%]

1 Introduction

This thesis is a continuation of the specialization project TMT4500 conducted in the spring semester in 2015 at NTNU.

Fatigue is recognized as the failure of a material after being subject to a cyclic load over a period of time. The failure occurs without warning and results in a brittle-looking fracture surface. After the phenomenon was identified in the 1830's it has become progressively more important with time, and today it is stated that 90 percent of all service failures due to mechanical causes are a result of fatigue.

Aluminium is a very light metal, with a density of 2,7 g/cm^3, and has excellent resistance to corrosion and oxidation. Aluminium does not display a true endurance limit, resulting in the possibility of fatigue fracture even at very low cyclic loads. Aluminium alloys may display up to 30 times the strength of pure aluminium.

Alloying elements, such as silicon and magnesium, can increase the hardness and strength of aluminium when heat treated. This effect is well documented and is now regarded as common knowledge. This thesis aims to investigate the effect of different temper state for AA6005.

2 Theory

In this chapter background information about aluminium in general and relevant theory to this thesis is presented. The background information is limited to the production of aluminium and aluminium in general, with special emphasis on the Al-Mg-Si alloys.

2.1 Aluminium

Aluminium is a light metal with a density of 2,7g/cm^3 and a FCC structure [1]. The low density reduces the amount of energy needed for transportation. The recycling process of aluminium is also very energy efficient, with only 5% of energy usage compared to production of aluminium from ore. This leads to less CO_2 emissions and saves a lot in energy usage. The total loss of metal during recycling is less than 3%, and 75% of all aluminium ever produced is still in use today, making aluminium a very sustainable metal [2].

Al-Mg-Si Alloys

Extruded Al-Mg-Si alloys are designated as 6xxx-alloys. They are heat treatable, i.e. they can be solution heat treated and precipitation heat treated, and have excellent corrosion resistance in natural environments. Alloys in the 6xxx-series also have good electric conductivity due to the low fraction of alloying elements [1].

2.2 Production and Extrusion

The extrusion process gives unlimited options in regard to design and application of aluminium. After the reduction of the bauxite ore, casting, and homogenization of the billet, the extrusion process can begin. The billet is preheated and pressed though an extrusion die, which gives the profile its shape. Figure 2.1 shows the production steps for aluminium [1].

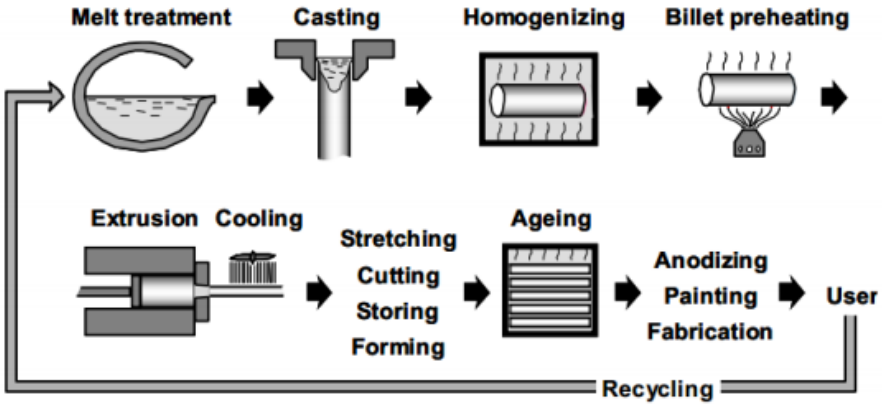

Figure 2.1: Production steps of aluminium [3].

Figure 2.2 shows an example of the temperature range from casting to finished product. Please note the difference in temperature increase during extrusion. This is a result of friction between the billet/profile and the extrusion die

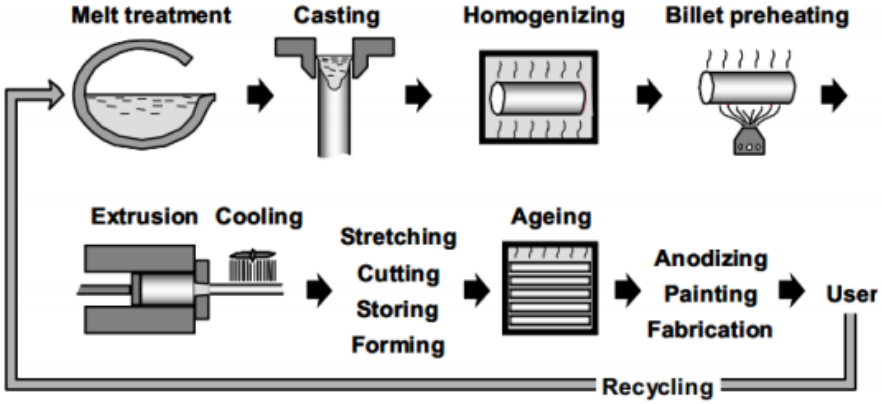

Figure 2.2: Example of temperature ranges during the production process [4].

2.3 Vickers Hardness

A materials hardness is usually defined as its ability to resist plastic deformation. There are several different types of hardness, depending on how the hardness was measured. In this thesis Vickers hardness (HV) is used. In this system a square-based diamond pyramid indenter, with the angle between the opposing pyramid faces being 136°, is used. A load is applied and the area of the indented area is measured. A value is then calculated using the equation below [4].

$$HV = 1{,}854\frac{P}{L^2} \qquad (1)$$

Where: HV is the Vickers hardness
P is the applied load [kg]
L is the average length of diagonals [mm]

2.4 Ageing

Some aluminium alloys are able to harden by precipitation hardening. Precipitation hardening can occur by the passing of time, referred to as natural ageing, or by applying heat to speed up the process, referred to as artificial ageing. Ageing is only possible if the solubility of the alloying elements is decreasing as the temperature decreases. The alloying elements will then be in a super saturated solution in the aluminium matrix when quenched to room temperature (RT). This is a metastable structure and the driving force will try to obtain equilibrium by precipitating out the alloying elements to another phase. This is why this process also is referred to as precipitation hardening. By controlling the temperature, and therefore also the energy put into the system, the amount of precipitates can, to a certain degree, be controlled [4, 5].

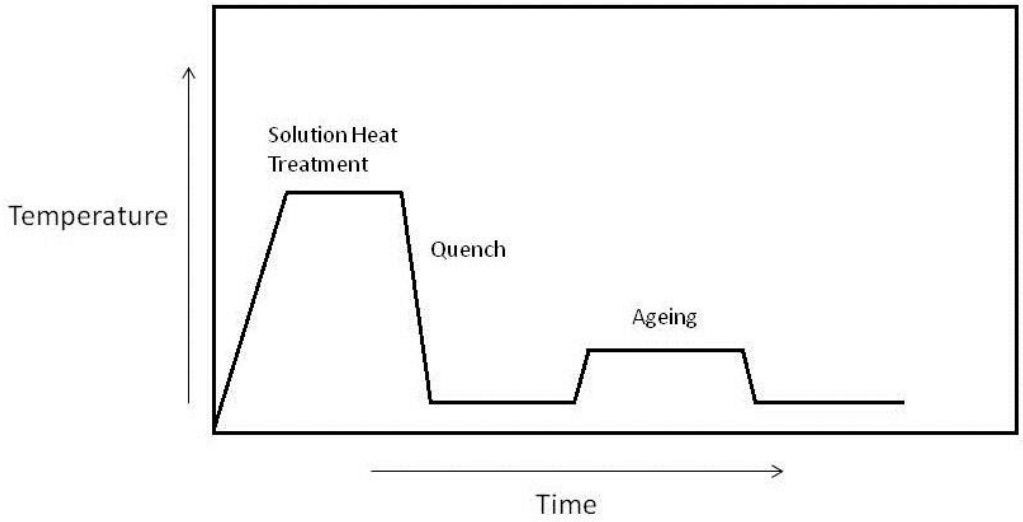

Figure 2.3: Typical steps taken during the ageing process [6].

In figure 2.3 a typical artificial ageing process is shown. The first step is to solution heat treat the alloy to dissolve any precipitated alloying elements back into a solid solution with the matrix. When this is done the aluminium as quenched and the alloying elements are now in a supersaturated solid solution. Finally the alloy is heated at a much lower temperature than before where the supersaturated elements can diffuse short distances and form ultrafine uniformly dispersed second phase precipitated particles [5].

Guinier-Preston Zones

Prior to precipitation of a second phase it is common for several other, intermediate phases, to occur. These phases were first detected by Guinier and Preston, and are therefore known as GP zones. The ageing sequence is shown in figure 2.4.

$$\text{Supersaturated } \alpha \longrightarrow \text{GP1} \longrightarrow \beta'' \longrightarrow \beta' \longrightarrow \beta(Mg_2Si)$$

Figure 2.4: The ageing sequence of 6000-series alloys [1].

During ageing clustering of the alloying elements first occurs. This is known as GP1 zones. In Al-Mg-Si alloys these are partly coherent, possibly monoclinic, needles along the <100> directions. As more atoms diffuse as ageing progresses the GP1 zones grow into GP2 , or β'' in Al-Mg-Si, zones. These are monoclinic, partly coherent needles in the <100> directions. With continued ageing even more diffusion occurs and a greater degree of order arises, and β' is formed. This is hexagonal partly coherent rods. At peak hardness the microstructure consists of a mixture of β'' and β'. Finally, the β' particles grow so large that they lose cohesion and precipitate out of the matrix. This can also be referred to as over-ageing [1, 5]

Figure 2.5 shows the area where the different zones are on the curve and the effect of artificial ageing temperature. Note that the figure is made for Al-4wt%Cu and not Al-Mg-Si alloys. Therefore the areas are somewhat offset according to the paragraph above.

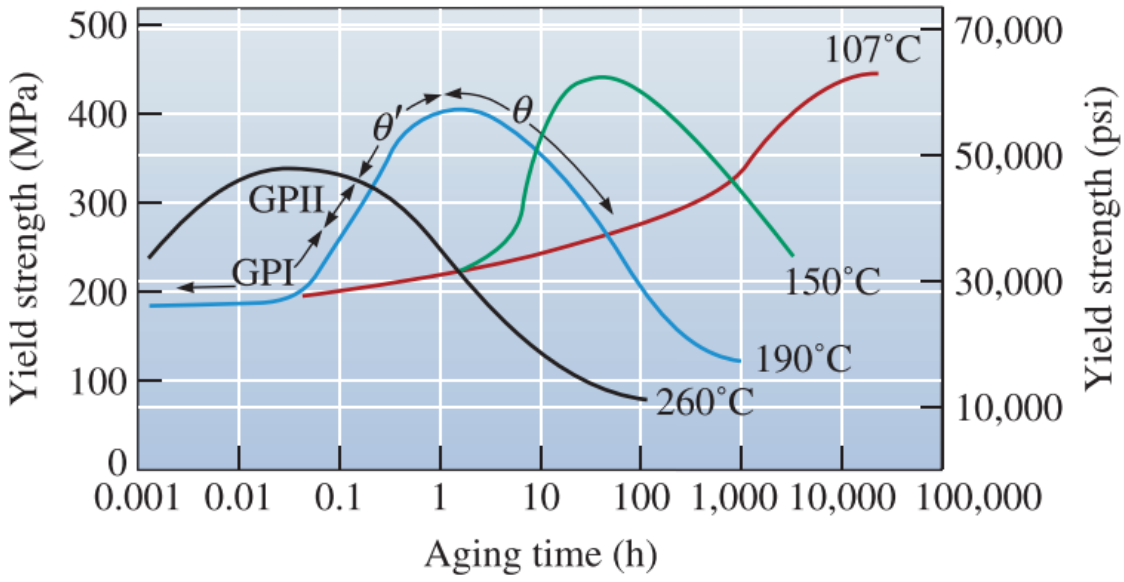

Figure 2.5: The effect of ageing temperature and time on the yield strength of an aluminium alloy. The alloy in a AL-4wt% Cu alloy, and θ is the equilibrium Cu phase [5].

Figure 2.5 shows the dependency of temperature and time during ageing on the resulting yield strength of the material. The peak strength increases with lower temperature and longer holding times. Although it is not shown in the figure it is possible to extrapolate the trend to room temperature. Over-ageing does not occur in naturally aged alloys [5].

Since the strength of aluminium alloys changes it is common to designate the different alloys by the treatment they have undergone. A selection of temper designations have been chosen and are described in table 2.1 below.

Table 2.1 : Description of a selection of temper designations [1].

T1	T4	T6
Cooled from hot working and naturally aged.	Solution heat treated and naturally aged.	Solution heat treated and artificially aged to maximum hardness.

2.5 Electric Conductivity

Electric conductivity is a measure of how easily electrons can move though a material. This movement can be hindered by imperfections in the crystal structure, resulting in a reduction in conductivity. Matthiessen's law, shown below, is used to describe the materials resistivity, i.e. a materials ability to hinder electron movement. It contains two parts, one describing the effect of temperature, and the other describing the effect of defects.

$$\rho = \rho_T + \rho_d \qquad (2)$$

Where: ρ is the total resistivity of the material
ρ_T is the resistivity contribution from temperature
ρ_d is the resistivity contribution from defects

The resistivity effect from defects is shown below.

$$\rho_d = b(1 - x)x \qquad (3)$$

Where: ρ_d is the resistivity contribution from defects
b is the defect resistivity coefficient
x is the atomic fraction of impurity or solid solution

As can be seen from equation 3 the resistivity of the material increases as the amount of impurities or solid solution fraction increases. Reduction of the fraction in solid solution by the means of precipitation hardening or ageing will have a positive effect on the conductivity of a material [5].

2.6 The Stress-Strain Curve

In a tensile test a force is applied to a specimen until fracture occurs. By measuring the area prior to testing, and the applied force and subsequent gage elongation during testing, an engineering stress-strain curve can be constructed.

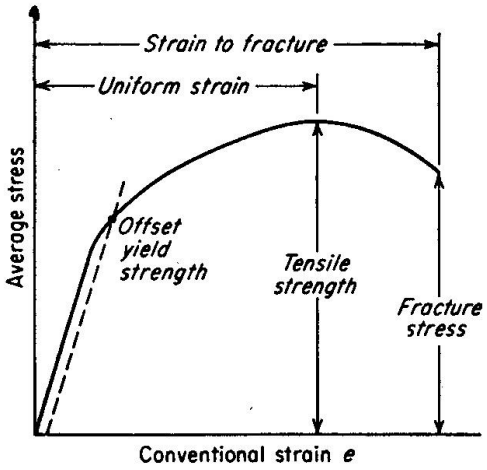

Figure 2.6: An engineering stress-strain curve. Note that the denomination on the axes are not coherent with the rest of this thesis [4].

An engineering stress-strain curve can be seen in figure 2.6. In the initial area of the curve, where it is straight, no permanent deformation occurs. This area is called the elastic zone. If more stress is applied permanent deformation will set in. This is called plastic deformation, and the area of the graph is therefore called the plastic zone.

The engineering stress is defined as the force divided by the original area.

$$\sigma = \frac{F}{A_0} \qquad (4)$$

Where: σ is the stress [MPa]
F is the force [N]
A_0 is the original cross section area of the sample [mm^2]

The strain is defined as the change in gage length divided by the original gage length. It is also common to give the strain as percent increase in length, as is done in this report.

$$\varepsilon = \frac{L - L_0}{L_0} \qquad (5)$$

Where: ε is the strain [mm/mm]
L is the specimens gage length after fracture [mm]
L_0 is the original gage length [mm]

There are several pieces of information the engineering stress-strain curve can provide. One crucial piece of information is the yield stress (σ_y), or the offset yield stress as it is called in figure 2.6, and it is defined as the stress value when the specimen is permanently deformed by 0,002, or 0,2%. This gives equation (6) below.

$$\sigma_y = \frac{F_{(strain\ offset=0{,}002)}}{A_0} \qquad (6)$$

Where: σ_y is the yield stress [MPa]
$F_{(strain\ offset=0,002)}$ is the force applied when to achieve a strain value of 0,002 [N]
A_0 is the original cross section area of the sample [mm^2]

The ultimate tensile strength is defined as the maximum force applied divided by the original cross section area.

$$\sigma_{UTS} = \frac{F_{max}}{A_0} \qquad (7)$$

Where: σ_{UTS} is the ultimate tensile strength [MPa]
F_{max} is the maximum force applied [N]
A_0 is the original cross section area of the sample [mm^2]

After the ultimate tensile strength is reached necking occurs and the engineering stress decreases until fracture. Necking is the term used to describe the plastic deformation shortly before fracture where the cross section area is reduced. Since equation (4) uses the original area the stress value seems to decrease. The true stress value uses the cross section area of any given point in time. This is difficult to measure accurately and the engineering stress is therefore more commonly used [4].

2.7 Fatigue

Fatigue is the term used when a material is subject to dynamic, or cyclic, loading over a period of time. If fracture occurs during such loading it is referred to as a fatigue fracture. Under constant loading a specimen acts in a very predictable way. First elastic elongation occurs, then plastic deformation, before necking sets in and the specimen fractures, as shown in the section 2.6. During cyclic loading the specimen can fracture even below yield stress.

To cause a fatigue fracture three basic factors are needed:

1. A maximum tensile stress of significant high value
2. A large enough variation or fluctuation in the applied stress
3. A sufficiently large number of cycles of the applied stress

2.7.1 Stress Cycles

There are several way an applied stress may vary or fluctuate to cause fatigue to occur. During fatigue testing cyclic loads, where the minimum and maximum stress values are set and consistently reached, are used, as shown in figure 2.7 (a) and (b).

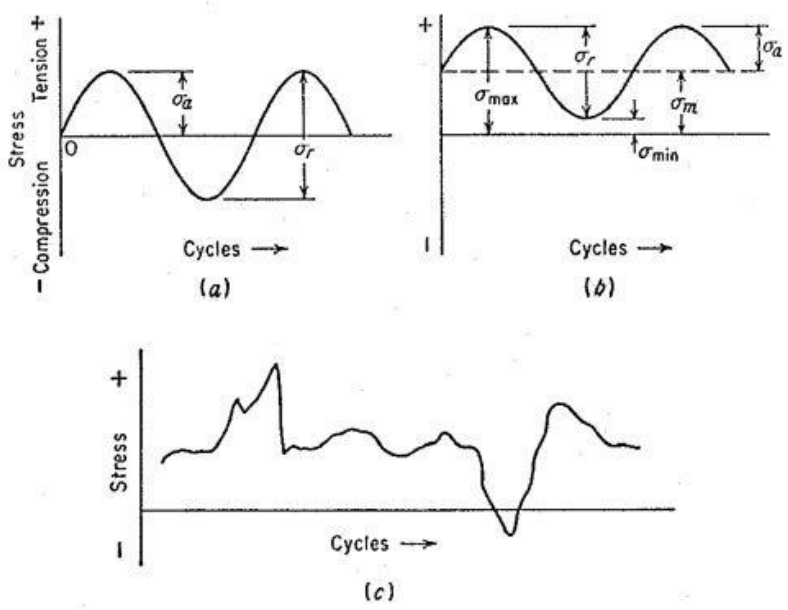

Figure 2.7: Sketches of different cyclic loading patterns. (a) shows uniform loading were the stress is the same in tension i.e. R=1. (b) shows a tension cycle were the specimen always is in tension, e.g. R=0,1. (c) shows a random stress cycle were R is difficult to determine. [4]

The symbols in figure 2.7 (a) and (b) are described in equations 6 to 9.

$$\sigma_a = \frac{\sigma_{max} - \sigma_{min}}{2} \quad (8)$$

$$\sigma_m = \frac{\sigma_{max} + \sigma_{min}}{2} \quad (9)$$

$$R = \frac{\sigma_{min}}{\sigma_{max}} \quad (10)$$

$$A = \frac{\sigma_a}{\sigma_m} = \frac{1 - R}{1 + R} \quad (11)$$

Where: σ_a is the stress amplitude [MPa]
σ_m is the mean stress [MPa]
σ_{max} is the maximum stress [MPa]
σ_{min} is the minimum [MPa]
R is the stress ratio
A is the Amplitude ratio

2.7.2 SN-curve

The usual way to present fatigue data is in a S-N curve. The maximum stress, S, the specimens have been exposed to is plotted against how many cycles, N, it endued until fracture. The curve as determined for a specific value for σ_m, R, or A. It is distinguished between high cycle fatigue ($N>10^5$) were the deformation of the specimen is largely elastic, and low cycle fatigue ($N<10^4$ or 10^5) were tests are conducted by controlled cycles of elastic plus plastic strain instead of load controlled strain as in high cycle fatigue.

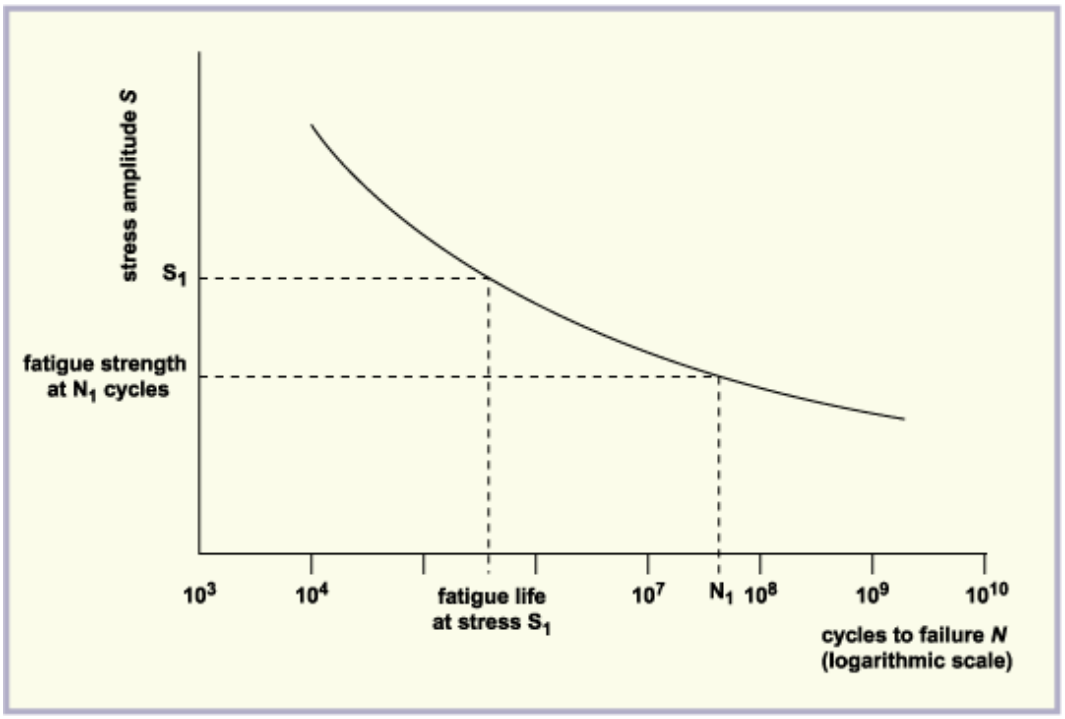

Figure 2.8: Example of a S-N curve without a fatigue limit [4].

Some materials, such as steels, have fatigue limits. This is a limit were the material is presumed to endure an infinite number of cycles without fracturing at a given stress value. Aluminium does not have such a limit as the curve never becomes horizontal. In these cases an arbitrary number of cycles, e.g. 10^7 cycles, is chosen and the test is stopped when a sample reaches this number. The sample is then deemed as a run out (RO) and is marked as such in the SN curve. The high-cycle region of the curve can sometimes be described by the Basquin equation [4]:

$$N\sigma_a^p = C \qquad (12)$$

Where: σ_a is the stress amplitude [MPa], and p and C are empirical constants.

2.8 Fatigue Fracture

The most accurate way to study a fracture and investigate the progression of the fracture is to examine the fracture surface. In this way it is possible to identify if the fracture was brittle or ductile, or where the different stages are located in fatigue fractures [7].

The fluctuating load experienced during fatigue causes local stress concentrations, and can with time result in crack formation. Fatigue cracks initiate usually on the surface, especially if the surface is scratched or damaged, or at an internal interface, such as the interface of a carburized surface layer and the base metal. During cyclic loading slip will occur on atomic planes, and the most persistent of the slip lines are embryonic fatigue cracks. The geometry of the specimen will also contribute as corners and other sudden changes in geometry act as stress intensifiers [4, 7].

A fatigue fracture is usually divided into three distinct stages named I-III.

Stage I

This is the stage where the crack is initiated and crack growth occurs along slip planes. This is usually 45° to the direction of the applied stress. The area of stage I crack growth is no larger than a few grains in polycrystalline metals [4, 7].

Stage II

In stage II the crack changes character and start to grow normal to the directions of the applied stress. The crack propagation occurs along specific crystallographic planes [7].

Stage III

In stage III the cross section is reduced to a degree that the material cannot support the applied stress and fracture is unavoidable. The fracture can be brittle, ductile or a combination of the two [7].

During macroscopic investigation the three stages can be identified. The most characteristic trait of a fatigue fracture are beach marks, on the macro scale, and striations, on the micro

scale. Beach marks and striations are orientated perpendicular to the crack propagation direction. Striations are a result of one, or more, loading cycles [7].

2.9 Energy Dispersive Spectroscopy

Energy dispersive spectroscopy (EDS) occurs in a SEM when an incoming electron interacts with the nucleus of an atom, causing an electron from the inner electron shells to be ejected. An electron from a higher energy electron shell then occupies this now vacant position, emitting a photon with the excess energy. Since the electrons in atoms have discrete energy levels the emitted photon will have an energy equal to the difference between the two energy levels of the electron shells. This energy is specific to each atom and when measured can be used to identify the atom. A photon emitted by an electron jumping from the L-shell to the K-shell, the two innermost electron shells, is called a K_α photon [7].

3 Experimental

In this thesis examinations of AA6005 have been conducted. The effect of long time natural ageing and artificial ageing in temper states pre- and post T6 on the fatigue properties was investigated. This includes electrical conductivity and hardness.

3.1 Delivered Material and Chemical Composition

The alloy used in this thesis was an AA6005 and was provided by Hydro Aluminium. It was delivered as an extruded profile with a width of 80mm, height of 10mm and length of 2000mm. An image of the cross section of the profile can be seen in figure 3.1.

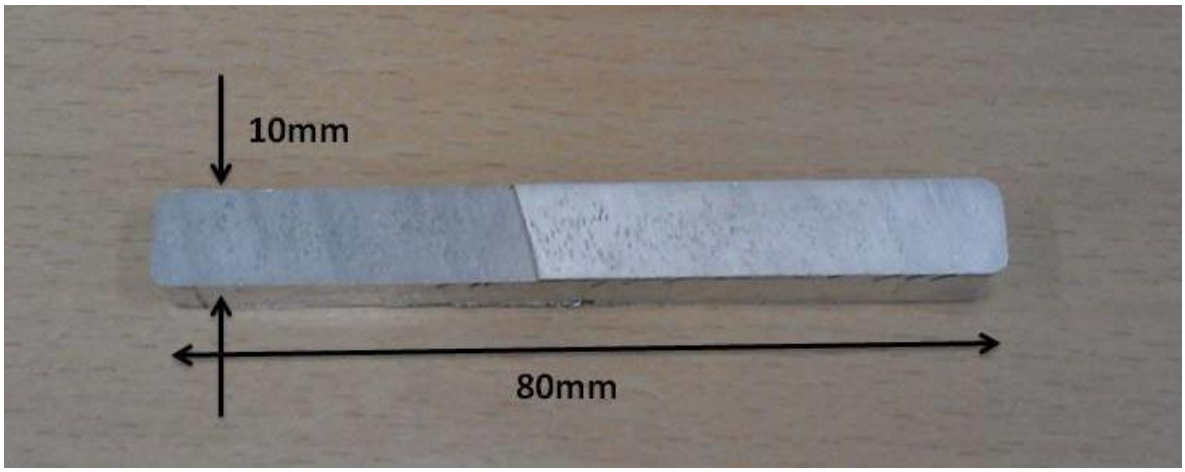

Figure 3.1: Cross section of the delivered profile [6].

The chemical composition of the alloy is shown in table 3.1.

Table 3.1: Chemical composition in wt% of the alloy used [8].

Alloy	Fe	Si	Mg	Mn	Cu	Zn	Ti	Al
AA6005 [wt%]	0.2	0.62	0.44	0.19	0.15	0.003	0.011	98.386

3.1.1 Production Process

The alloy was Direct Chill (DC) cast by Hydro RTD at Sunndalsøra to billets with a diameter of 203mm [8]. The billet was homogenized according to the parameters shown in table 3.2.

Table 3.2: Homogenization parameters used at Hydro RTD [8].

Alloy	Heating rate [°C/h]	Holding temperature [°C]	Holding time [Hours]	Cooling rate [°C/h]
AA6005	100	580	3	300-350

After homogenization, the billet was extruded by Hydro Aluminium Profiles AS at Raufoss. The parameters used are in this process are shown in table 3.3. Note that this was done in 2003 [8].

Table 3.3: Extrusion parameters used at Hydro Aluminium Profiles [8].

Alloy	Billet temperature [°C]	Ram speed [mm/min]
AA6005	500	4.2

After extrusion the profile was in storage until used in this thesis.

3.1.2 Definitions of Directions of Extruded Profile

In this thesis the extrusion direction (ED), the traverse direction (TD), and the normal direction (ND) are shown in figure 3.2. Together these directions form planes, such as the ND-TD plane shown below in grey. The planes and directions are used to describe where examinations were conducted compared to the delivered profile.

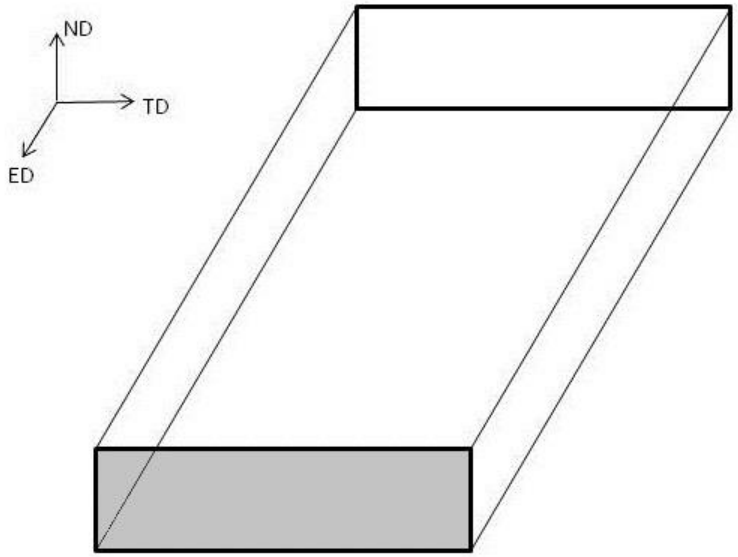

Figure 3.2: Definition of directions used in this thesis. The ND-TD plane is shown in grey [6].

3.1.3 Definition of Temper States

In this thesis three temper states are used: T1, under-aged (UA) and over-aged (OA). The T1 temper state indicates the as delivered condition where the alloy has only undergone natural ageing since fabrication. The UA and OA temper states have both been solution heat treated and artificially aged in accordance to sub-chapter 3.2. The difference between these temper states is the length of artificial ageing. The UA temper state is artificially aged to a condition before reaching peak hardness (T6), and the OA temper state is artificially aged to a condition past peak hardness. Figure 3.3 shows a graph highlighting where on the ageing curve these conditions are.

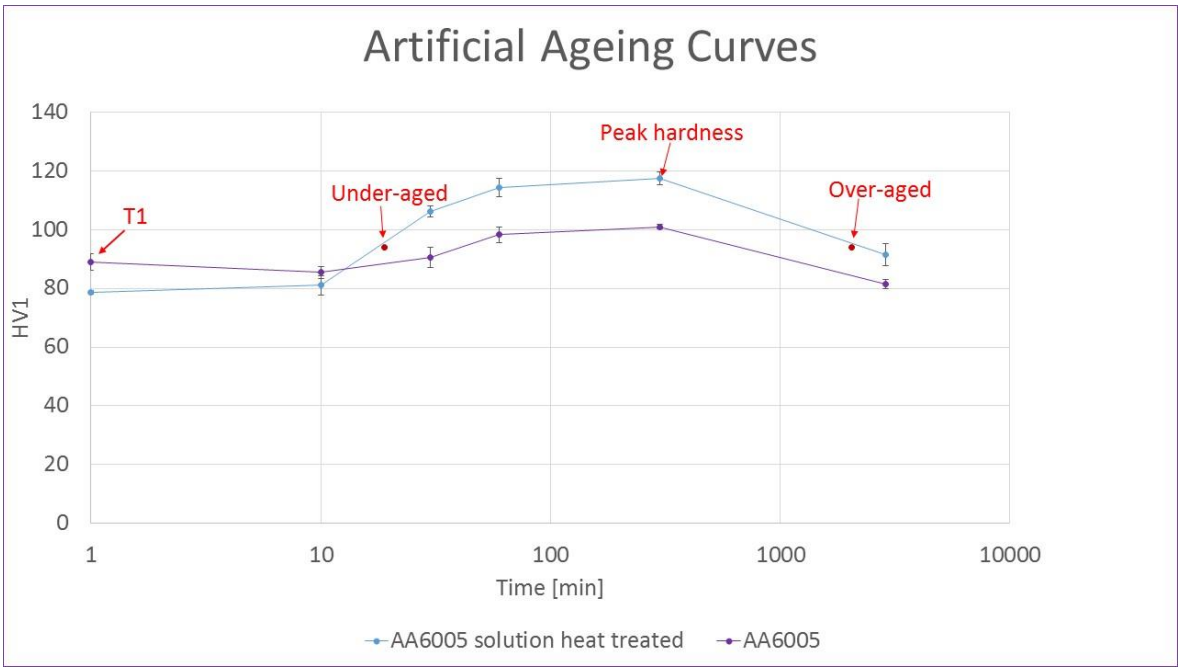

Figure 3.3: Graph defining the regions meant by under-aged and over-aged.

3.2 Artificial Ageing

Artificial ageing was conducted in order to examine the effect of this heat treatment on the alloy, and to identify the artificial ageing time to obtain the temper states UA and OA. In both these cases the process was the same. Frist, the alloy was cut using a Struers Discotm-2 into samples measuring 10x10x10mm. The samples were then solution heat treated in a salt bath at 540°C for 15 minutes, before being quenched, and rested at RT for 15 minutes. Thereafter the samples were submerged in an oil bath at 185°C and retrieved according to table 3.4.The samples were quenched upon retrieval.

Table 3.4: Time samples were submerged in an oil bath at 185°C before being retrieved.

Sample number	1	2	3	4	5	6
AA6005	0 min	10 min	30 min	60 min	5 hours	48 hours

Before hardness testing was conducted the samples were grinded down using P#1200 SiC paper until all visible surface defects were removed. This was done to ease measuring of the hardness, as well as to remove any suspected contamination from a previous extrusion though the same die used to produce the profile used in this thesis [8]. A selection of samples were measured and the thickness had been reduced by about 150µm [6].

Hardness measurements were done using a Matsuzama DVK-15 on the ED-TD plane. A total of five measurements were taken for each sample and a mean value calculated. The parameters used during hardness testing are shown in table 3.5.

Table 3.5: Parameters used during hardness testing.

Load [kg]	Loading time [s]	Loading speed [µm/s]
1	15	100

The targeted hardness for UA and OA was 94 HV1. This was found to be after 19 minutes for UA, and 34 hours for OA. See appendix A for measurements.

3.3 Microstructure Examination

Examination of the microstructure by microscopy requires a polished surface to obtain satisfactory results. This was done by casting the sample in epoxy resin, before grinding and polishing the sample surface with subsequently finer particles. Grinding and polishing was done with SiC paper and DiaPro Mol, respectfully. The steps used are shown in table 3.6. These steps were also taken to prepare the samples used for chemical composition analyses of the primary particles.

The machines used for grinding and polishing were a Streuers Knuth-Rotor and a Streuers DP-U3, respectfully.

Table 3.6: Steps taken during grinding and polishing, from left to right. The numbers are the coarseness level of the SiC paper during grinding, and the average particle size during polishing.

Grinding	P#320	P#1200	P#2000
Polishing	6 µm	3 µm	1 µm

3.3.1 Primary Particle Optical Microscopy

The primary particles were investigated in the ED-ND plane. This was done after solution heat treatment at 540°C for 15 minutes. A Leica MEF4M optical microscope was the used to provide images of the primary particles, and the software used for analyses was iSolutions DT

3.3.2 Primary Particle Chemical Composition Analyses

The samples used for chemical composition analyses were enclosed in Al-foil

The electric circuit between the given sample and the Al-foil was closed by adding a conducting tape to them. The samples were then stored in an oven at 73°C until examination. This was done to remove gas from the epoxy [9].

The primary particles were investigated in the ND-TD plane. This was done for all temper states. A FESEM Zeiss Ultra 55, Limited Edition scanning electron microscope (SEM) at the Department of Materials Science and Engineering at NTNU in Trondheim. The technique used was energy dispersive spectroscopy (EDS), with the acceleration voltage set to 20kV and the aperture was 120 μm for all images. The software used for the analyses was esprit 1.94.

3.4 Electrical Conductivity

Electrical conductivity was measured after soloution heat treatment and artificial ageing. Measurements were taken after the samples had been used for hardness testing. The apparatus used to conduct the measurement was a Foerster SIGMATEST 2.

3.5 Tensile Testing

To identify the yield stress tensile testing was done. The specimens used were produced at "Finmekanisk verksted" at NTNU with the specifications shown in figure 3.4. Note that the thickness of the specimen is halved compared to the delivered profile. This was done by milling each side down by 2,5 mm.

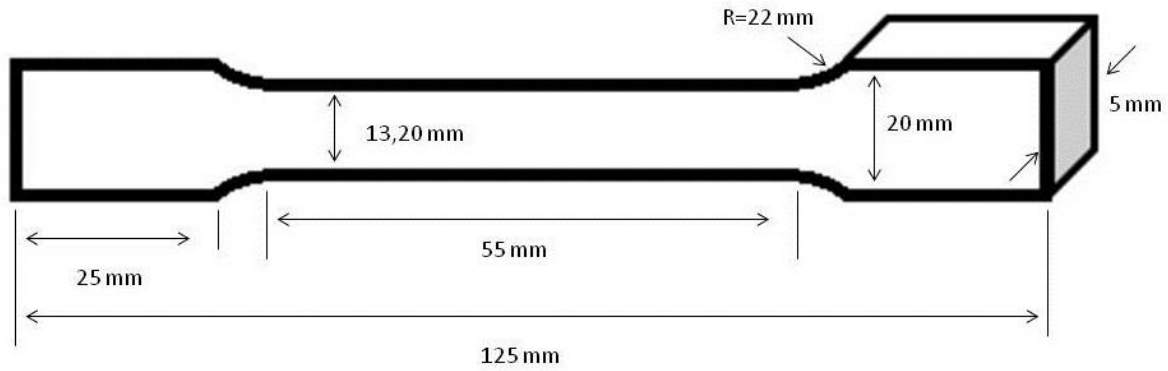

Figure 3.4: Dimensions of the tensile test specimens used [6].

The tensile test specimens were machined parallel to the extrusion direction as shown in figure 3.5.

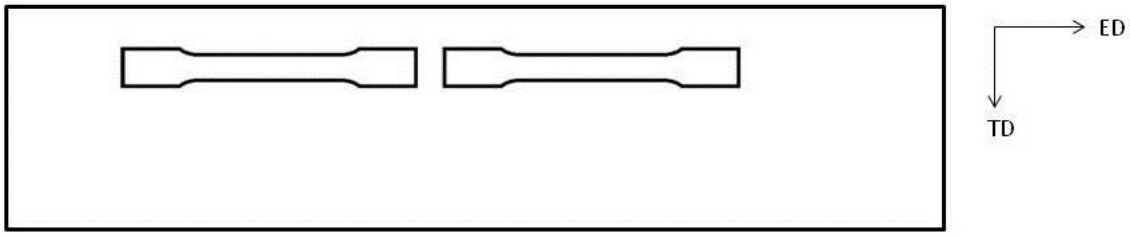

Figure 3.5: Direction of tensile test specimen compared to the delivered profile [6]. Not to scale.

A MTS 810 was used to perform tensile testing. During tensile testing an extensometer was used with the initial length of 5 mm. The strain rate was 2mm/min. Testing was done in room temperature.

3.6 Fatigue Testing

3.6.1 The Fatigue Specimen

The specifications for the fatigue specimen were chosen in compliance with ASTM standard E466-07 [10], and the dimensions are shown in figure 3.6. Fabrication was, as for the tensile test samples, done by "Finmekanisk verksted" at NTNU. Note that the thickness of the sample is reduced compared to the received profile. This was done by milling down each side by 3,5 mm.

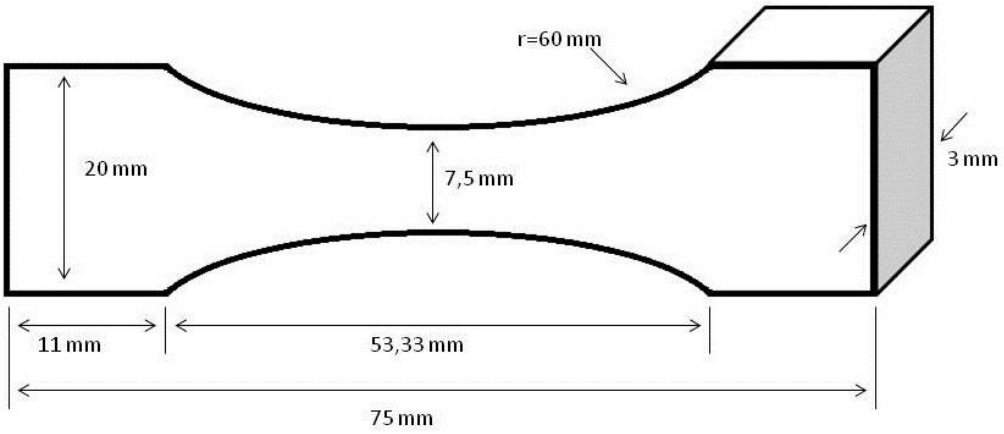

Figure 3.6: Dimensions of the fatigue specimens [6].

Specimens were machined parallel to the extrusion direction, as shown in figure 3.7.

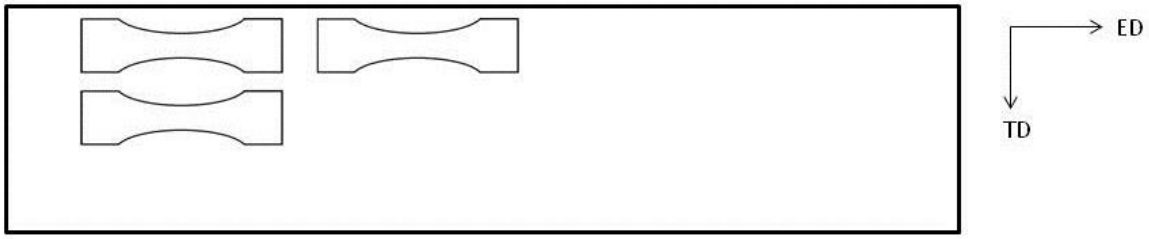

Figure 3.7: Direction of fatigue test specimens compared to the extruded profile [6]. Not to scale.

Prior to testing the samples were grinded to remove surface roughness caused by machining. The surfaces in the ED-TD plane were grinded using a Streuers Knuth-Rotor with a grit size of P#320 until surface markings from milling were removed, and then with a grit size of P#1200 to smoothen the surface. The curved surfaces were machined by water jet cutting and

had therefore a large surface roughness. This surface was therefore grinded down by hand with grit size increasing from P#80 to P#1200 until all visible markings on the surface were removed. The edges between the surfaces were grinded 40 times using a grit size of P#1200. One time is defined as both a back and forth motion. The corners between the surfaces were also grinded by hand with the same process. This was done to minimize stress concentrations due to geometry.

Fatigue testing was done using a MTS 810. The stress ratio chosen was R=0,1 to avoid buckling of the sample. The frequency during testing was set to f=20Hz. During testing the axial displacement limits were 1,8 mm and -0,5 mm to avoid damage to the machine and sample. The upper limit was later changed to 2,0 mm as the MTS 810 machine shut down during the 8th specimen in the UA series. The visible fracture of the specimen was then about halfway through the specimen in the TD. The cyclic limit was set to $N=2\cdot10^6$ cycles. Samples achieving this were deemed as run outs (RO). A total of ten samples ten specimens were tested in the T1 temper state, and nine specimens were tested in the UA and OA temper states.

3.6.2 Testing after Cyclic Loading

After fatigue testing was done new measurements of hardness and electric conductivity were performed to determine the effect of cyclic loading on these properties.

The hardness was measured about 5 mm from the fracture, and in the middle of the specimen if it was deemed a RO. Fractures occurred mostly to within the area shown in figure 3.8, as not all fractures were middle on the specimen. A few specimens fractured outside this area, and these specimens had their hardness measured towards the area shown in figure 3.8. In total five measurements were taken parallel to the fracture surface, and only on one specimen part after fracture.

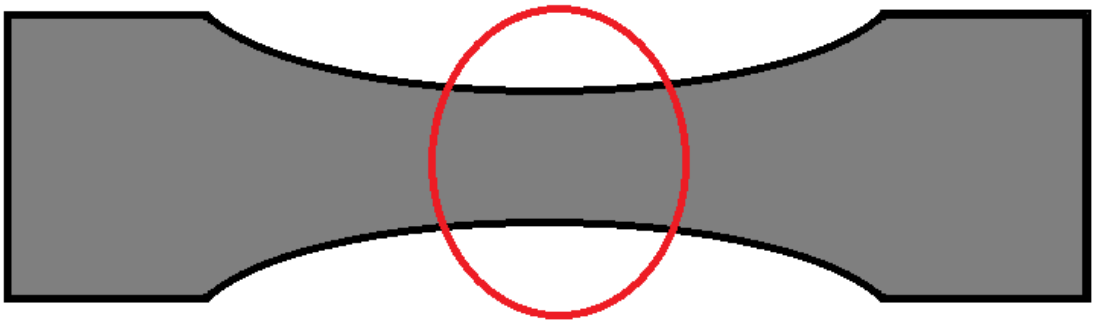

Figure 3.8: Area enclosed shows where hardness measurements were taken [6]. When fracture occurred outside this area, measurements were taken on the specimen part containing this area.

Electric conductivity was measured once on each specimen part. Electric conductivity measurements were done slightly outside the enclosed are in figure 3.8 as the probe used was large and precaution was taken not to damage the fracture surface. In the case of ROs the electric conductivity measurements were taken in the middle of the specimen.

3.7 Fractography

Fractography was done in a FESEM Zeiss Ultra 55, Limited Edition scanning electron microscope (SEM) at the Department of Materials Science and Engineering at NTNU in Trondheim. A selection of fractured fatigue samples were selected for examination. The technique used was secondary electron detection. The acceleration voltage used was set to 15 kV and the aperture was 30 μm for all images. The examined specimens were put in an ultrasound bath for 90-120 seconds to remove contaminations on the fracture surfaces.

4 Results

In this chapter the results from the conducted experiments will be presented. Some of the presented results were found during the previous project work done in the spring of 2015. This is mainly analyses of the T1 temper state.

4.1 Micrograph of the Grain Structure

In the preliminary project work to this thesis [6], the grain structure was examined after anodizing, and in polarized light. Figure 4.1 shows the resulting micrograph of this examination. The black spots in the image are a result of over-anodizing the sample. The profile surface can be seen at the bottom of the image. It is evident that the grain structurer is fibrous in the extrusion direction. The average grain thickness is 7µm.

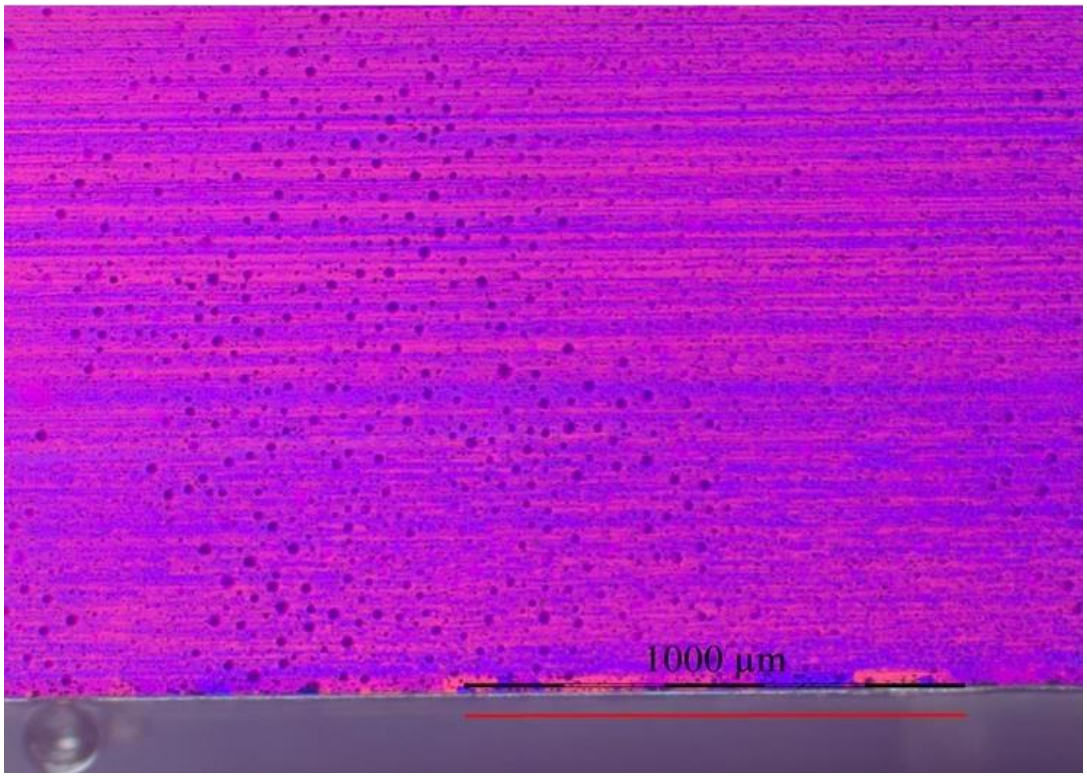

Figure 4.1: Micrograph of the grain structure in the T1 temper state. A red line, the same length of the scale bar, has been added as the placement of the scale bar can hinder its visibility. The image is taken in the ED-TD plane. The black spots are a result of over-anodizing [6].

The anodizing was done with 1,0A current and 20,0V voltage for 90 seconds.

4.2 Primary Particles

Primary particle analyses was done by taking several images of the alloy in the ED-TD plane using an optical microscope and counting the amount of particles in each image. The particles were grouped into six categories: <2µm^2, 2-5µm^2, 5-10 µm^2, 10-15 µm^2, 15-25 µm^2, and >25 µm^2. The image area of the particle were also measured.

The chemical composition of the primary particles was examined using EDS. This was done in the ND-TD plane.

4.2.1 Optical Microscopy Analyses of the T1 Temper State

Analyses of the alloy in the T1 temper state were conducted in the spring of 2015, and have been presented on the report generated by that project [6].

The images used to analyses the particles are shown in figure 4.2a and 4.2c, with the corresponding bar charts shown in figure 4.2b and 4.2d, respectfully. The bar charts show a similar size distribution of primary particles, with figure 4.2a containing more primary particles than figure 4.2c.

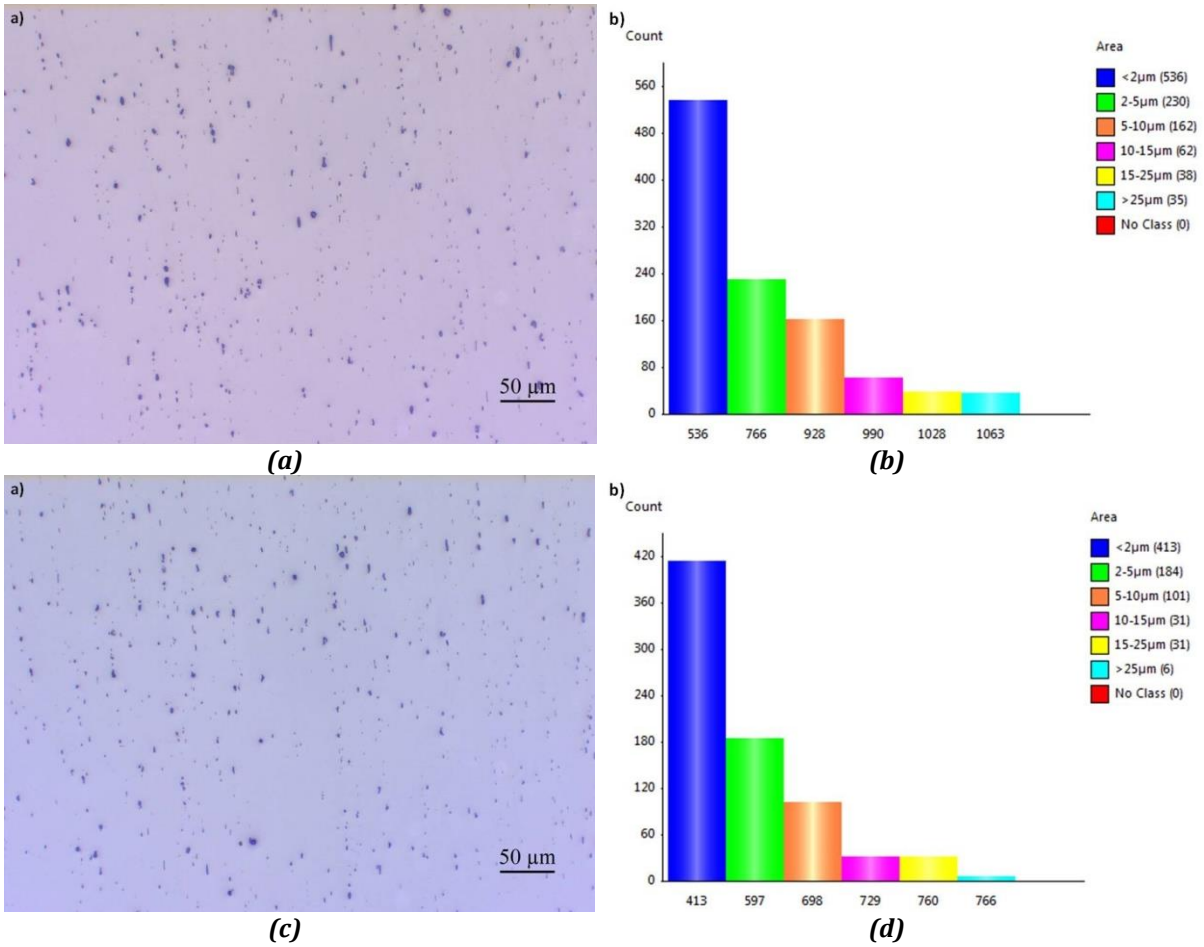

Figure 4.2: Results of primary particles in the T1 temper state. The images used in the analyses are shown on the left, and the corresponding particles counts are shown on the right [6].

The total area of the primary particles by size category in percent of total image area is shown in table 4.1. It is apparent that figure 4.2a has a much larger fraction of the image area covered by primary particles than figure 4.2c. The mean value is also shown in table 4.1.

Table 4.1: Area of particles in figure 4.2a and 4.2c by size category, and the mean value between them [6].

Particle size	Particle Area in Figure 4.2a [%]	Particle Area in Figure 4.2c [%]	Mean
<2µm	0.186	0.155	0.1705
2-5µm	0.345	0.265	0.305
5-10µm	0.529	0.329	0.429
10-15µm	0.347	0.179	0.263
15-25µm	0.337	0.271	0.304
>25µm	0.685	0.083	0.384
Total particle area [%]	2.429	1.282	1.856

The mean values for the total particle area of each size category, shown in table 4.1, are used to construct the bar chart shown in figure 4.3. In figure 4.3 it can be seen that the amount of primary particles in a size category does not indicate the amount of total image area that category occupies in the image. This is evident by the fluctuation in figure 4.3, and by comparing the size category with the highest amount of primary particles, <2µm, to the size category with the least amount of primary particles, >25µm.

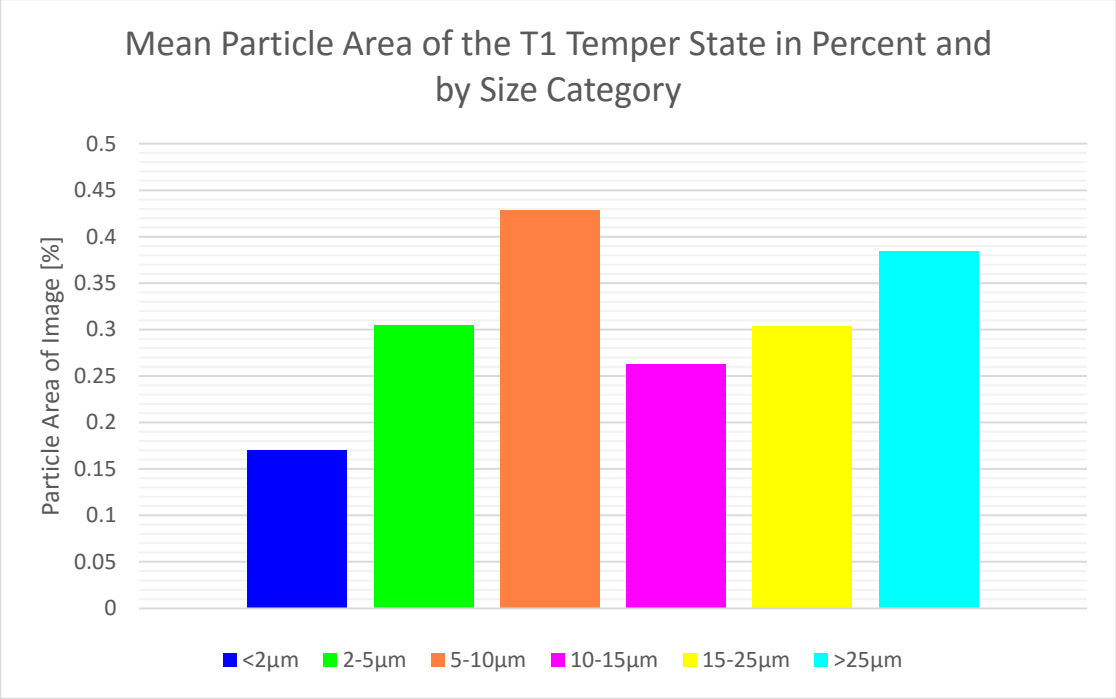

Figure 4.3: Mean primary particle area of the T1 temper state in percent and by size category [6].

4.2.2 Optical Microscopy Analyses after Solution Heat Treatment

A sample was solution heat treated at 540°C for 15 minutes to examine the effect of solution heat treatment on the primary particles of the alloy, if any. Figure 4.4 shows the images used for the analyses on the left, and the corresponding bar chart of primary particle count is shown on the right. The primary particle distribution and total count is similar in all three images shown in figure 4.4, with the only significant difference being the decreased primary particle count of size category <2µm in figure 4.4b compared to figures 4.4d and 4.4f.

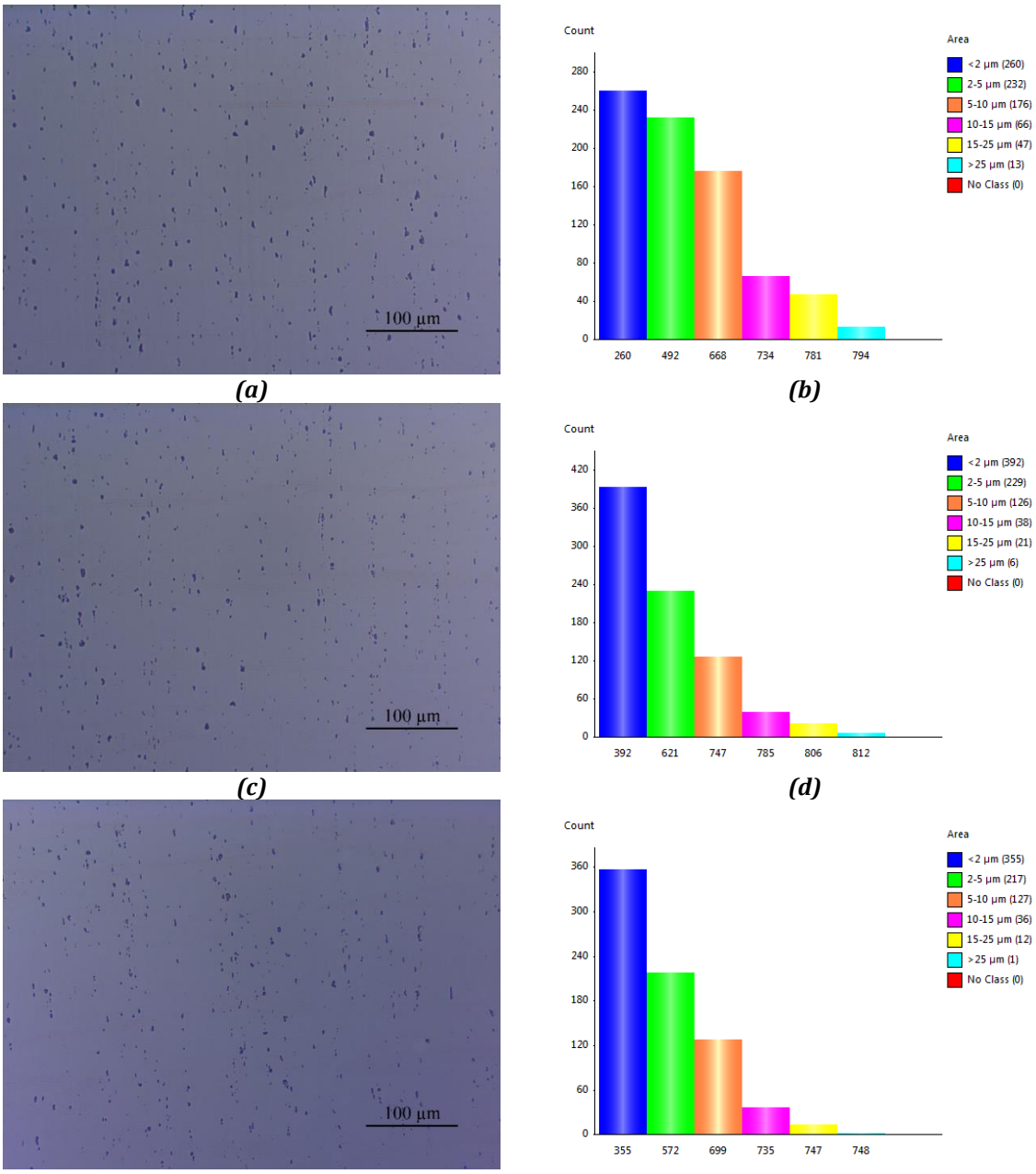

Figure 4.4: Results of primary particle analyses after solution heat treatment. No artificial ageing has been conducted on the sample. The images used are shown on the left and the corresponding particle count can be seen to the left, i.e. b) shows the particle count in a).

The total area of primary particles by size category in percent of total image area is shown in table 4.2. In table 4.2 it can be seen that the total primary particle area of each size category fluctuates between the images used. This can clearly be seen when comparing the two largest size categories, 15-25µm and >25µm, to the same size category in the different images. The largest difference is in the size category <25µm, where figures 4.4a has 15 times its area covered by this size category compared to figure 4.4e.

Table 4.2: Area of particles in figure 4.4 by size category, and the mean value of them.

Particle size	Particle Area in Figure 4.4a [%]	Particle Area in Figure 4.4c [%]	Particle Area in Figure 4.4e [%]	Mean
<2µm	0.111	0.157	0.153	0.140
2-5µm	0.372	0.342	0.316	0.343
5-10µm	0.580	0.407	0.413	0.467
10-15µm	0.372	0.209	0.199	0.260
15-25µm	0.405	0.182	0.106	0.231
>25µm	0.166	0.089	0.011	0.089
Total particle area [%]	2.006	1.386	1.198	1.530

The mean values for the total particle area of each size category, shown in table 4.2, are used to construct the bar chart shown in figure 4.5. In figure 4.5 the distribution of the mean total primary particle area by size category shows a tendency to follow a normal distribution centred on the 5-10µm size category.

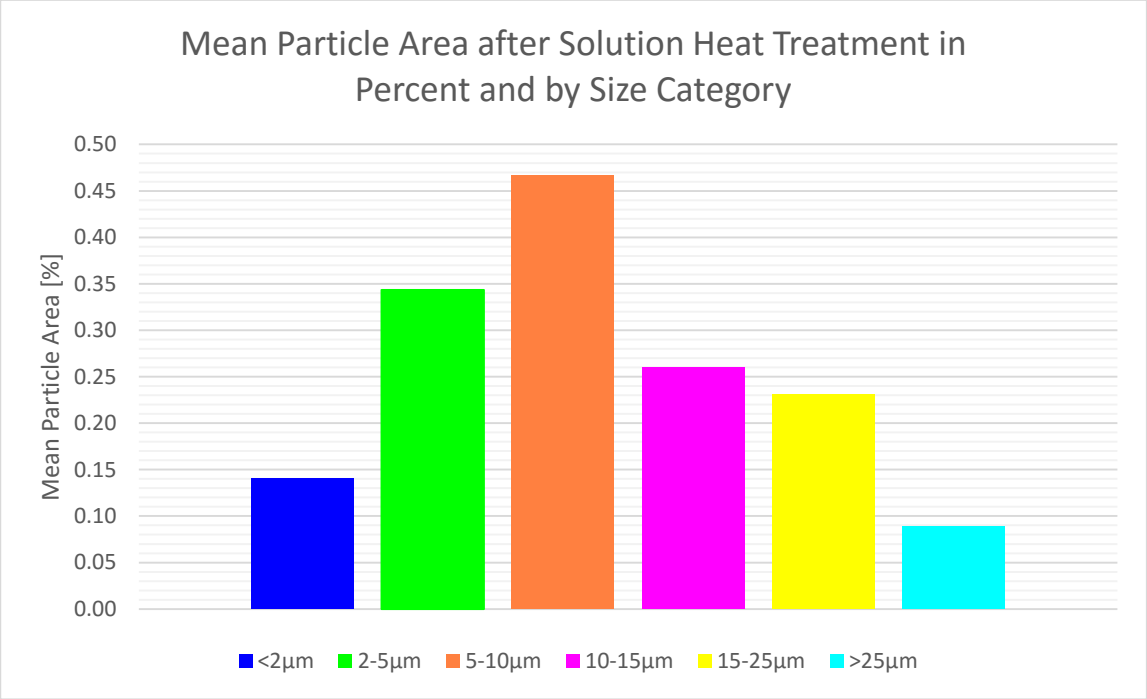

Figure 4.5: Mean primary particle area after solution heat treatment at 540°C for 15 minutes, in percent and by size category.

4.2.3 Chemical Composition Analyses

Chemical composition analyses was done on all temper states using EDS in a SEM. The parameters used are shown on the images. To analyse the entire primary particle box selection was used. This resulted in inclusion of the matrix, and the results can therefore not be used to identify the exact chemical composition of the particles, but rather identify the elements included in the primary particle, e.g. the presents of iron.

T1 Temper State

Figure 4.6 shows the image used to examine the chemical composition of the T1 temper state. The number of particles examined in the T1 temper state is 16. Three of the primary particles are darker than the surrounding matrix, while the rest are lighter, suggesting differences in chemical composition. From figure 4.6 it is apparent that the particles can be grouped into two groups: elongated particles and circular particles. The larger particles tend to be of an elongated shape, while the smaller particles tend to be more circular in shape.

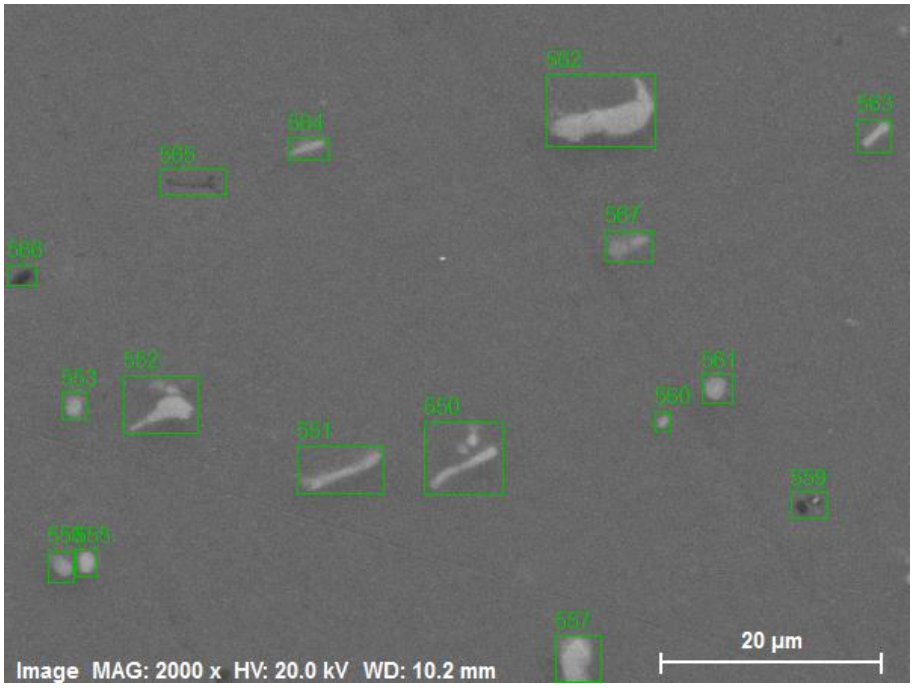

Figure 4.6: Image used to examine the chemical composition of the primary particles in the T1 temper state. The primary particles are differentiated by a given number.

Table 4.3 shows the chemical composition of the primary particles shown in figure 4.6. The particles can be identified by the number associated with each particle. The darker particles are marked in the table by *. Note that that chromium was found in some particles. This element is not included in the chemical composition received from Hydro Aluminium. It is apparent that the darker particles do not include iron.

*Table 4.3: The chemical composition of the particles shown in figure 4.6. The darker particles can be identified with *.*

Particle Number	Al [%]	Mg [%]	Si [%]	Mn [%]	Fe [%]	Cr [%]	Ti [%]
550	94.13	1.29	1.62	1.59	1.36		
551	94.64	1.29	1.64	1.22	1.04	0.16	
552	92.52	1.25	2.09	2.12	2.03		
553	97.27	1.39	1.00	0.29	0.06		
554	94.47	1.30	1.79	1.27	1.18		
555	94.47	1.30	1.79	1.27	1.18		
556	97.19	1.38	1.04	0.39			
557	86.35	1.17	3.48	4.15	4.02	0.83	
559*	96.91	1.35	1.56	0.18			
560	97.36	1.38	0.92	0.26			0.07
561	97.34	1.33	0.99	0.34			
562	89.79	1.21	2.74	2.82	2.95	0.48	
563	97.26	1.31	0.97	0.33	0.13		
564	97.24	1.32	0.99	0.43	0.02		
565*	97.64	1.34	0.83	0.12			0.07
566*	97.37	1.38	1.06	0.18			
567	97.05	1.29	1.07	0.59			

Under-Aged Temper State

Figure 4.7 shows the image used to examine the chemical composition of the UA temper state. The number of particles examined in the UA temper state is 18. Five of the primary particles are darker than the surrounding matrix, while the rest are lighter, suggesting differences in chemical composition. When comparing the UA temper state with the T1 temper state it is apparent that the particles are more circular in shape, with the elongated particles having a more oval shape than the needle-like appearance of some particles in the T1 temper state.

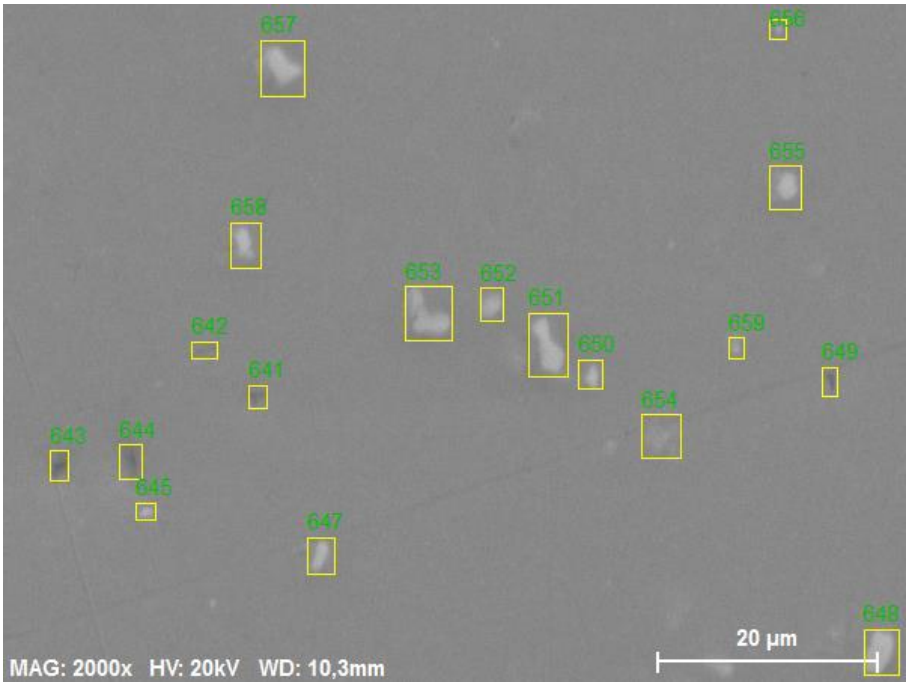

Figure 4.7: Image used to examine the chemical composition of the primary particles in the UA temper state. The primary particles are differentiated by a given number.

Table 4.4 shows the chemical composition of the primary particles shown in figure 4.7. The particles can be identified by the number associated with each particle. The darker particles are marked in the table by *. Note that that chromium was found in some particles, predominantly particles including iron. It is apparent that the darker particles do not include iron.

*Table 4.4: The chemical composition of the particles shown in figure 4.7. The darker particles can be identified with *.*

Particle Number	Al [%]	Mg [%]	Si [%]	Mn [%]	Fe [%]	Cr [%]
641*	97.42	1.36	0.97	0.25		
642*	97.30	1.38	0.99	0.33		
643*	97.18	1.36	1.20	0.27		
644*	97.36	1.37	0.98	0.29		
645	96.38	1.35	1.25	0.82	0.20	
647	95.08	1.32	1.61	1.07	0.76	0.16
648	90.94	1.25	2.52	2.48	2.39	0.41
649*	97.38	1.38	0.95	0.29		
650	95.05	1.25	1.57	1.15	0.76	0.22
651	94.37	1.28	1.66	1.39	1.07	0.22
652	96.76	1.33	1.22	0.50	0.19	
653	95.88	1.32	1.46	0.80	0.45	0.10
654	97.14	1.50	1.11	0.22	0.02	0.02
655	97.16	1.34	1.03	0.41	0.06	
656	97.23	1.37	1.02	0.38		
657	96.57	1.32	1.29	0.67		0.15
658	94.71	1.31	3.64	0.34		
659	97.45	1.38	0.93	0.25		

Over-Aged Temper State

Figure 4.8 shows the image used to examine the chemical composition of the UA temper state. The number of particles examined in the OA temper state is 14. No darker particles were found in the OA temper state. In the OA temper state the particles seem to have different shapes compared to the other two tamper states. From figure 4.8 both elongated, circular, and crescent shaped particles are found, but still no needle-llike shaped particles as in the T1 temper state.

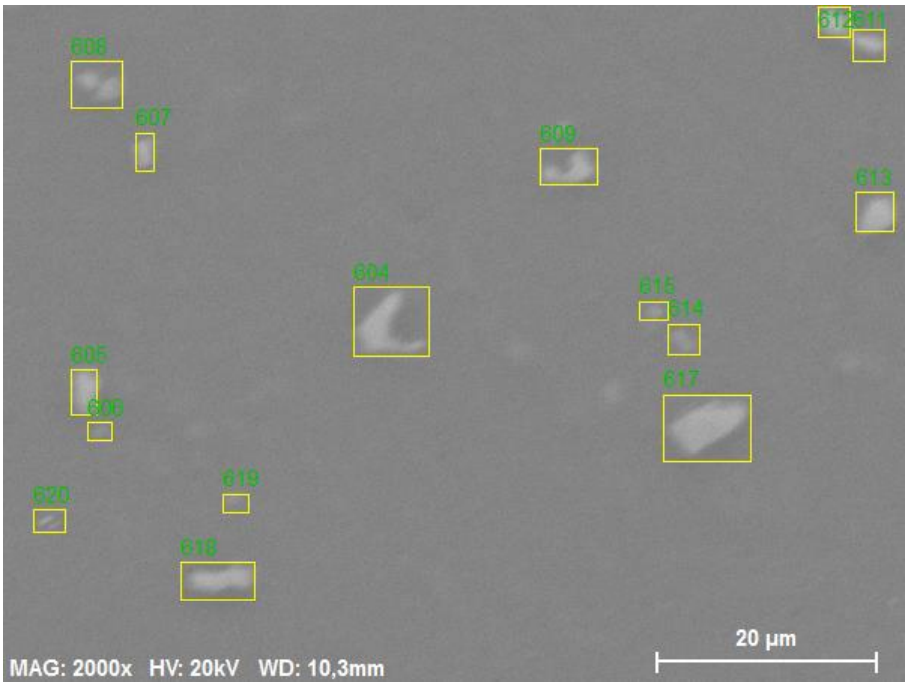

Figure 4.8: Image used to examine the chemical composition of the primary particles in the OA temper state. The primary particles are differentiated by a given number.

Table 4.5 shows the chemical composition of the primary particles shown in figure 4.8. The particles can be identified by the number associated with each particle. Chromium was found in most particles, but in varying concentrations.

Table 4.5: The chemical composition of the particles shown in figure 4.8.

Particle Number	Al [%]	Mg [%]	Si [%]	Mn [%]	Fe [%]	Cr [%]
604	87.50	1.19	2.67	4.01	3.82	0.81
605	88.85	1.22	2.53	3.35	3.50	0.55
606	96.59	1.27	0.98	0.75	0.41	
607	94.47	1.31	1.38	1.47	1.14	0.22
608	95.09	1.30	1.85	0.95	0.68	0.13
609	90.05	1.25	2.23	3.15	2.83	0.50
611	94.55	1.08	1.21	1.56	1.30	0.31
612	93.82	1.28	1.50	1.70	1.38	0.32
613	93.04	1.27	1.74	1.97	1.63	0.35
614	97.19	1.32	0.90	0.50	0.03	0.05
615	97.40	1.35	0.82	0.39		0.05
617	89.10	1.21	2.47	3.25	3.33	0.63
618	95.02	1.29	1.40	1.07	1.05	0.16
619	97.58	1.34	0.77	0.32		

4.3 Artificial Ageing

Artificial ageing experiments have been conducted from the T1 temper state and after solution heat treatment at 540°C for 15 minutes. The T1 temper state was done in the preliminary work [6]. From figure 4.9. It is apparent that the T1 temper state has undergone natural ageing, as expected, as the hardness is higher before being exposed to the artificial ageing process. After 10 minutes the hardness is about the same, before the solution heat treated sample surpasses it. The hardness of the two series seem to follow the same overall curve after artificial ageing for 30 minutes, with the solution heat treated series at elevated levels compared to the T1 series. Note also that the hardness of the T1 series drops slightly after artificial ageing for 10 minutes.

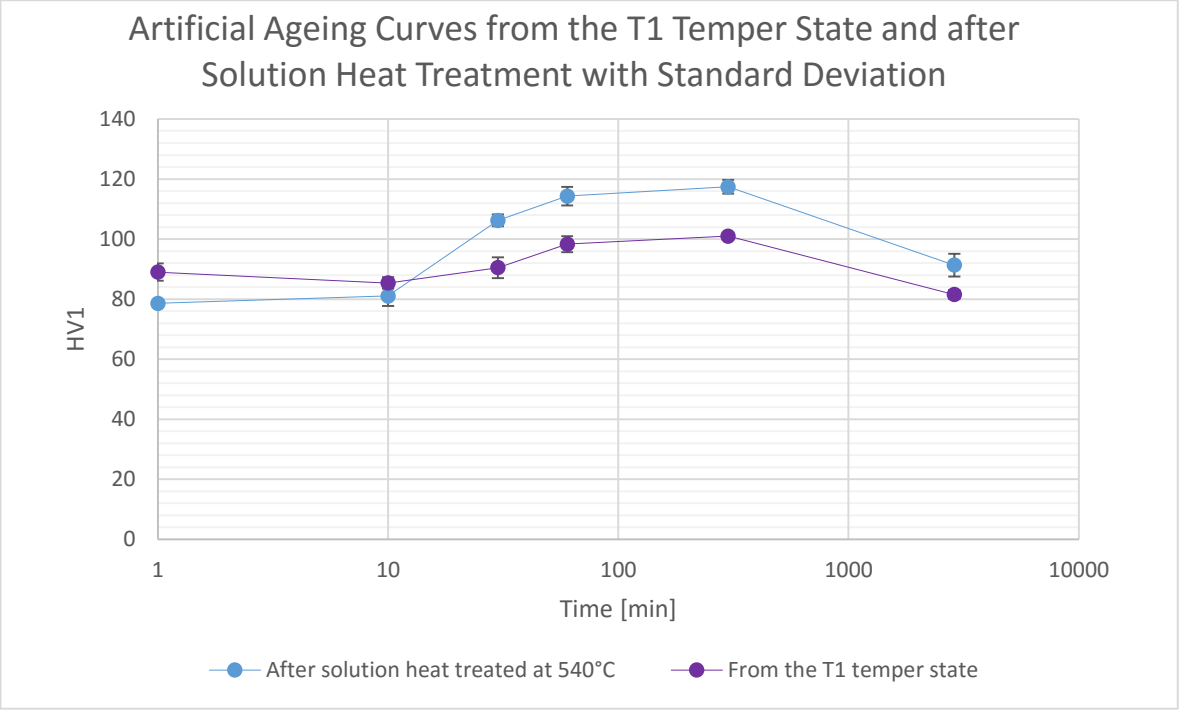

Figure 4.9: Artificial ageing curves from the T1 temper state [6] and after solution heat treatment. Solution heat treatment was done at 540°C for 15 minutes, and artificial ageing was done at 185°C.

The mean hardness values with their standard deviation used to construct figure 4.9 are shown in table 4.6.

Table 4.6: Mean hardness values for artificial ageing from the T1 temper state, and after solution heat treatment. Data for artificial ageing from the T1 temper state taken from preliminary work [6].

Ageing time	0 min	10 min	30 min	60 min	5 hours	48 hours
From T1 [HV1]	89 ± 2.9	85 ± 1.9	90 ± 3.4	98 ± 2.7	101 ± 0.9	82 ± 1.5
Solution heat treated [HV1]	79 ± 0.6	81 ± 3.4	106 ± 1.9	114 ± 3.1	117 ± 0.3	91 ± 3.8

4.4 Electrical Conductivity

The electrical conductivity was measured on the same samples used to measure the hardness, and the results are shown in figure 4.10. Measurements from the T1 temper state were conducted in the preliminary project work [6]. From 4.10 it can be seen that the T1 temper state shows a slightly higher electrical conductivity when subject to little to no artificial ageing, and when subject to artificial ageing for a long period of time. It appears that the solution heat treated series experiences a large increase, ~1,7MS/m, in electrical conductivity between artificial ageing for 10 minutes and artificial ageing for 30 minutes, while the T1 series experiences this increase, ~2,0MS/m, later, between artificial ageing for 60 minutes and 5 hours.

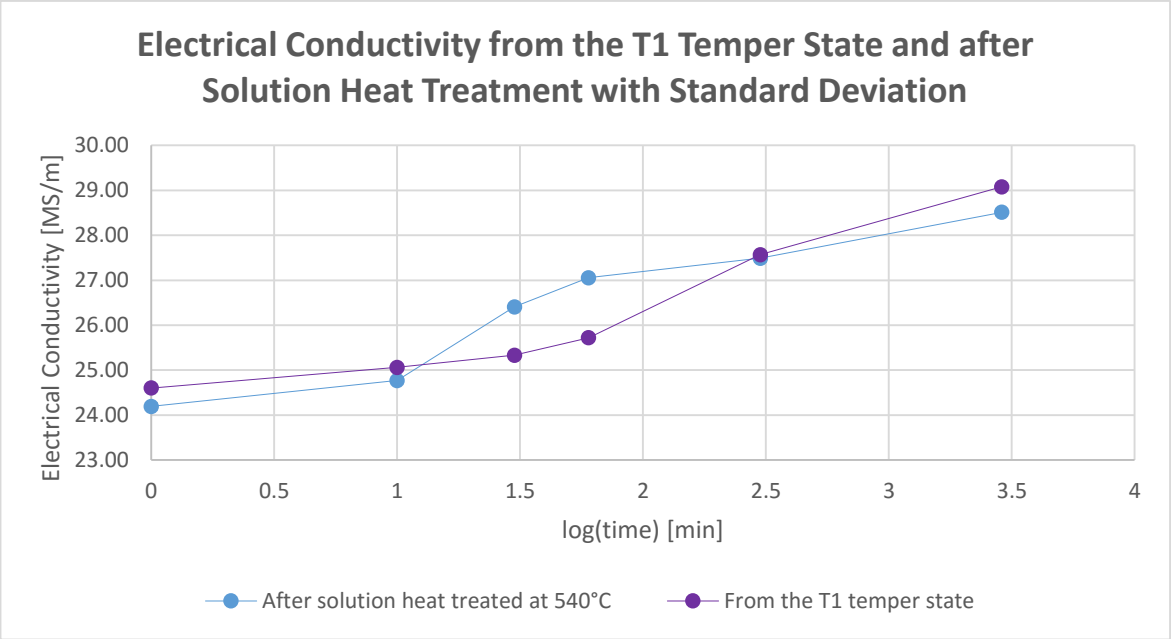

Figure 4.10: Electrical conductivity from the T1 temper state [6] and after solution heat treatment and artificial ageing up to 48 hours. Note that the highest standard deviation value is 0,07 and subsequently the error bars are not visible. Only one measurement was taken for the T1 temper state and subsequently no standard deviation is available for this series.

Table 4.7 shows the values used to construct figure 4.10. The standard deviation calculated for the solution heat treated sample is very small, with the largest standard deviation being 0,07. Multiple measurements were not taken on the T1 series in the preliminary project work, and subsequently this series does not have a standard deviation value.

Table 4.7: Electrical conductivity values used in figure 4.10. Standard deviation was only done for the solution heat treated samples. Data for the T1 series is taken from preliminary work where only one measurement was taken [6].

Ageing time	0 min	10 min	30 min	60 min	5 hours	48 hours
Solution heat treated [MS/m]	24.19 ± 0.07	24.77 ± 0.07	26.41 ± 0.04	27.05 ± 0.05	27.49 ± 0.07	28.51 ± 0.04
From T1 [MS/m]	24.60	25.06	25.33	25.72	27.72	29.08

4.5 Tensile Testing

Tensile tests were done in all three temper states: T1, UA and OA. Note that the T1 temper state was done in the preliminary project work [6]. Three test specimens were used to examine the tensile properties in temper states T1 and UA, while four were used to examine the OA temper state. For each temper state a close-up of the initial part of the stress-strain curve is also shown in a separate figure. The close-up figures are limited to the range where fatigue testing was done.

The result from the T1 temper state is shown in figure 4.11. The yield stress was found to be 210±1 MPa, and the ultimate tensile strength was found to be 331±1 MPa. All specimens followed a similar course during tensile testing and fractured roughly in the middle of the specimen.

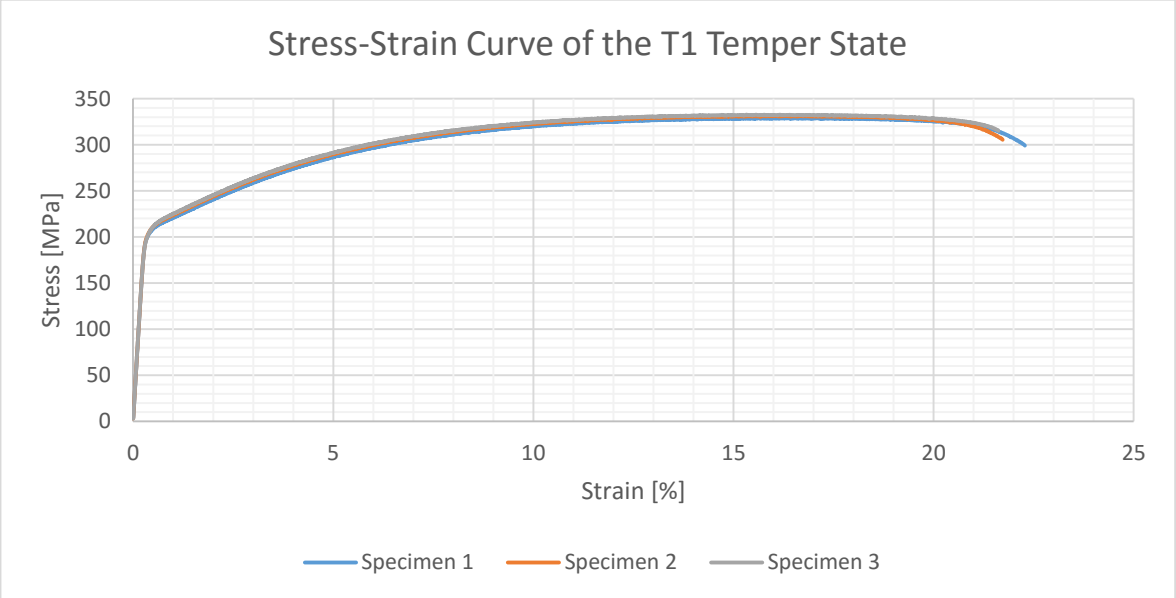

Figure 4.11: Stress-strain curve in the T1 temper state [6].

In figure 4.12 a close-up of the initial part of the stress-strain curve is shown. This figure is limited to the area where fatigue testing took place. In the case of the T1 temper state the fatigue specimen was subject to a maximum stress of 280 MPa, and was subsequently subject to about 4,5% elongation.

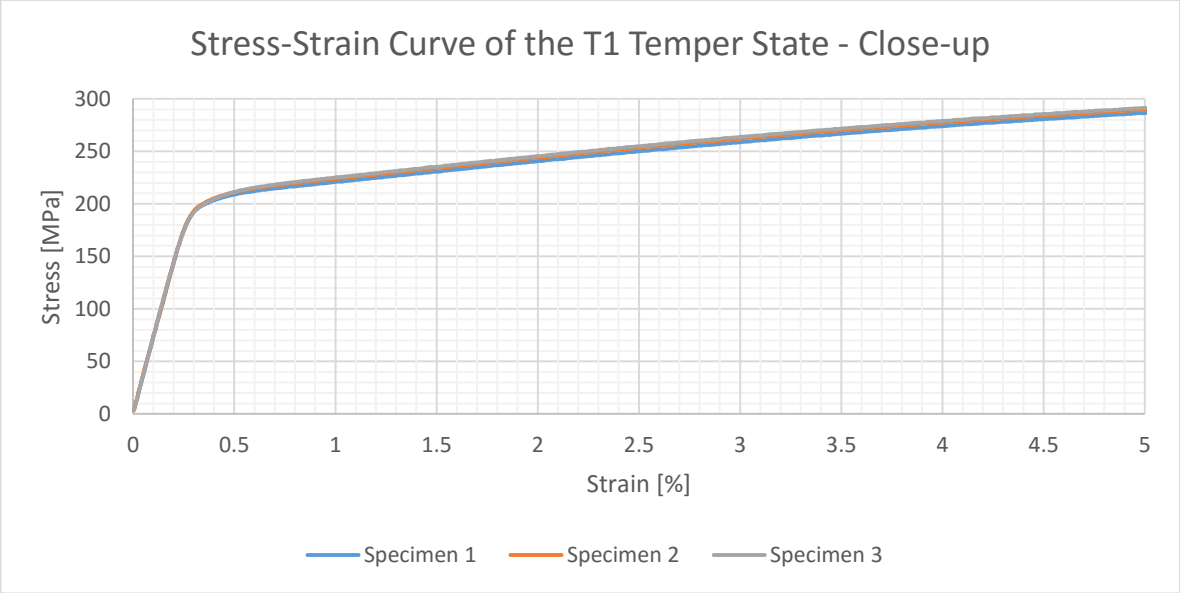

Figure 4.12: Close-up of the stress region in figure 4.11, where fatigue testing was conducted [6]. The maximum stress applied to a fatigue sample was 280 MPa in this temper state.

The results from the tensile testing of the UA temper state is shown in figure 4.13. The yield stress was found to be 259±9 MPa and the ultimate tensile strength was found to be 331±5 MPa. From figure 4.13 it is apparent that the UA series was not as uniform as the T1 series. Specimen 2 in this series follows the other specimens, but with slightly decreased values, thus causing a much larger standard deviation compared to the other two temper states. The most likely cause of this difference in behaviour of specimen 2 is small individual variations in the specimen caused by the short artificial ageing time of 19 minutes the specimen was subject to, as the alloy is in an area of the artificial ageing curve, see figure 4.9, where the hardness increases rapidly. All the specimens fractured at roughly the middle of the specimen.

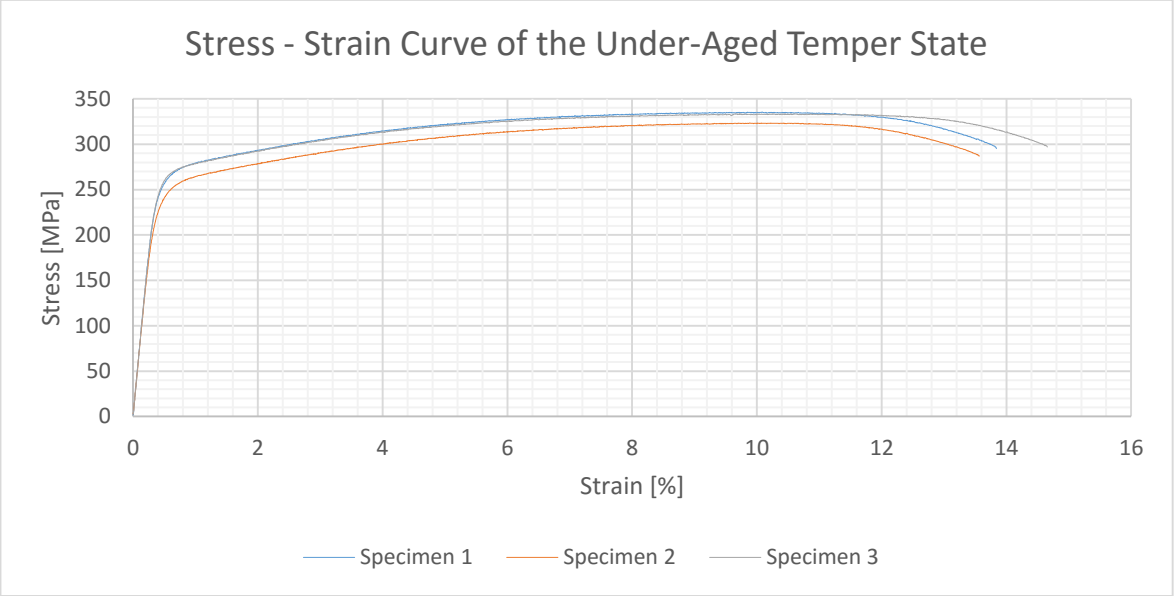

Figure 4.13: Stress-strain curve of the UA temper state.

Figure 4.14 shows a close up of the initial part of the stress-strain curve for the UA temper state. The curve is limited to the area where the fatigue testing was conducted. The maximum stress used during fatigue testing was 285 MPa, and was subsequently subject to between 1,4% and 2,2% elongation, depending on which tensile specimen used. Note that the elongation axis is cropped at 2,5% and not 5% as the case is for the T1 temper state.

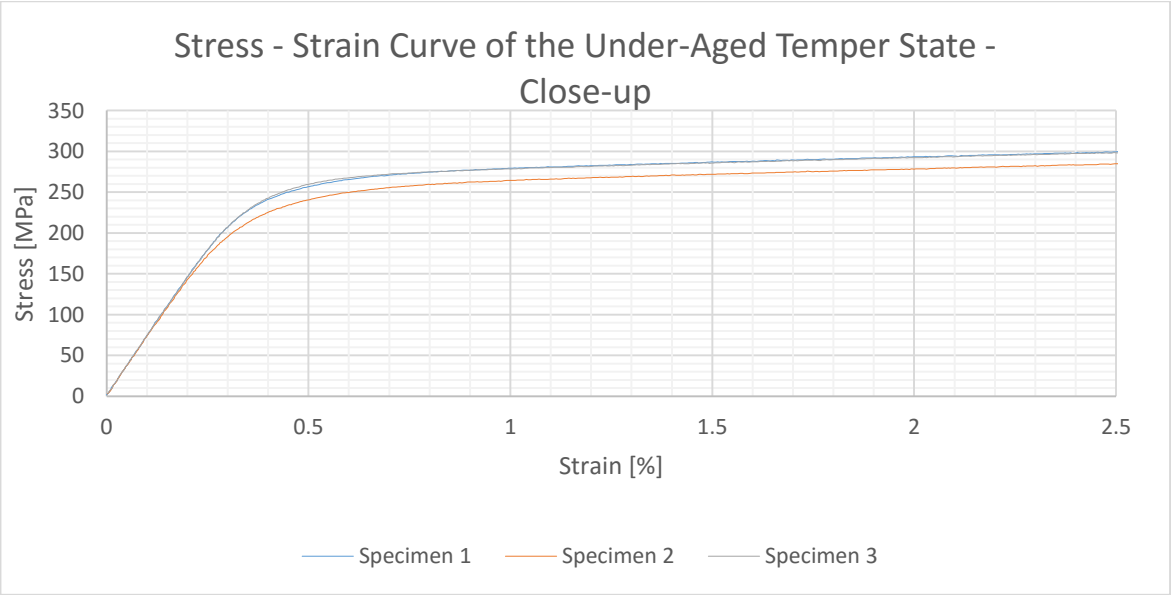

Figure 4.14: Close-up of the stress region figure 4.13, where fatigue testing was conducted. The maximum stress applied to a fatigue sample was 285 MPa in this temper state.

The result from the OA temper state is shown in figure 4.15. The yield stress was found to be 248±1 MPa, and the ultimate tensile strength was found to be 294±0 MPa. All specimens followed a similar course during tensile testing and fractured roughly in the middle of the specimen.

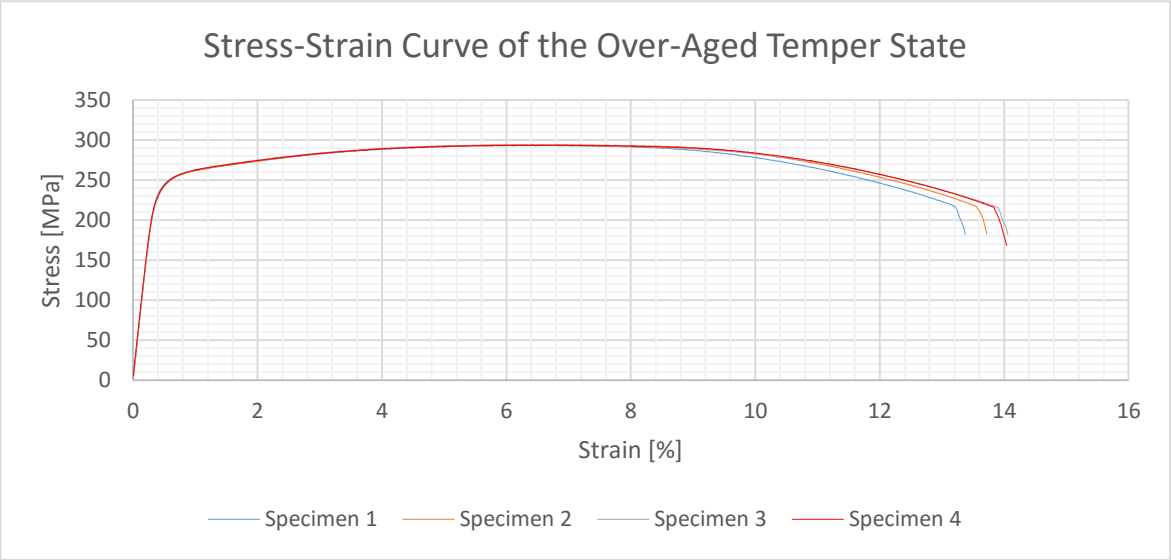

Figure 4.15: Stress-strain curve of the OA temper state.

Figure 4.16 shows a close up of the initial part of the stress-strain curve for the OA temper state. The curve is limited to the area where the fatigue testing was conducted. The maximum stress used during fatigue testing was 280 MPa, and was subsequently subject to 2,5% elongation. Note that the elongation axis is cropped at 2,5% and not 5% as the case is for the T1 temper state.

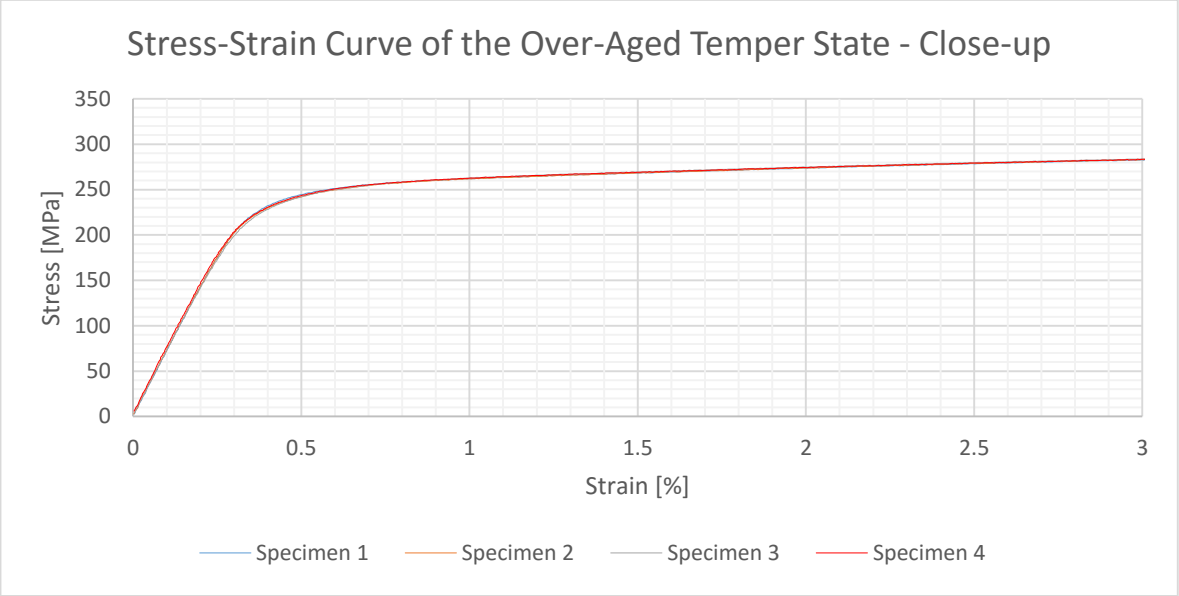

Figure 4.16: Close-up of the stress region figure 4.15, where fatigue testing was conducted. The maximum stress applied to a fatigue sample was 280 MPa in this temper state.

Table 4.8 shows some selected values from the stress-strain curves of the different temper states. The yield stress increases with increased artificial ageing, as expected, and the uniform elongation and the fracture elongation decreases with increased artificial ageing. It is apparent that the effect of work hardening decreases with increased artificial ageing.

Table 4.8: Mean values for the yield stress, ultimate tensile stress, uniform elongation, and fracture elongation for the stress-strain curves presented in figures 4.11 – 4.15. Note that that the values for the T1 temper state are from preliminary work [6].

Temper State	σ_y [MPa]	σ_{UTS} [MPa]	ε_u [%]	ε_f [%]
T1	210 ± 1	331 ± 1	15.8 ± 0.3	21.9 ± 0.4
UA	259 ± 9	331 ± 5	10.3 ± 0.3	14.0 ± 0.5
OA	248 ± 1	294 ± 0	6.3 ± 0.2	13.8 ± 0.3

4.6 Fatigue Testing

The fatigue tests done resulted in a S-N curve for each temper state. These S-N curves are shown individually in figures 4.17 -4.19, and later in figure 4.20 the trend lines from each temper state are shown together. All S-N curves are plotted as the maximum stress applied vs the number of cycles to fracture. The run out (RO) limit was set to $2 \cdot 10^6$ cycles. Any experiment exceeding this limit was aborted and marked as RO.

The hardness and electrical conductivity was also measured to see if cyclic loading effected these properties.

All tests were done in room temperature and the relative humidity was between 43% and <10%.

4.6.1 S-N Curves

The S-N curve for the T1 temper state is show in figure 4.17. The minimum stress applied to cause fracture was 236 MPa and experienced 212.735 cycles before fracture, and the maximum stress for a RO was 235 MPa.

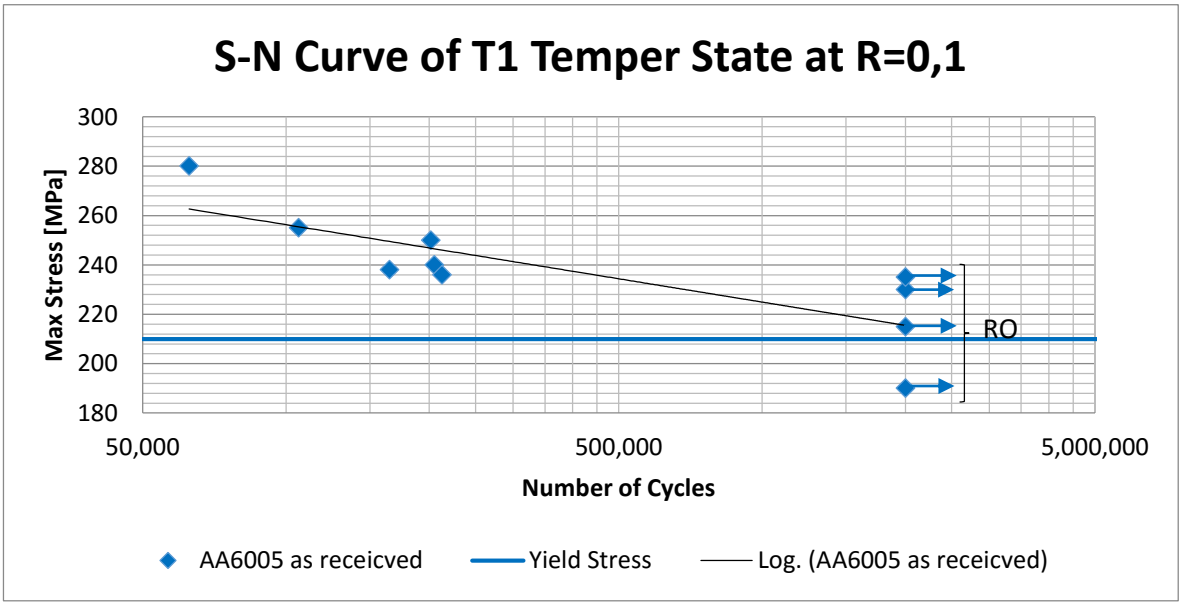

Figure 4.17: S-N curve of the T1 temper state at 20Hz and R=0,1.

The S-N curve for the UA temper state is show in figure 4.18. The minimum stress applied to cause fracture was 243 MPa and experienced 299.791 cycles before fracture, and the maximum stress for a RO was 240 MPa. During the 8th specimen, run at a maximum stress of 265 MPa, in this series the limit for the axial displacement was exceeded. The visible fracture of the specimen was then about halfway through the specimen in the TD. This was deemed to be close enough to a complete facture with regard to number of cycles that this specimen is included in the S-N curve for the UA temper state.

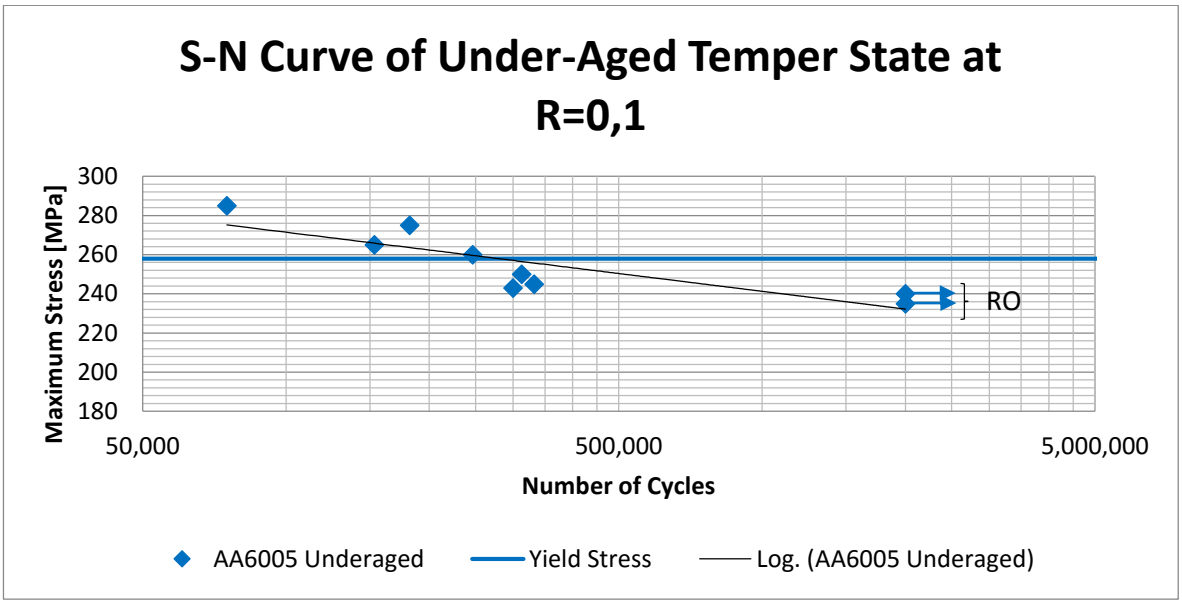

Figure 4.18: S-N curve of the UA temper state at 20Hz and R=0,1.

The S-N curve for the OA temper state is show in figure 4.19. The minimum stress applied to cause fracture was 218 MPa and experienced 663.730 cycles before fracture, and the maximum stress for a RO was 215 MPa.

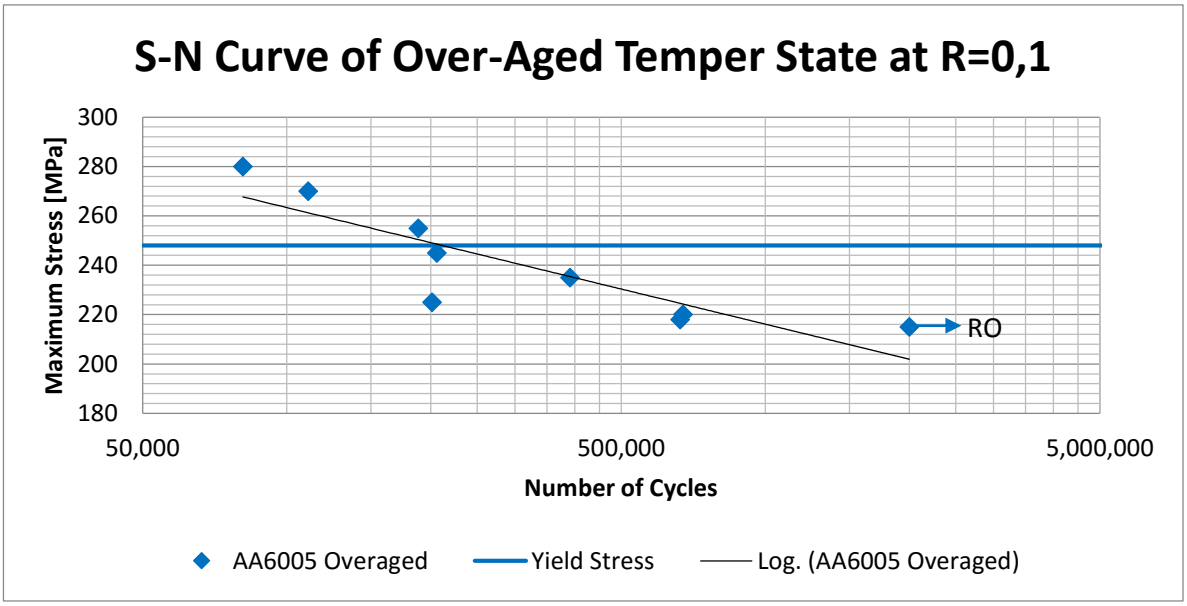

Figure 4.19: S-N curve of the OA temper state at 20Hz and R=0,1.

The trend lines from the S-N curves presented previously are shown together in figure 4.20. The trend lines are plotted from 60.000 to 2.000.000 cycles. It is apparent that the T1 and UA trend lines seem to be almost parallel, while the OA trend line has a sharper slope. One consideration to make is that the ROs are included in the trend lines. As the number of ROs are different for all temper states, decreasing with increased amount of artificial ageing, the trend lines could be considered to be slightly skewed towards sharper slopes. If the ROs were not included the trend lines would have even sharper slopes than presented in figure 4.20, and the OA temper state would most likely have the shallowest slope as it has a data point at 663.730 cycles, while the T1 and UA temper states have their last data point at about 210.000 and 300.000 cycles, respectfully.

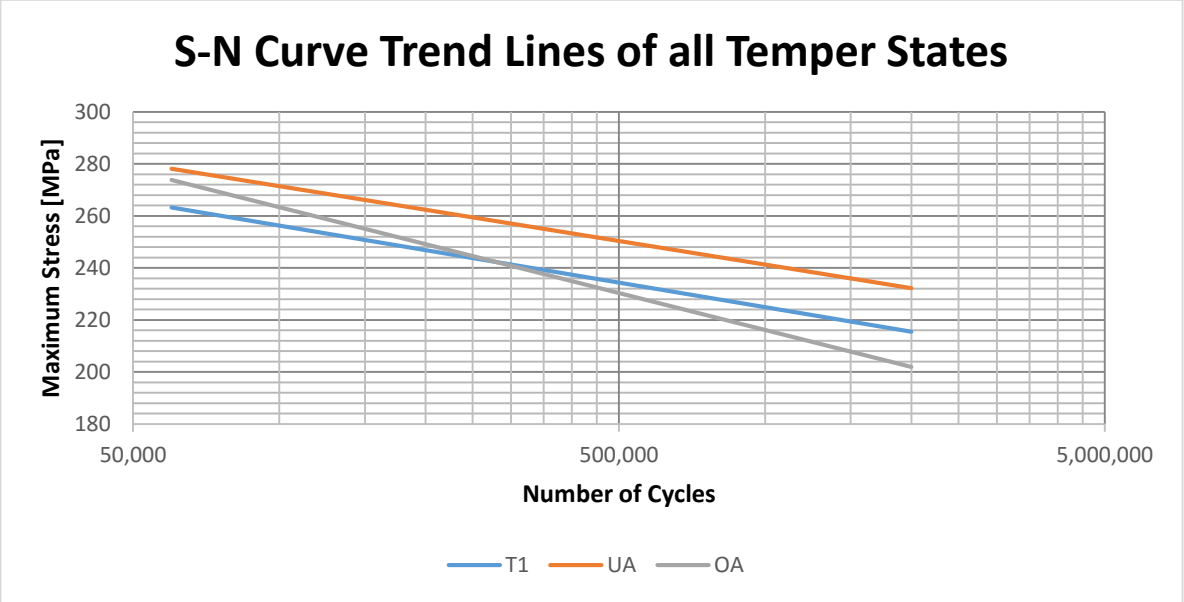

Figure 4.20: Trend lines from the S-N curves of each temper state.

4.6.2 Hardness after Fatigue testing

All plots are shown with the same intervals on the axis to ease comparison. The yield stress of the temper state is shown in with a red line and the mean hardness is shown with a blue line in all figures.

The hardness after cyclic loading of the T1 temper state is shown in figure 4.21. It is apparent that cyclic hardening has occurred for this temper state, and is increasing with higher applied stress. As most of the specimens are loaded at a higher stress than the yield stress this is probably caused by work hardening. Also of note is that at lower applied stress, i.e. experienced more cycles, the cyclic hardening impact is less.

The trend line follow the equation y=0,1073x+65,034.

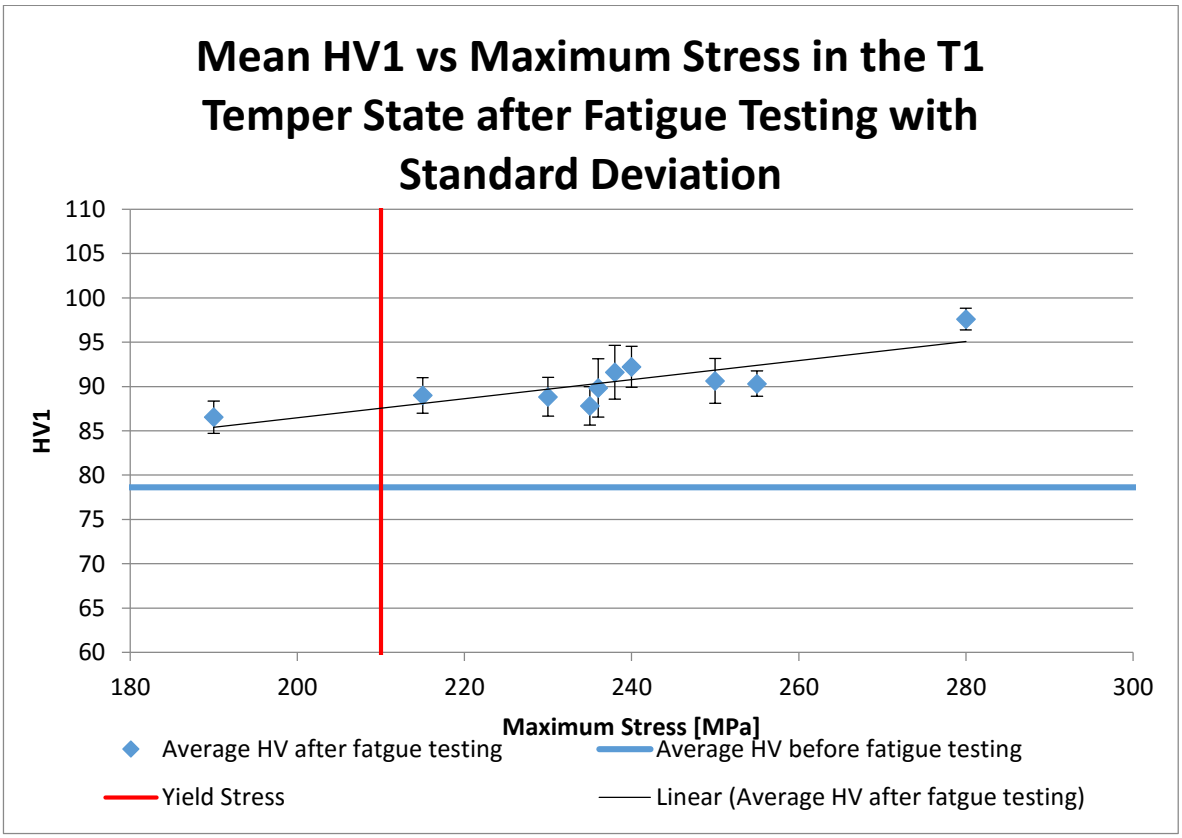

Figure 4.21: Hardness measurements of the T1 temper state after fatigue testing with standard deviation compared to the hardness prior to testing. The yield stress is also shown to identify which specimens have been exposed to plastic deformation.

The hardness after cyclic loading of the UA temper state is shown in figure 4.22. A large amount of the hardness values in this temper state is below the mean hardness value before cyclic loading indicating cyclic softening has occurred. Note that the measurements fall into two groups divided by the yield stress. Below the yield stress the values are erratic, varying from slightly above the mean hardness before cyclic loading to values well below this initial value. Above the yield stress however, the hardness values are fairly similar, with a slight trend towards the mean hardness prior to cyclic loading with increasing applied stress, i.e. fewer cycles.

The trend line follow the equation y=0,1065x+60,7.

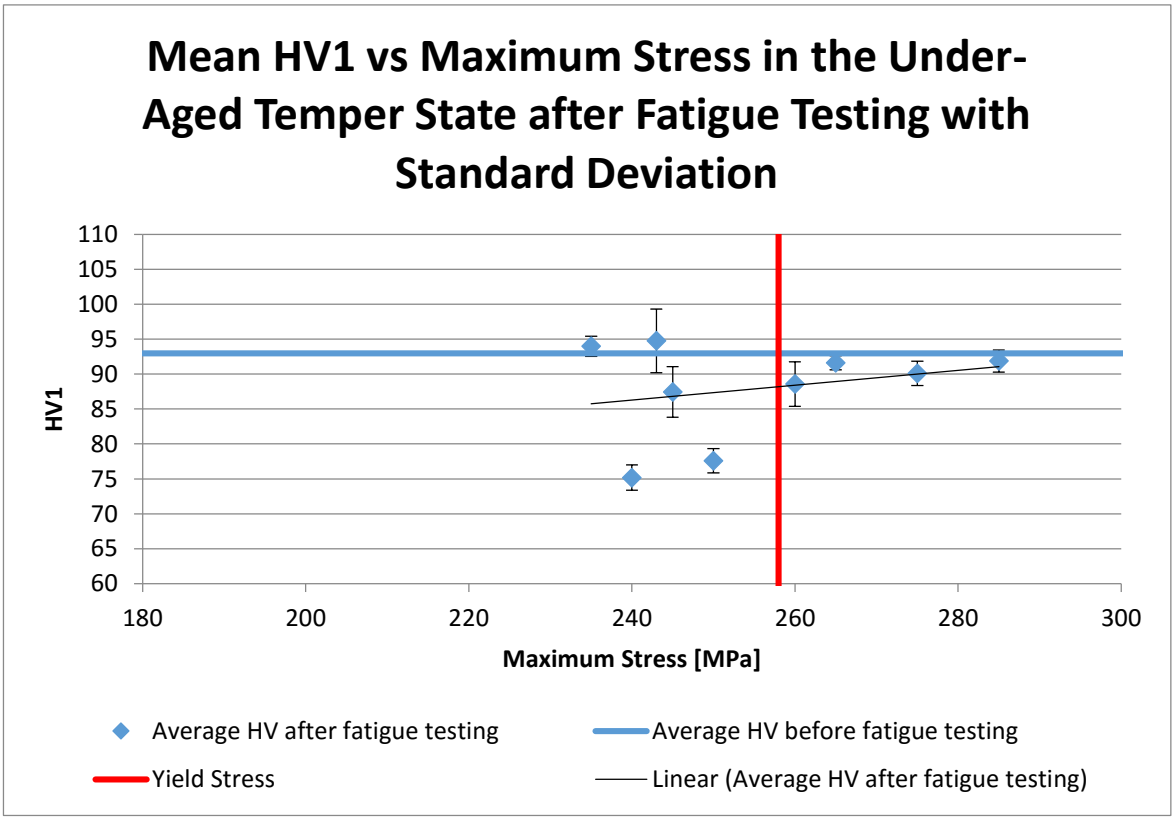

Figure 4.22: Hardness measurements of the UA temper state after fatigue testing with standard deviation compared to the hardness prior to testing. The yield stress is also shown to identify which specimens have been exposed to plastic deformation.

The hardness after cyclic loading of the OA temper state is shown in figure 4.23 It is apparent that cyclic softening has occurred for this temper state, and is fairly constant regardless of the applied stress.

The trend line follow the equation y=-0,0023x+89,951.

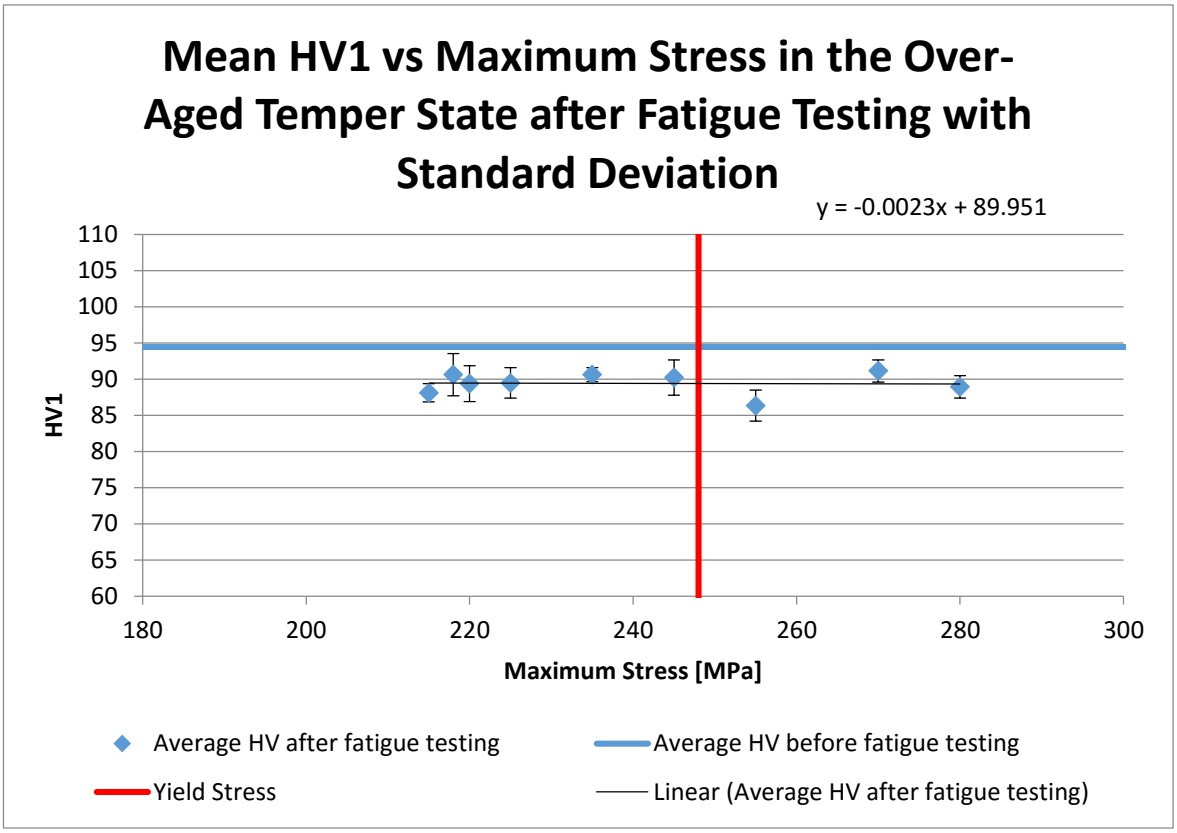

Figure 4.23: Hardness measurements of the OA temper state after fatigue testing with standard deviation compared to the hardness prior to testing. The yield stress is also shown to identify which specimens have been exposed to plastic deformation.

4.6.3 Electrical Conductivity after Fatigue Testing

All plots are shown with the same interval on the axis to ease comparison.

In figure 4.24 the electrical conductivity measurements after cyclic loading for the T1 temper state is presented and compared to the electrical conductivity prior to cyclic loading. As can be seen in figure 4.24 no significant change has occurred. Although the change is slight a small decrease in electrical conductivity can be seen especially around 240 MPa and 280 MPa.

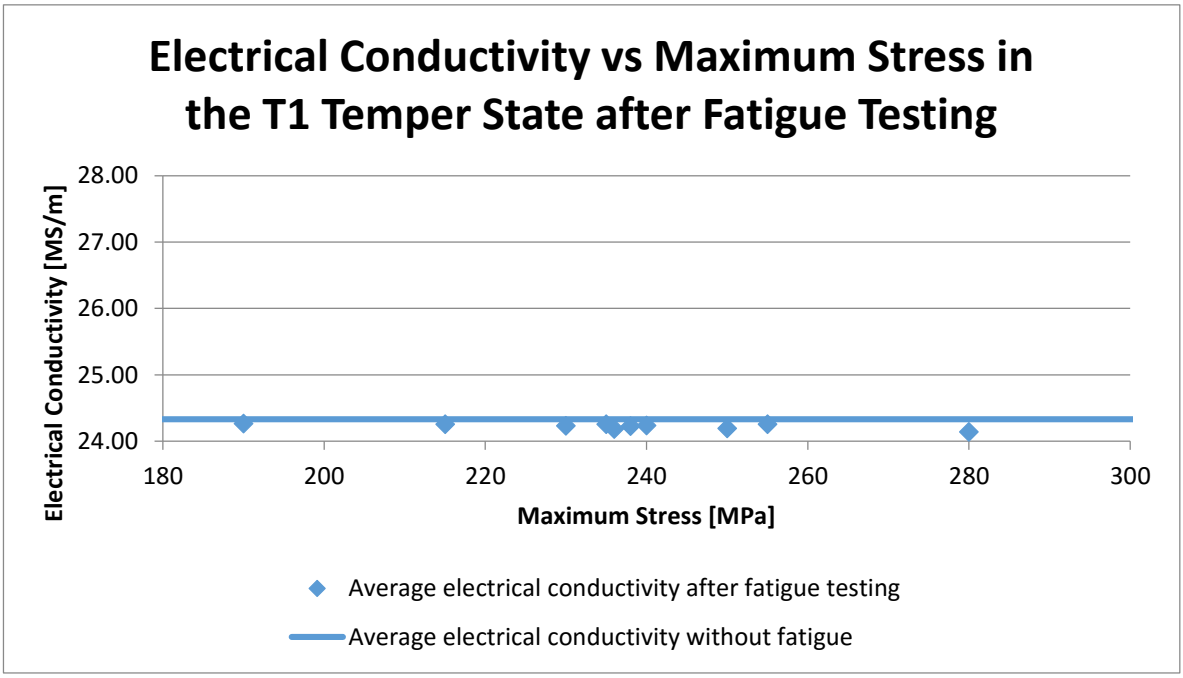

Figure 4.24: Electrical conductivity measurements of the T1 temper state done after fatigue testing compared to the electrical conductivity prior to fatigue testing.

In figure 4.25 the electrical conductivity measurements after cyclic loading for the UA temper state is presented and compared to the electrical conductivity prior to cyclic loading. As can be seen in figure 4.25 no significant change has occurred, and the measured values are centred around the value prior to cyclic loading.

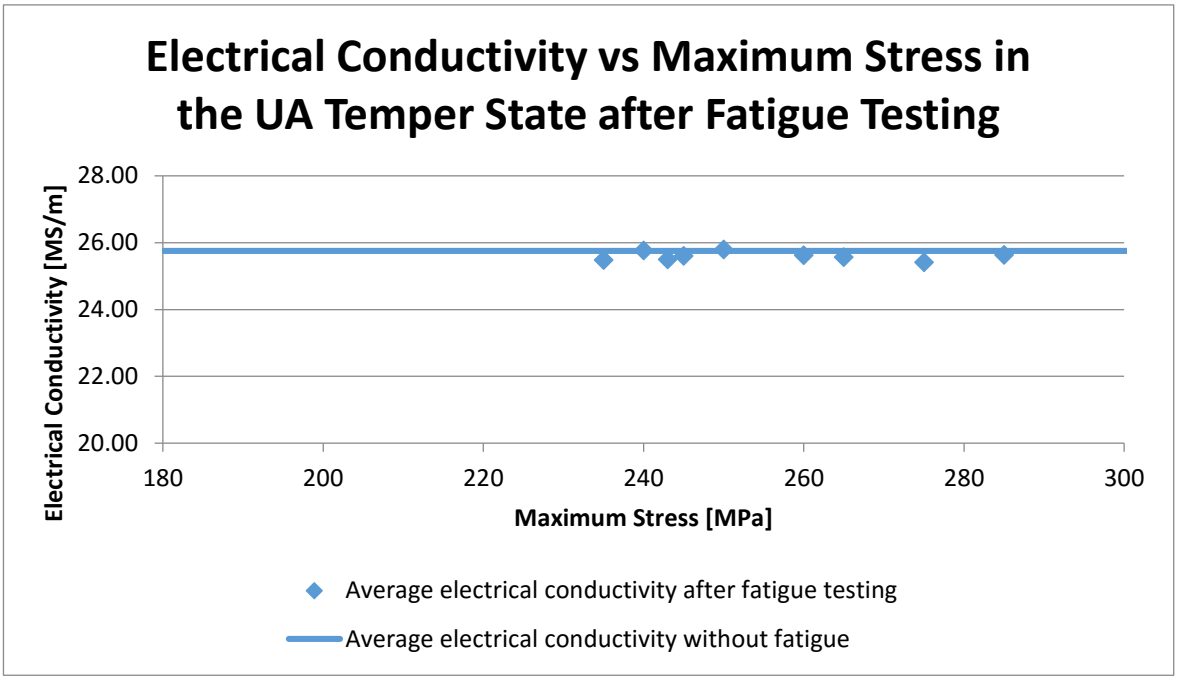

Figure 4.25: Electrical conductivity measurements of the UA temper state done after fatigue testing compared to the electrical conductivity prior to fatigue testing.

In figure 4.26 the electrical conductivity measurements after cyclic loading for the OA temper state is presented and compared to the electrical conductivity prior to cyclic loading. As can be seen in figure 4.26 no significant change has occurred, and the measured values are centred around the value prior to cyclic loading.

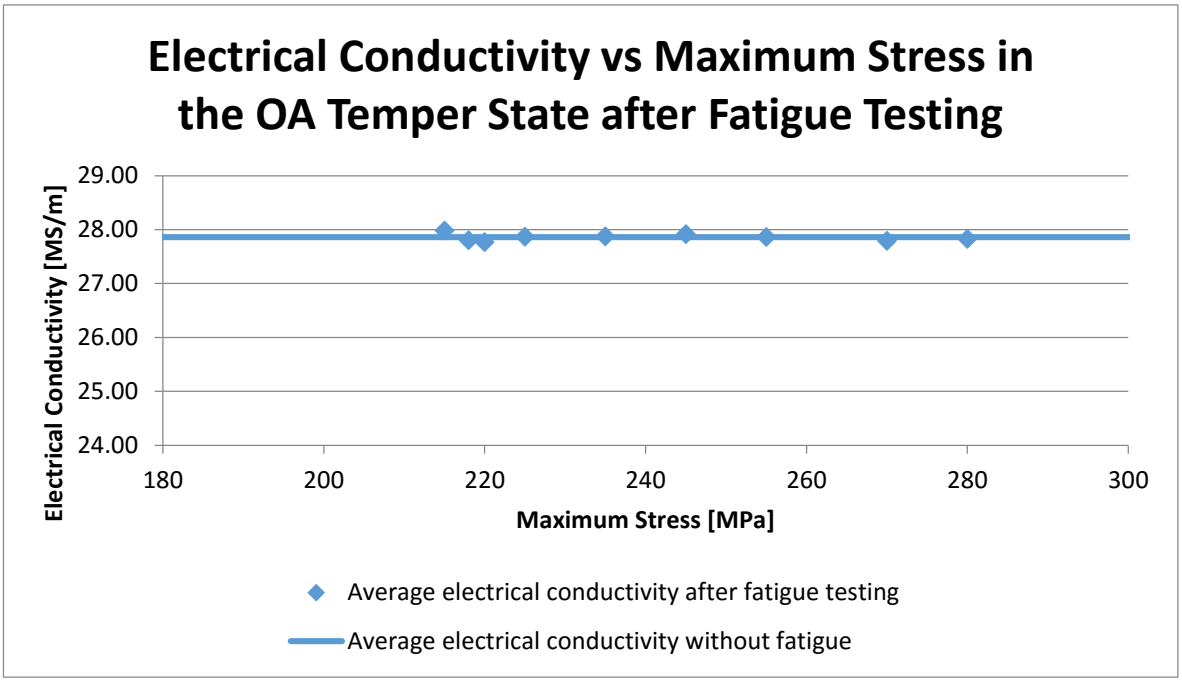

Figure 4.26: Electrical conductivity measurements of the OA temper state done after fatigue testing compared to the electrical conductivity prior to fatigue testing.

4.7 Fractography

A selection of fatigue specimens were chosen to be further investigated. In this sub-chapter the specimen with the longest fatigue life before RO have been presented, as the purpose is to underline the fatigue properties of each temper state, and attempt to identify differences between the different temper states.

All fatigue specimens examined had a fracture surface ~45° to the direction of the applied stress, especially the stage III crack growth areas. The fractographs are taken in the direction of the applied stress and fatigue crack growth traits such as striation length, cannot easily be measured. It was deemed too difficult to identify probable crack initiation sites, stage I, and therefore only stage II and III are investigated. It was evident that crack initiation occurred several places simultaneously as all examined specimens have an area perpendicular to the applied stress direction with stage II areas, at a ~45° to the direction of the applied stress, on several sides. These areas varied from some 100 µm in length to about 1 mm in length, and are therefore probably not areas of stage I crack growth.

4.7.1 Overview of Examined Specimens

An overview the fracture surfaces presented are shown in this sub-chapter. First the T1 temper state is presented, followed by the under-aged specimen, and lastly the over-aged specimen. This will be the order all fractographs are presented. The stage II area is shown enclosed by a red line, and the area of the specimen where other fractographs are taken from are marked with name and an arrow. The stage III fractographs are taken from the opposite side of the stage II area.

In figure 4.27 the fracture surface of the specimen from the T1 temper state can be seen. The area shown as normal to the applied stress if horizontal, while the rest of the specimen is at a ~45° to the applied stress. This specimen was run at a maximum stress of 236 MPa, and its fatigue life was 212.725 cycles.

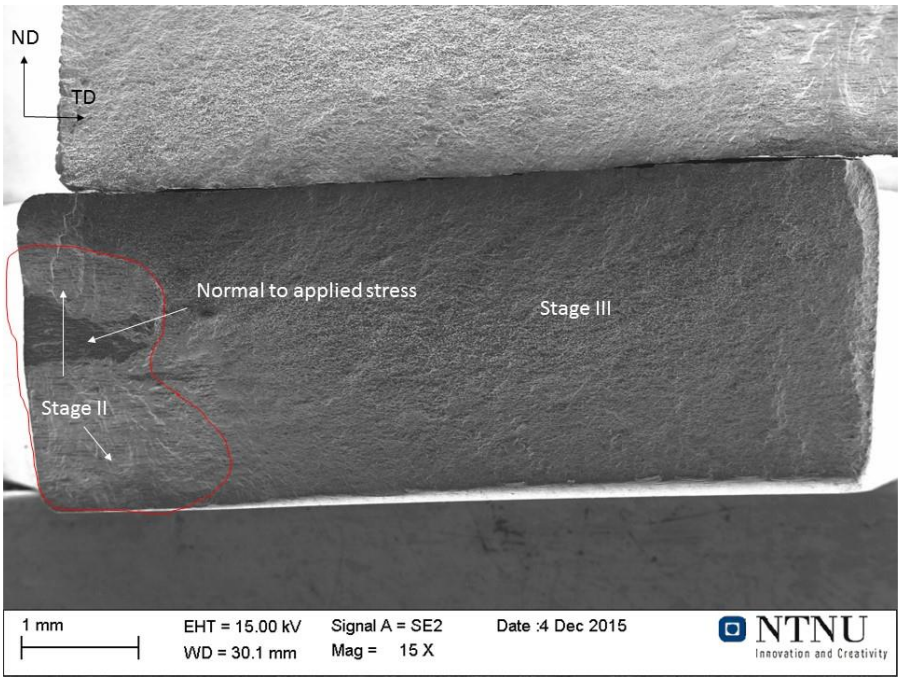

Figure 4.27: An overview of the fracture surface in the T1 temper state. The maximum applied stress was 236 MPa and the fatigue life was 212.725 cycles.

In figure 4.28 the fracture surface of the specimen from the UA temper state can be seen. The area shown as normal to the applied stress if horizontal, while the rest of the specimen is at a ~45° to the applied stress. The areas indicated by the stage II arrows are of a cup-and-cone nature. This specimen was run at a maximum stress of 243 MPa, and its fatigue life was 299.791 cycles. Due to technical issues during microscopy the parameters were not included when capturing the image.

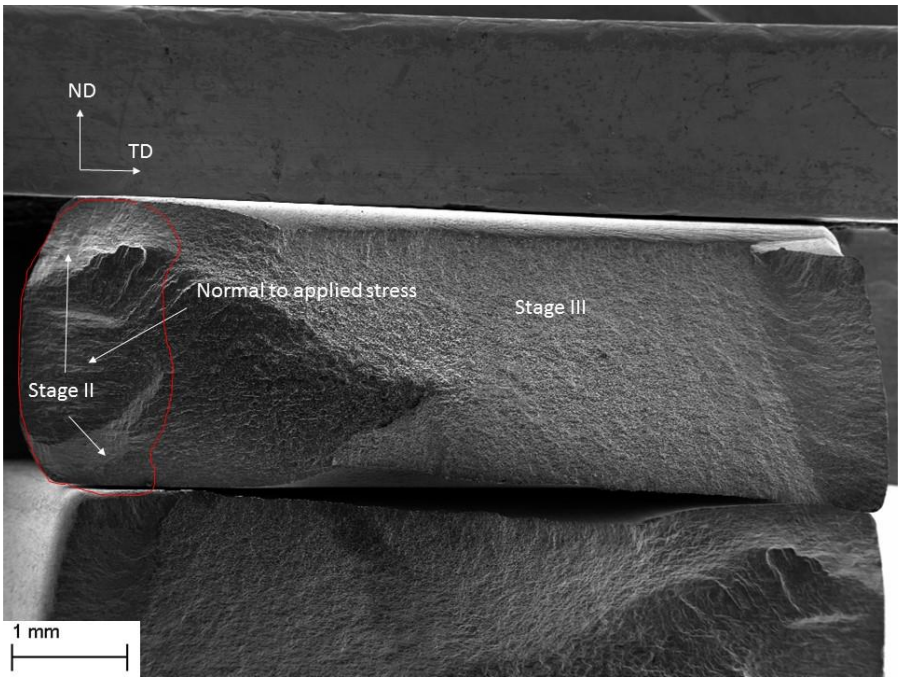

Figure 4.28: An overview of the fracture surface in the UA temper state. The maximum applied stress was 243 MPa and the fatigue life was 299.791 cycles.

In figure 4.29 the fracture surface of the specimen from the UA temper state can be seen. The area shown as normal to the applied stress if horizontal, while the rest of the specimen is at a ~45° to the applied stress. The areas indicated by the stage II arrows are of a cup-and-cone nature. This specimen was run at a maximum stress of 218 MPa, and its fatigue life was 663.730 cycles.

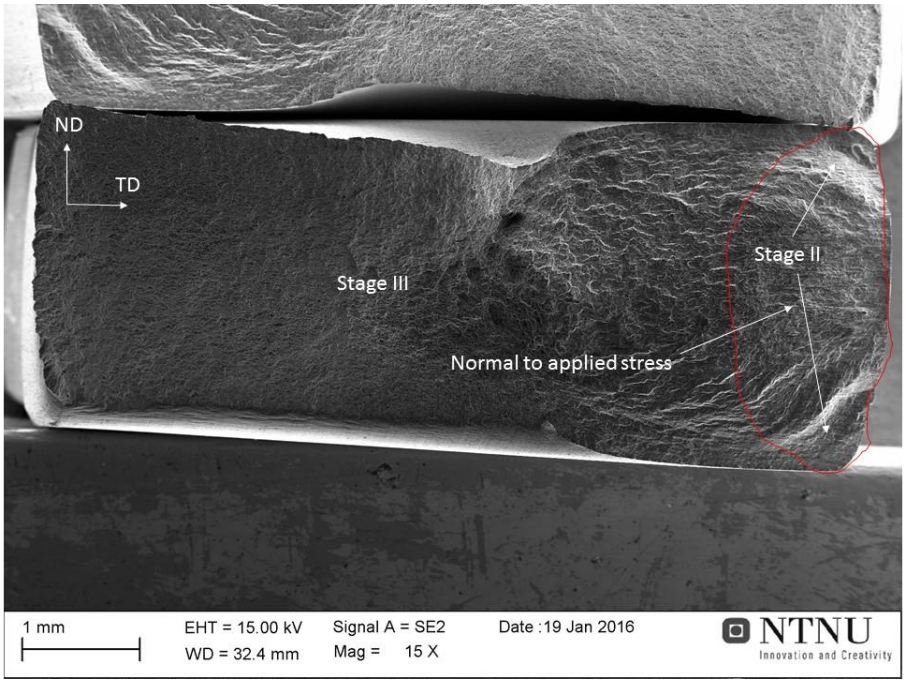

Figure 4.29: An overview of the fracture surface in the OA temper state. The maximum applied stress was 218 MPa and the fatigue life was 663.730 cycles.

4.7.2. Stage II Crack Growth

The stage II crack growth area are presented with the T1 temper state first, then the UA temper state, and lastly the OA temper state is presented. In each temper state three areas are shown: first the areas that are ~45° to the applied stress direction, i.e. the area marked as stage II on the overview image, then the horizontal area normal to the applied stress direction is presented. Compared to the overview image the top area is presented first, then the bottom area. The three areas are presented with two images: one with a low magnification, and one with higher magnification. The image with higher magnification is taken from the area enclosed by a red rectangle in the image with lower magnification.

The T1 Temper State

In figures 4.30 to 4.32 the areas marked in the overview image in figure 4.27 is shown. From the beach marked is can be seen that the crack growth direction was in the traverse direction.

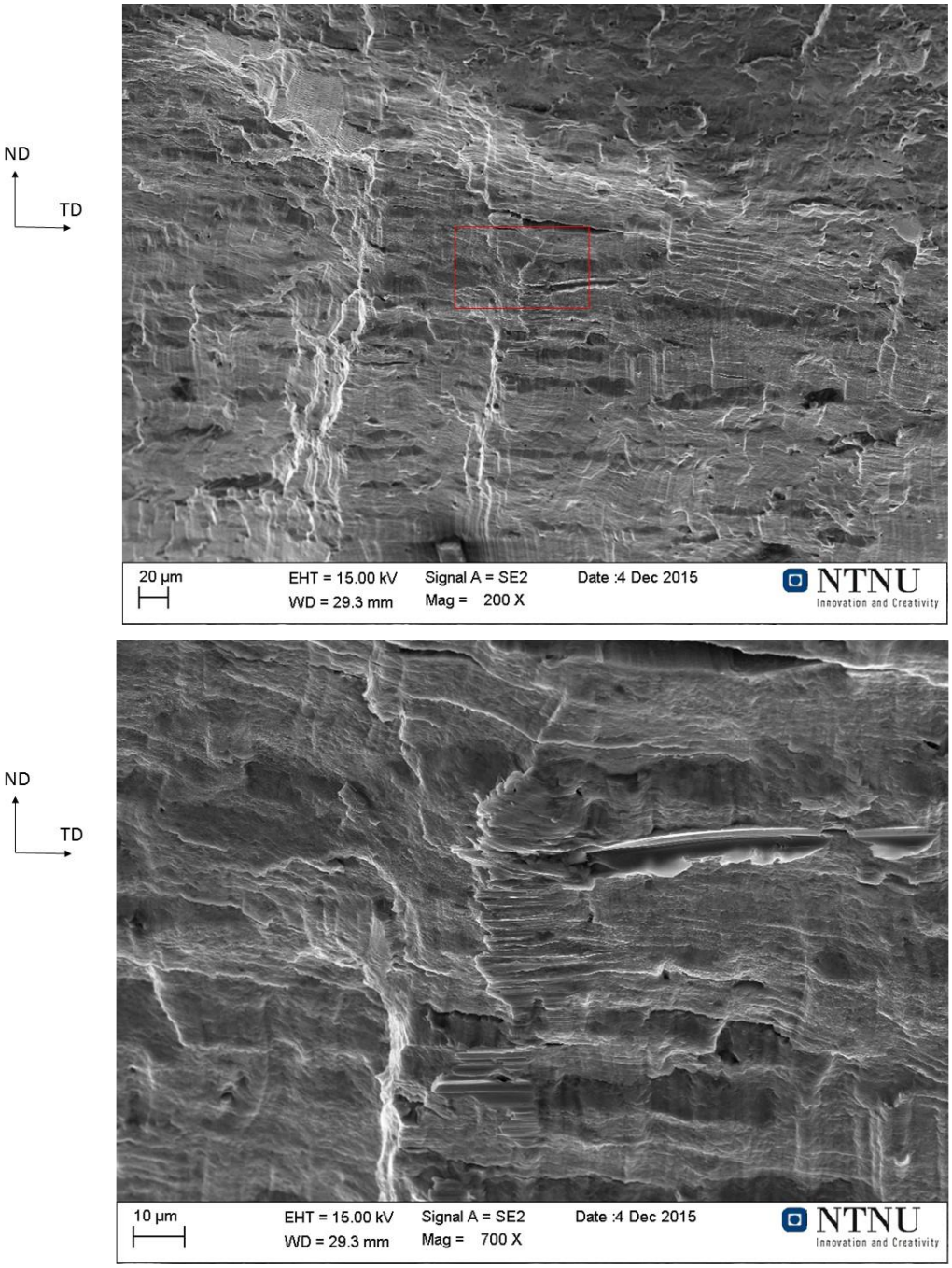

Figure 4.30: Stage II crack growth of the T1 temper state located on the top of the specimen. Bottom image is located in the red rectangle in the top image.

From the beach marked is can be seen that the crack growth direction was in the traverse direction. Note also the corrosion on the sample.

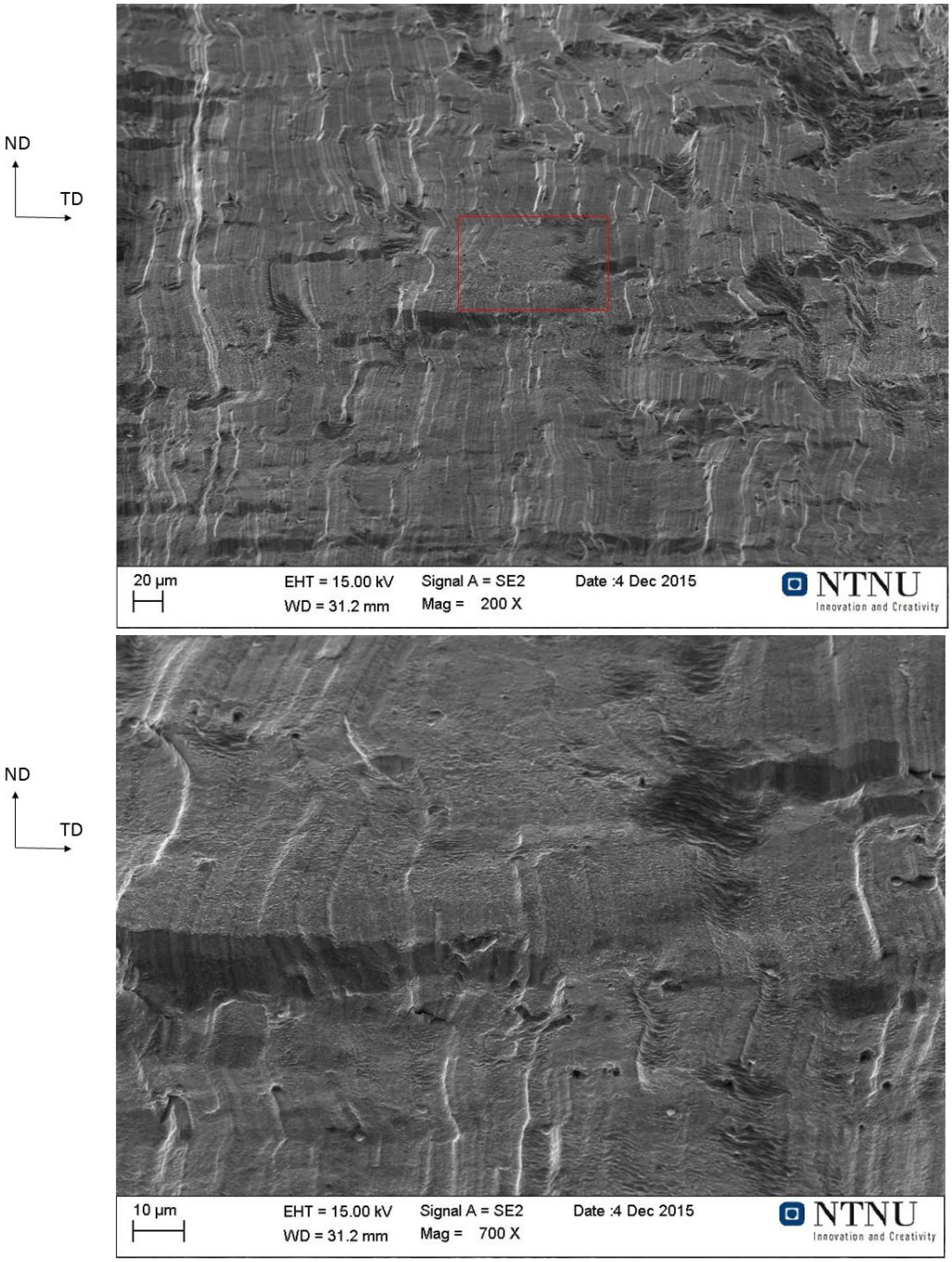

Figure 4.31: Stage II crack growth of the T1 temper state located on the bottom of the specimen. Bottom image is located in the red rectangle in the top image.

The area normal to the applied stress direction is dominated by the presents of secondary cracks, and the directions of the beach marks are erratic.

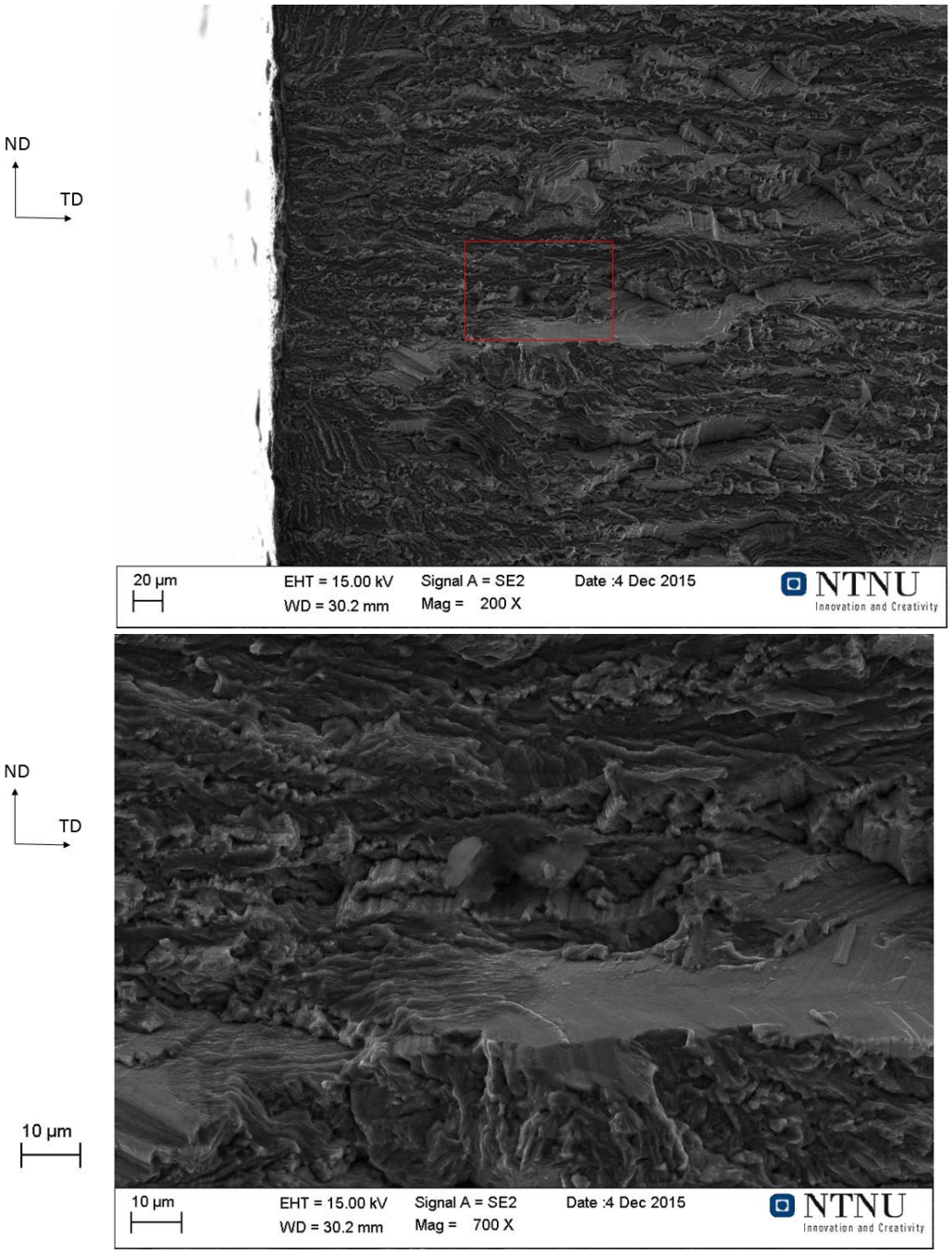

Figure 4.32: Stage II crack growth of the T1 temper state normal to the applied stress direction. Bottom image is located in the red rectangle in the top image.

The UA Temper State

In figures 4.33 to 4.35 the areas marked in the overview image in figure 4.28 is shown. From the beach marked is can be seen that the crack growth direction was in the traverse direction.

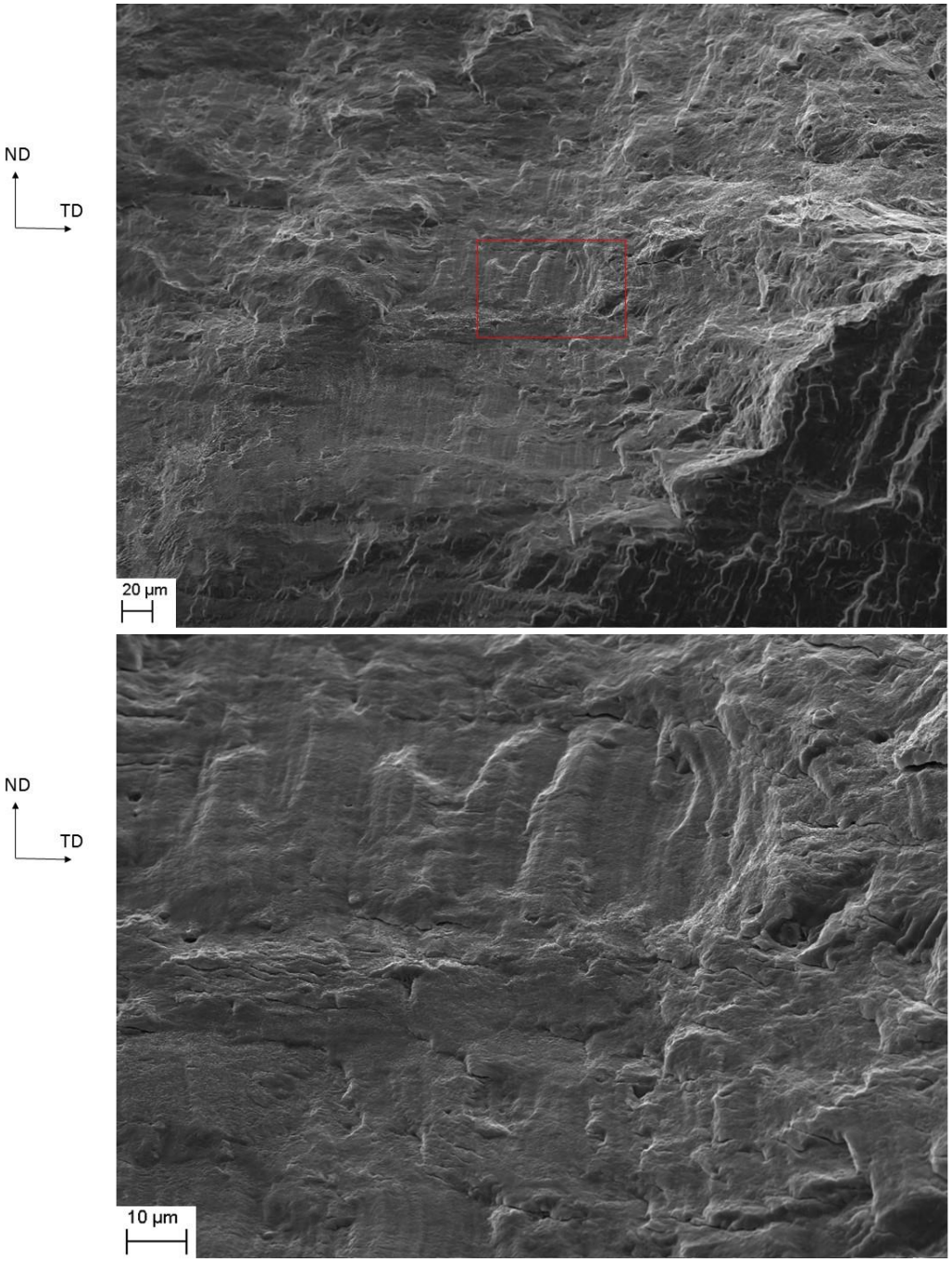

Figure 4.32: Stage II crack growth of the UA temper state located on the top of the specimen. . Bottom image is located in the red rectangle in the top image.

From the beach marked is can be seen that the crack growth direction was in the traverse direction. Figure 4.34 show evidence that crack closure has occurs.

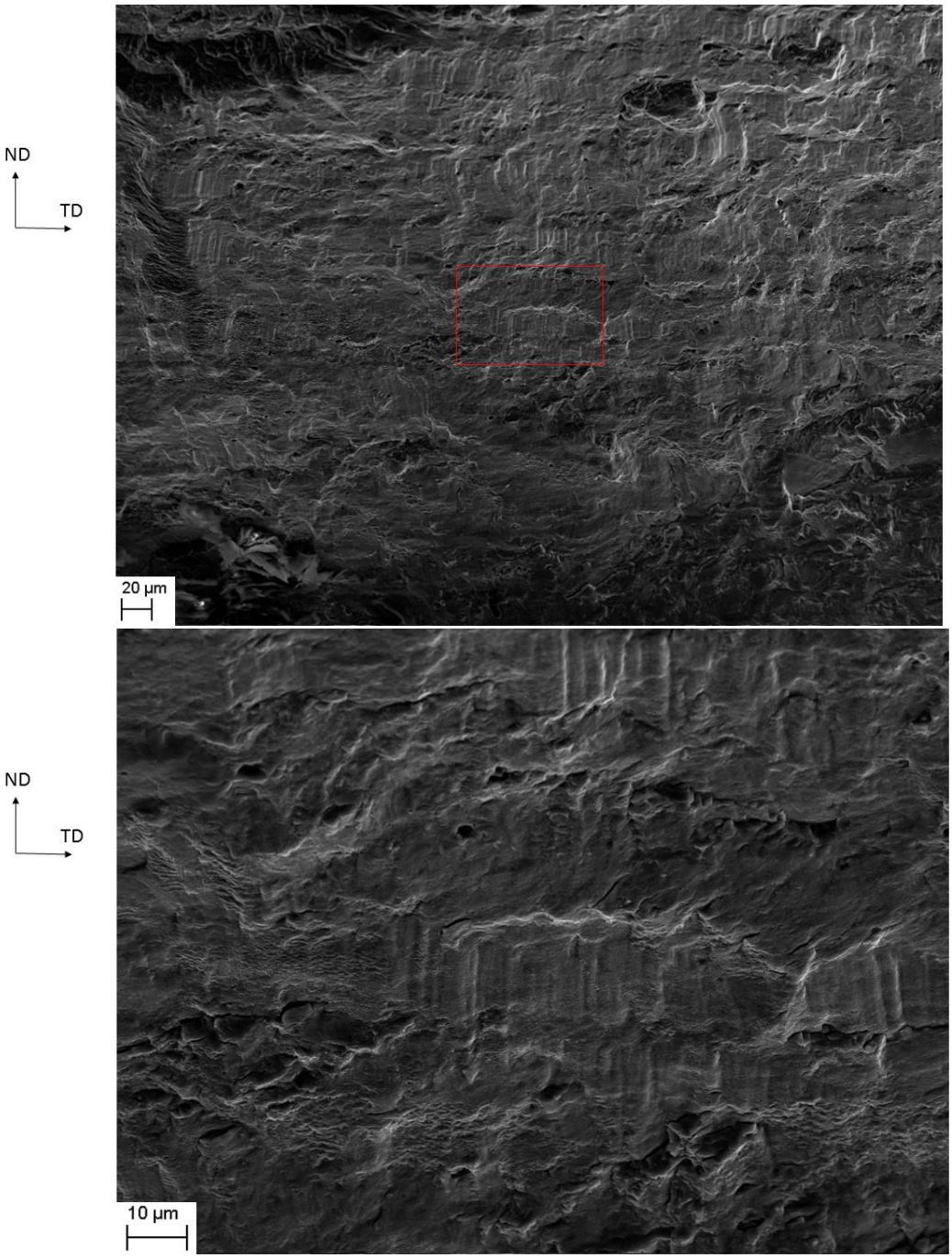

Figure 4.34: Stage II crack growth of the UA temper state located on the bottom of the specimen. Bottom image is located in the red rectangle in the top image.

The area normal to the applied stress direction is dominated by the presents of secondary cracks, and the directions of the beach marks are erratic.

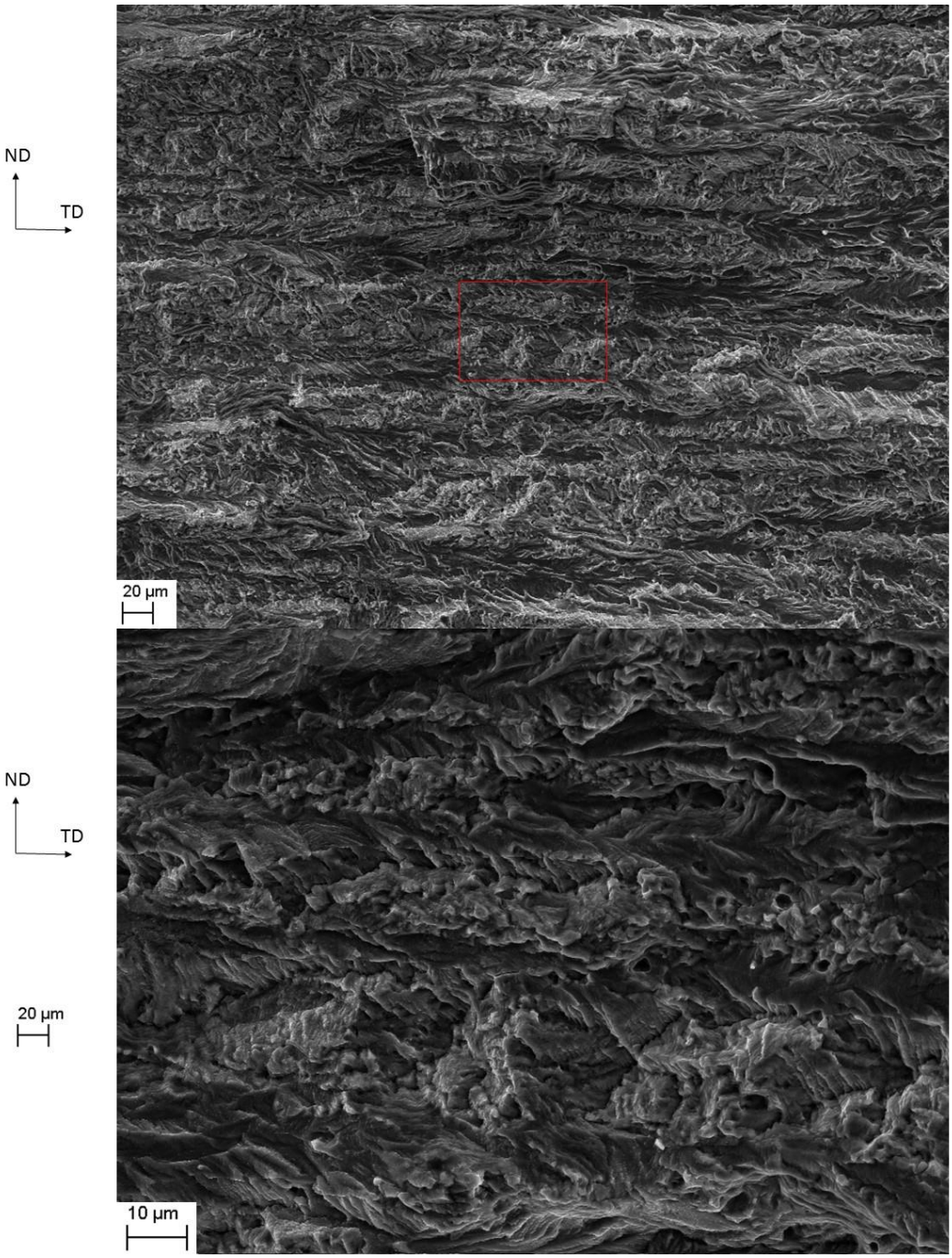

Figure 4.35: Stage II crack growth of the UA temper state normal to the applied stress direction. Bottom image is located in the red rectangle in the top image.

The OA Temper State

In figures 4.36 to 4.38 the areas marked in the overview image in figure 4.29 is shown. From the beach marked is can be seen that the crack growth direction was in the traverse direction.

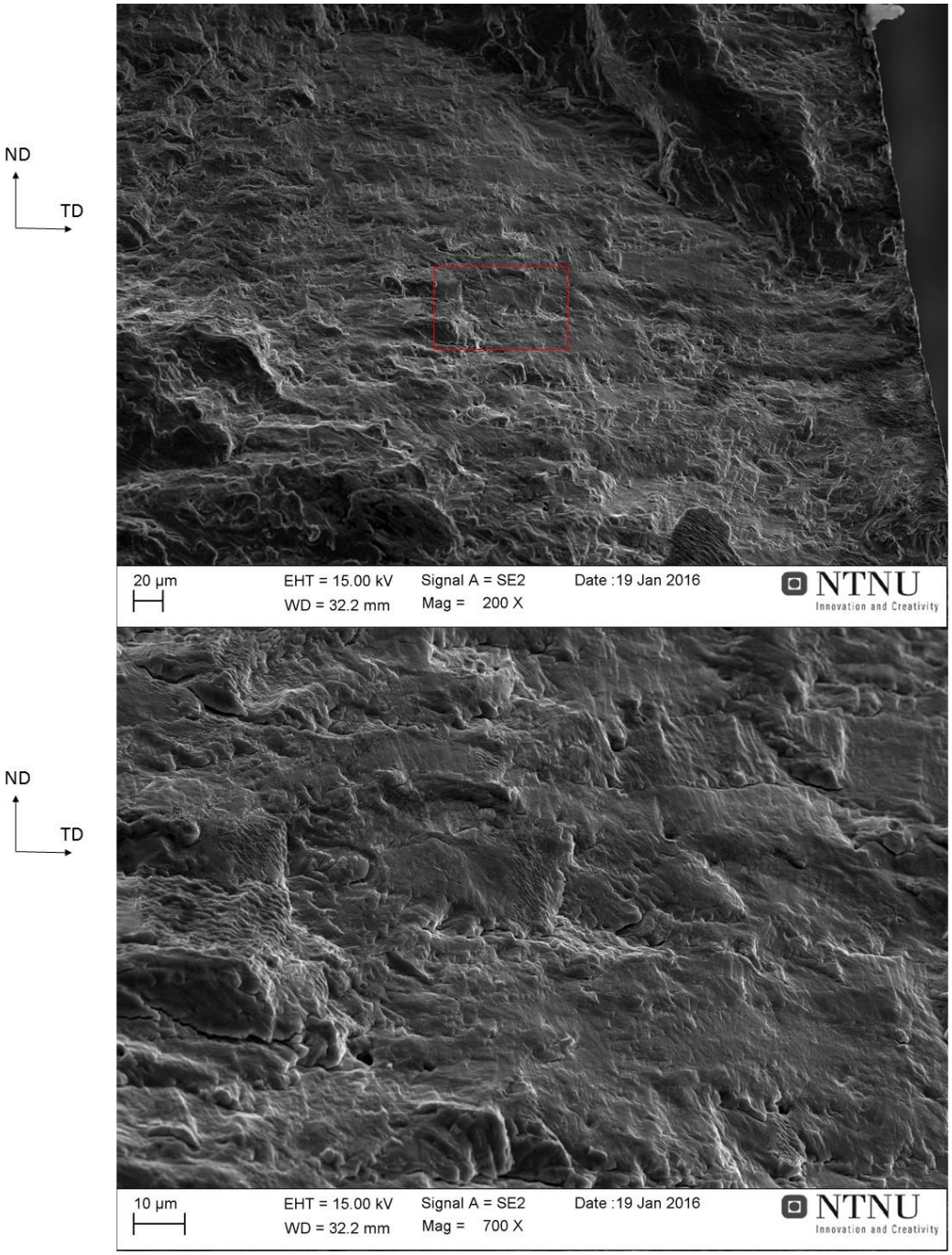

Figure 4.36: Stage II crack growth of the OA temper state located on the top of the specimen. . Bottom image is located in the red rectangle in the top image.

From the beach marked is can be seen that the crack growth direction was in the traverse direction.

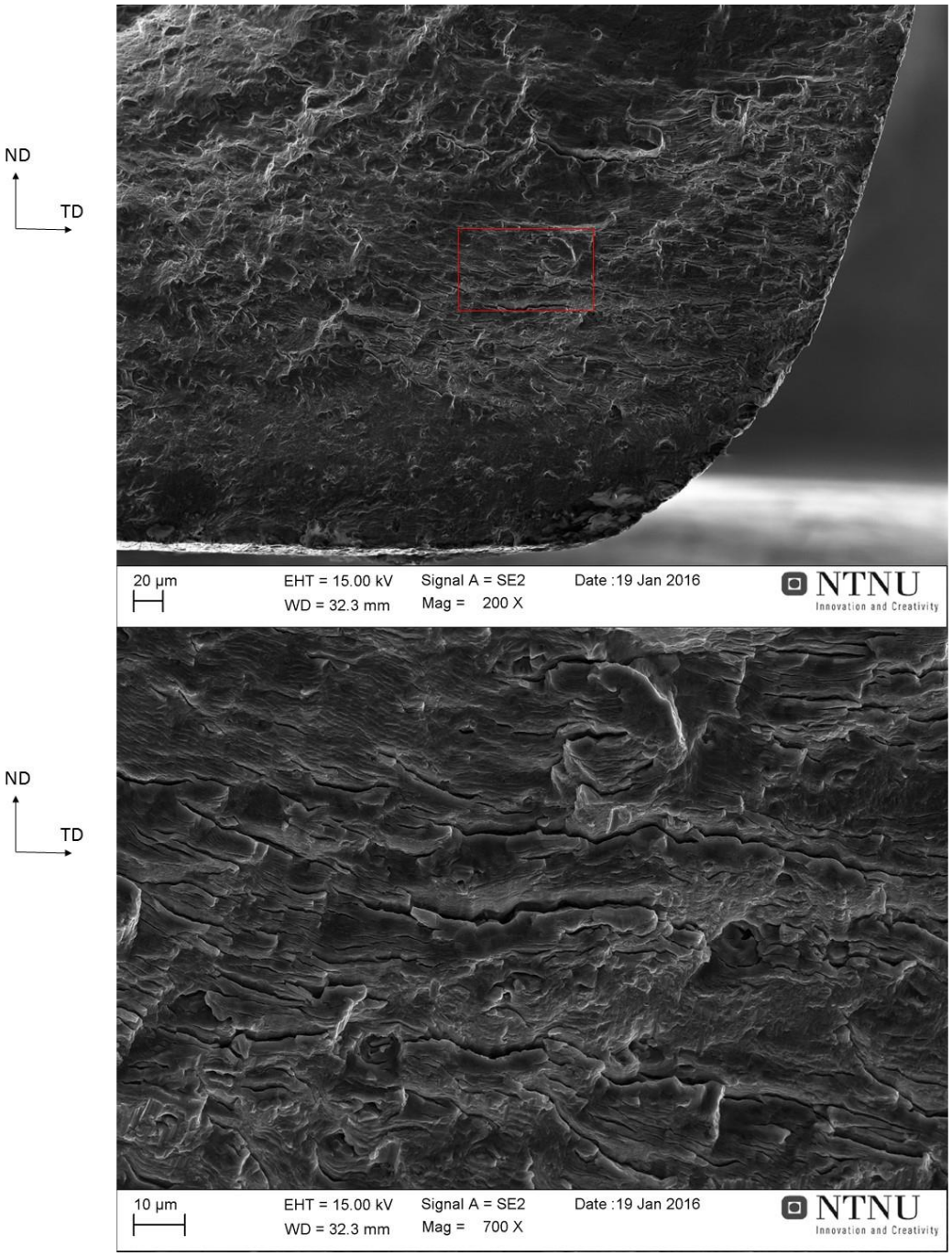

Figure 4.37: Stage II crack growth of the OA temper state located on the bottom of the specimen. Bottom image is located in the red rectangle in the top image.

The area normal to the applied stress direction is dominated by the presents of secondary cracks, and the directions of the beach marks are erratic.

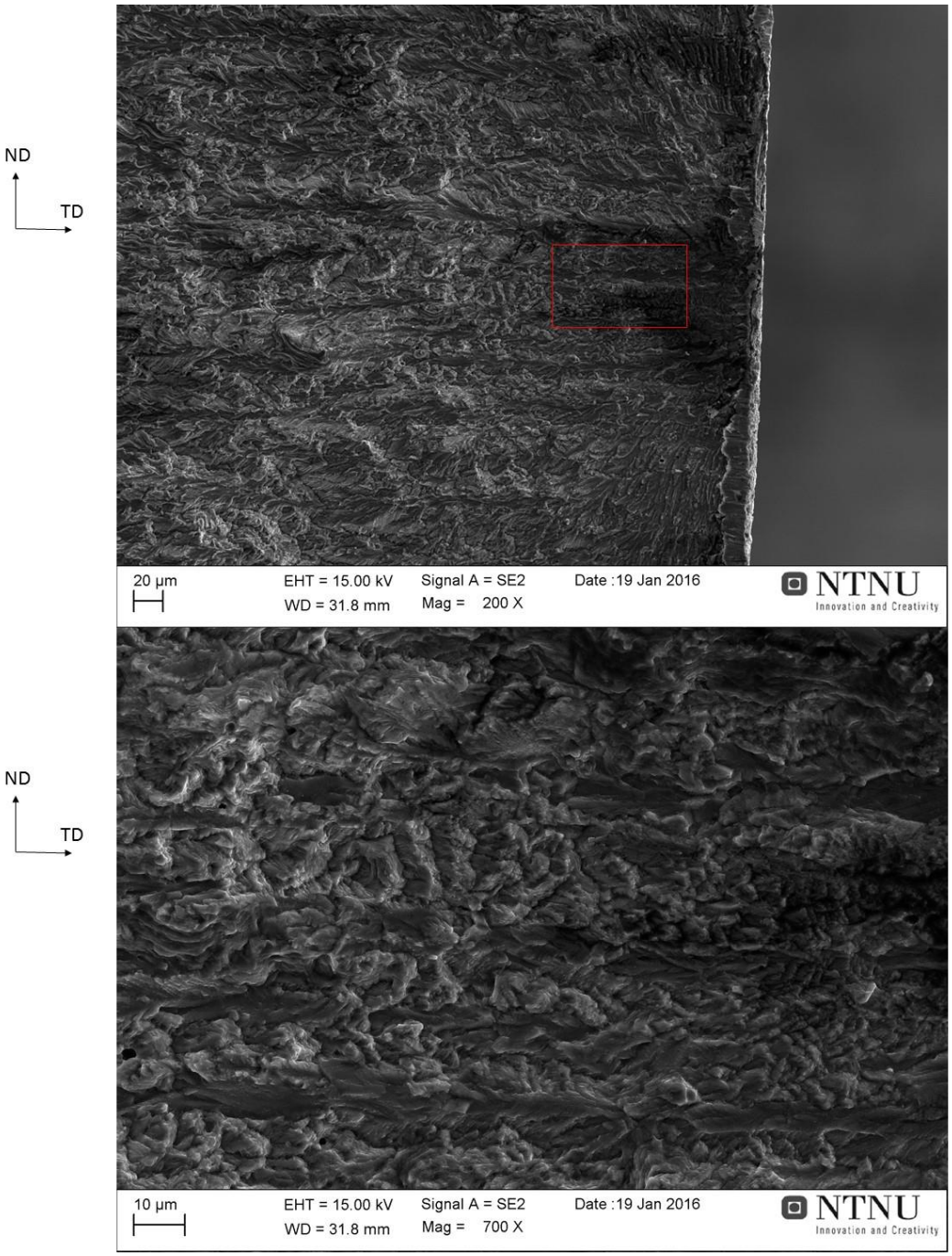

Figure 4.38: Stage II crack growth of the OA temper state normal to the applied stress direction. Bottom image is located in the red rectangle in the top image.

4.7.3. Stage III Crack Growth

The images of the stage III crack growth area are taken from the opposite side of the specimen compared to the stage II crack growth area. Only one image from each temper state is taken. The stage III area is ~45° to the direction of the applied stress. The temper states are presented in the following order: T1, UA, and OA.

Figure 4.39-4.41 shows the stage III crack growth area of the different temper states. The images are dominated by dimples and some small areas of local shear. Shear is more prominent in the UA and OA temper states.

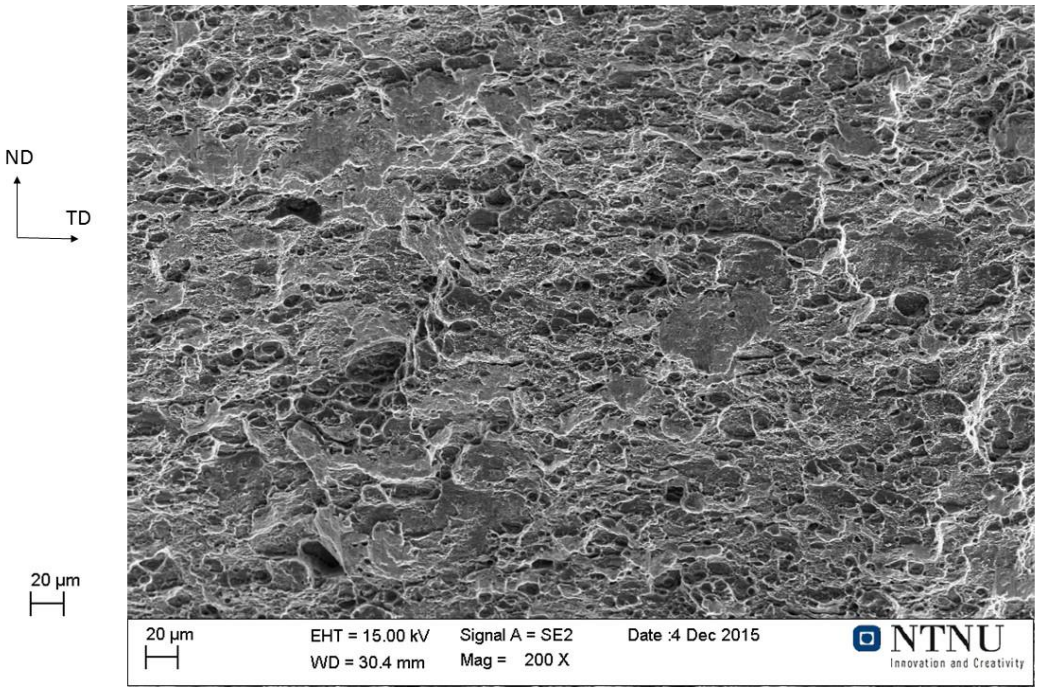

Figure 4.39: Stage III crack growth area of the T1 temper state.

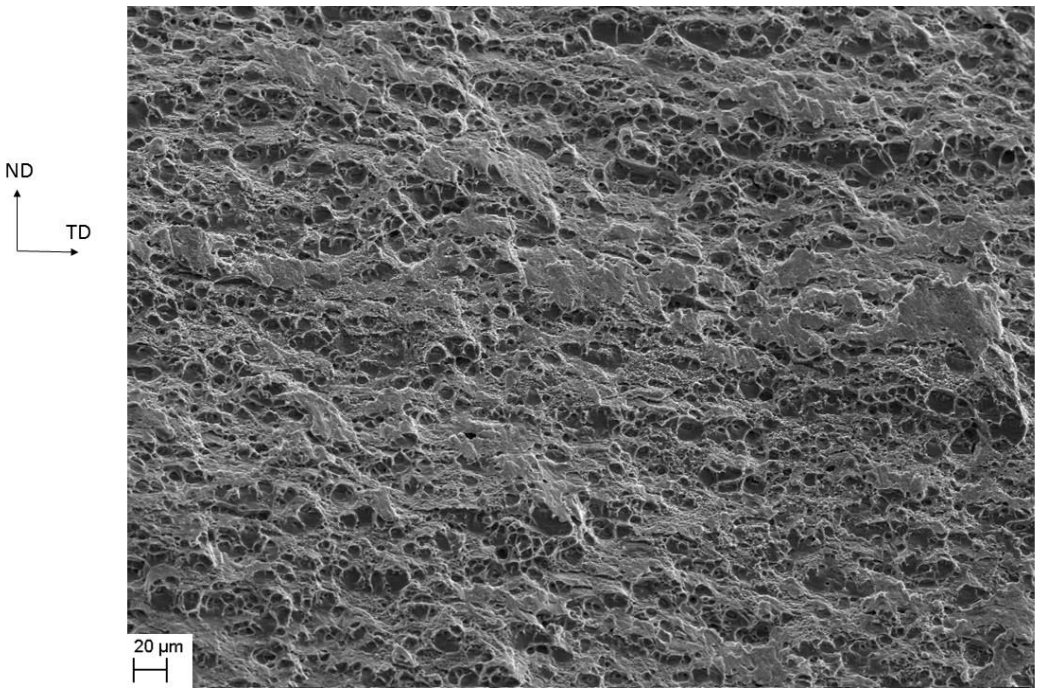

Figure 4.40: Stage III crack growth area of the UA temper state.

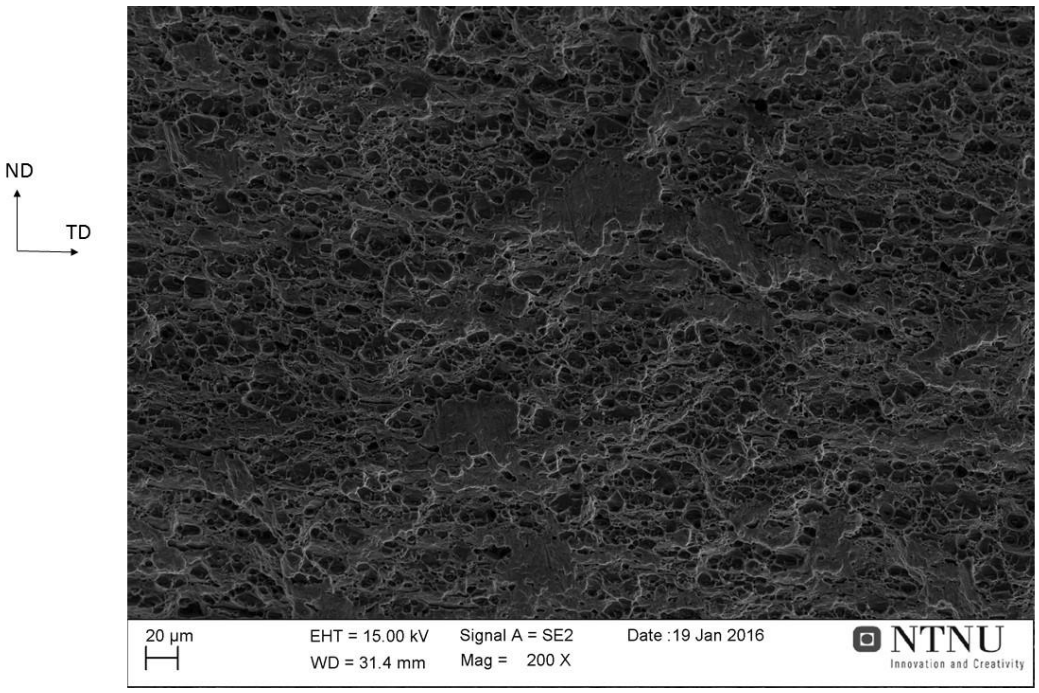

Figure 4.41: Stage III crack growth area of the OA temper state.

5 Discussion

5.1 The Effect of Artificial and Natural Ageing on AA6005

Observed Microstructural and Material Property Changes

Primary Particles

The primary particle analyses showed a decrease in particle size after solution heat treatment. It should be mentioned that the images used in the T1 temper state varied greatly as one had a particle area twice as large as the other image. This alone indicates that the distribution of primary particles can be regarded as highly heterogeneous, especially with regard to larger primary particles.

According to Fick's first law the diffusion rate is dependent on time and temperature. It could therefore be expected that the particles in the alloy would grow during solution heat treatment as the Si and Mg clusters disperse. According to Y. Agura Si-clusters in naturally aged Al-Mg-Si retards the growth of clusters during artificial ageing [11]. If this is also a mechanism in particle growth it could explain the decrease in particle area.

The EDS examinations showed the presents of chromium in particles. Chromium was virtually only present in particles containing iron, with only one deviating result. The element was not included in the chemical composition of the alloy, but due to its relative low wt% in the measured particles the fraction can be assumed to be low.

The presents of nonferrous Mg-Si-rich particles decreased with increased artificial ageing. By means of unaided eye observations the particles also seemed to decrease in size with increased ageing, and were not present in the over-aged sample. These particles could be formed by natural ageing during storage for a long time storage, and disperse when heat treated.

Grain Structure and Recrystallized Layer

The grain structure was only examined in the T1 temper state. During heat treatment the surface of a metal will be recrystallized [5], as can be seen in figure 4.1. During machining of the specimens a combined thickness of up to 500 µm was removed though grinding. The amount of material removed through manual grinding is unknown. It is uncertain if this was enough to remove the recrystallized layer from the specimen surface as no examination was conducted. According to K. Pedersen et al. the recrystallized layer eases initiation and propagation of a fatigue crack [12].

5.1.2 Hardness

The hardness of AA6005 was decreased after solution heat treatment, but during artificial ageing the solution heat treated sample passed the naturally aged sample. According to Y. Agura et al. this is due to Si-clusters hindering the hardness growth during artificial ageing [11].

5.1.3 Electrical Conductivity

The electrical conductivity of the samples artificially aged from the T1 temper state and after solution heat treatment both experienced an increase in electrical conductivity. Artificial ageing from the T1 temper state experienced this increase at a delayed rate compared to the soliution heat treated condition. According to Mattheissen's law this is caused by a decrease in the atomic fraction of solid solution present. The work done by Y. Agura et al. [11] shows the cluster growth is hindered by Si-clusters present from natural ageing. This translates to an increase in solid solution present and could be the reason of the delay.

5.2 The Effect of Ageing Time on Fatigue Properties

Figures 5.1-5.3 shows the correlation between the S-N curves and the stress-strain curves of the different temper states. It can be seen that the T1 temper state exhibits very good fatigue properties as is needed to exceed the yield stress to fracture.

The fatigue life is increased with increased amount of artificial ageing, with the fatigue life of the OA temper state being over 600.000 cycles in comparison to the T1 temper state of only 200.000 cycles. It is also observed that the UA and OA temper states have similar fatigue life with regard to the yield stress, but the yield stress of the OA temper state is less than that of the UA temper state. Also it should be pointed out that the range between run out and fracture is very little, and the change can be sudden, especially for the T1 temper state.

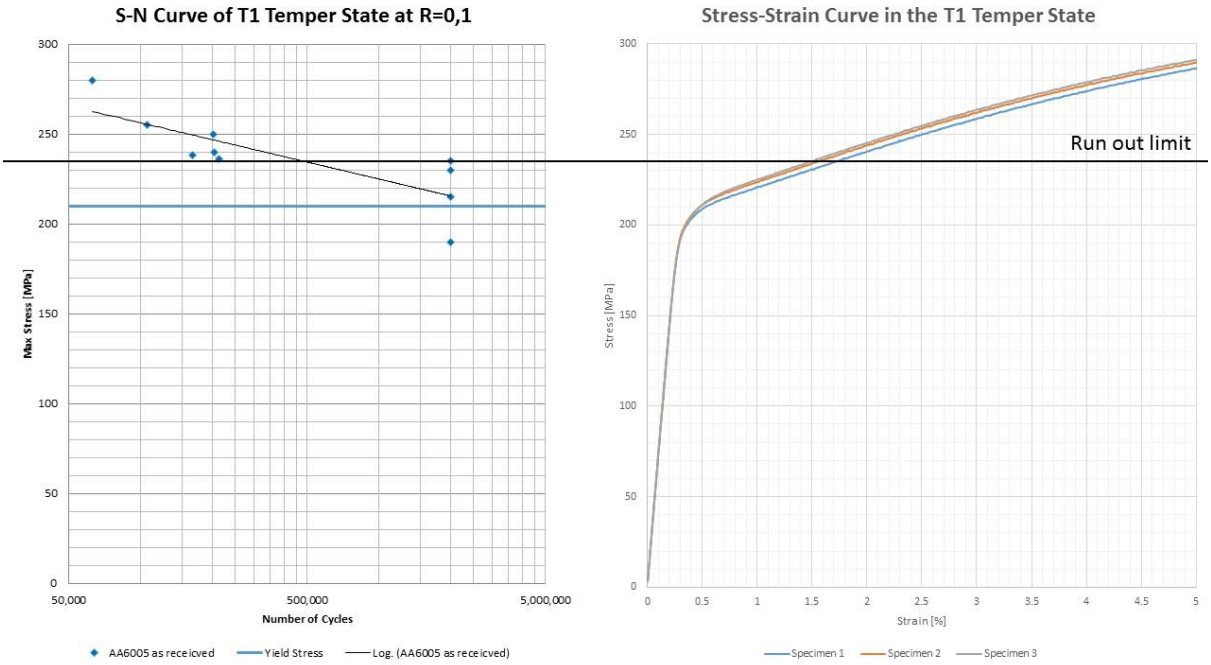

Figure 5.1: The correlation between the S-N curve and the strain-stress curve of the T1 temper state

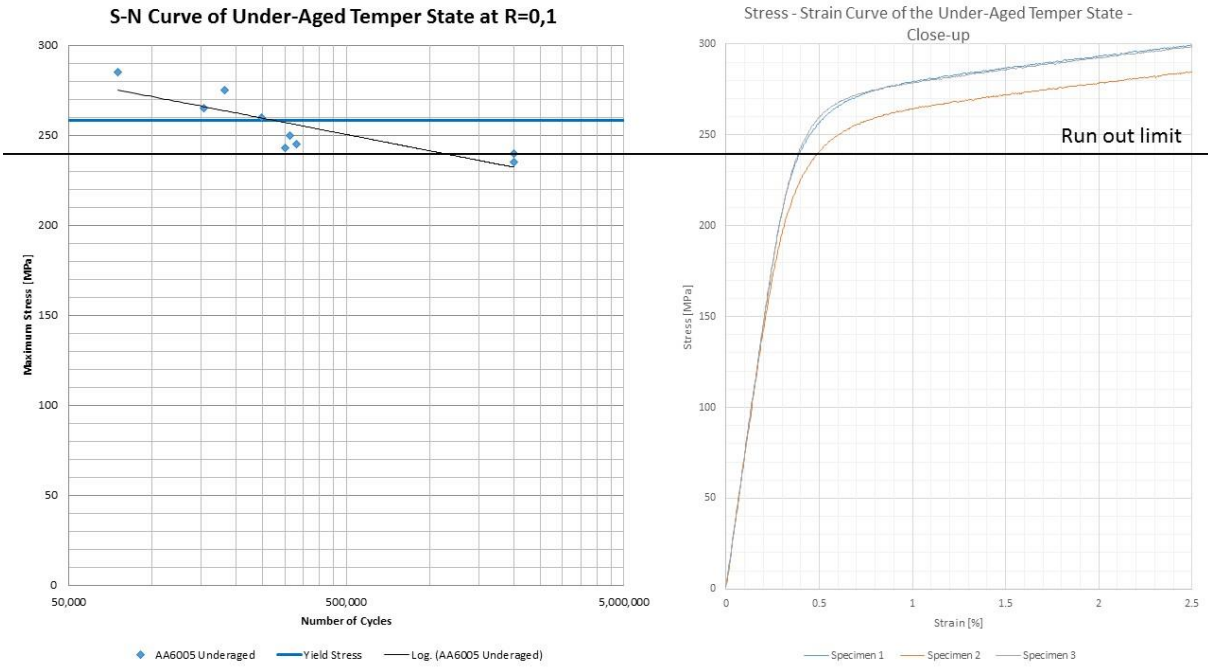

Figure 5.2: The correlation between the S-N curve and the strain-stress curve of the UA temper state.

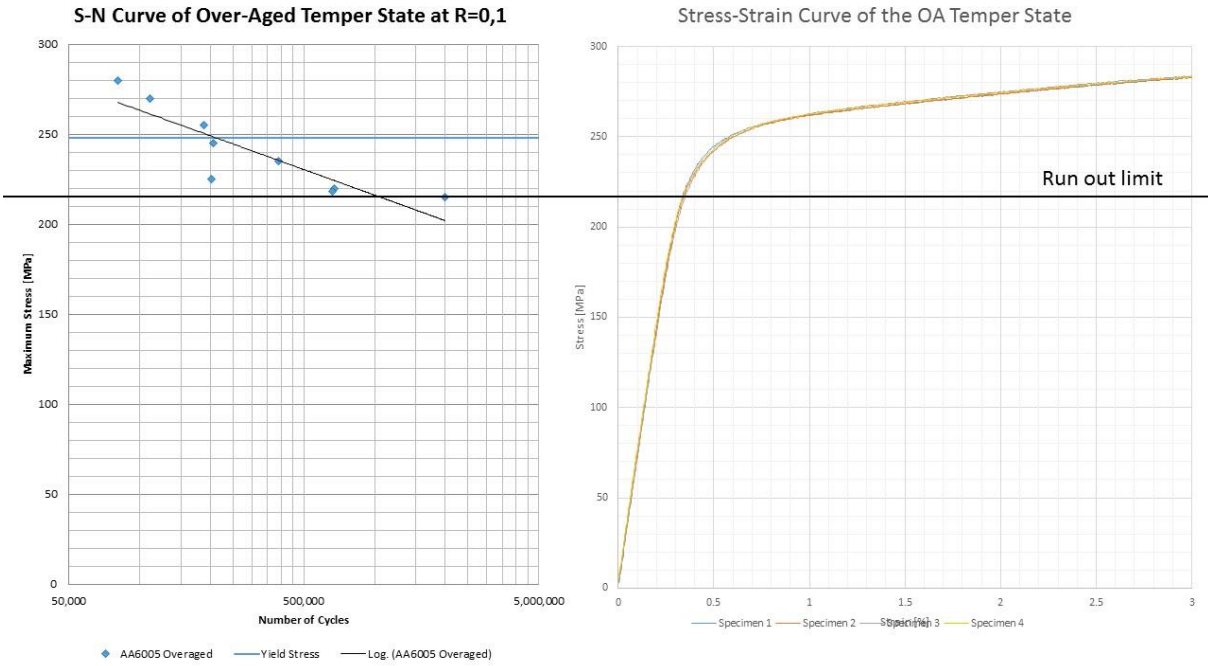

Figure 5.3: The correlation between the S-N curve and the strain-stress curve of the OA temper state.

5.2.1 Stress Correction

It was observed that some specimens did not fracture in the vicinity of the centre of the specimen. As the specimens were hourglass shaped it would be expected that the fracture occurred where the cross section was smallest, and the calculations of the applied stress were therefore done with this in mind. This, however, was not the case for some specimens, and a new stress was calculated on the bases of this new cross section area.

The stress was corrected by measuring the base of the fracture on each fracture surface. As the hourglass shape of the specimens necessitates the cross section to change along the extrusion direction, and the fractures were at a ~45°, the mean value of the measurements was used for calculations.

The reasons for the unexpected fracture area can have many explanations. It could arise from local microstructural deviations within the specimens to make more favourable crack initiation areas, e.g. local stress concentrations prior to fatigue testing, especially large incoherent particles, continued natural ageing after heat treatment. User error during fatigue testing is another explanation as some of the specimens were found to be installed in the MTS 810 slight offset compared to the direction of the applied stress. The preparation of the specimen was done by hand and checked using the unaided eye. The nature of this method in itself may cause fluctuating results in the end product, and it is possible that the grinding of the specimens corners was inadequate in the areas where unexpected fracture occurred.

In figures 5.4-5.6 the corrected maximum stress calculations are presented with the experimental data. When comparing the three figures it is evident that the T1 and over-aged temper states present a much higher degree of stability between the specimens tested, with only slight deviations from the test specimen. The under-aged temper state on the other hand shows a much larger deviations between the specimens, up to a difference of ~20 MPa. This, variations during tensile testing and the fact that the under-aged temper state also showed fluctuations in hardness after fatigue testing brings the stability of this temper state into question. Due to time restrictions this could not be investigated further, but further

investigations of this temper state could determine the stability of this temper state, and this is noted in chapter 7 Further Work.

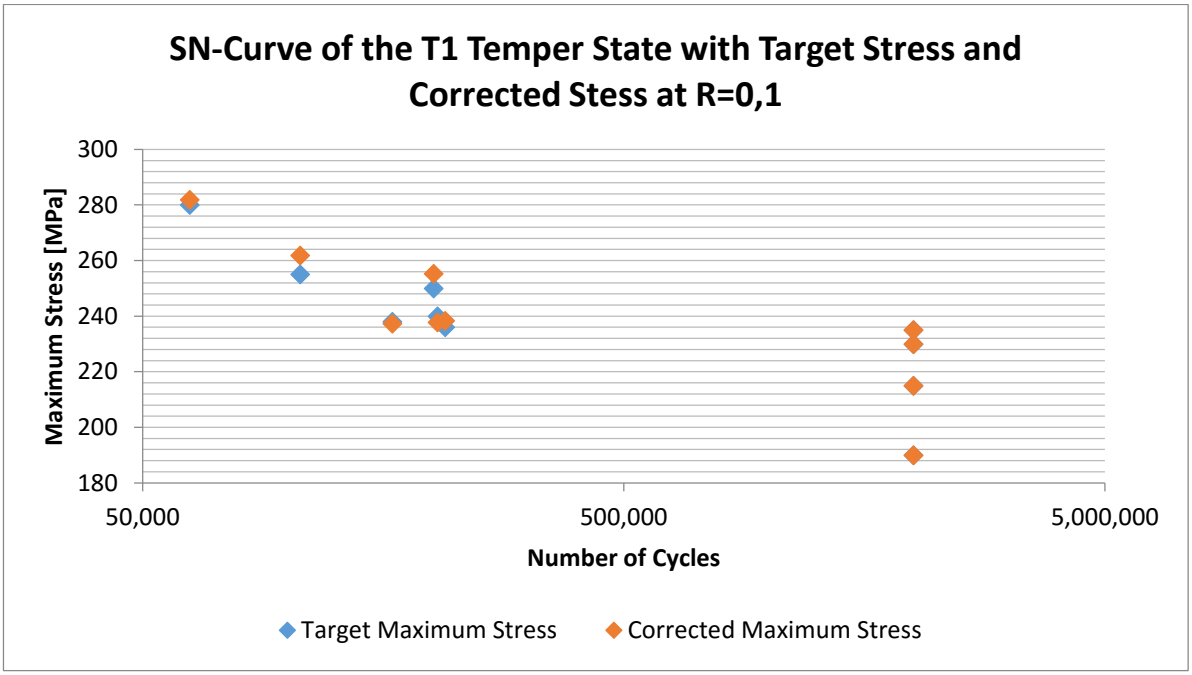

Figure 5.4: The targeted maximum stress and the corrected maximum stress calculated from the cross section area of the fracture for the T1 temper state.

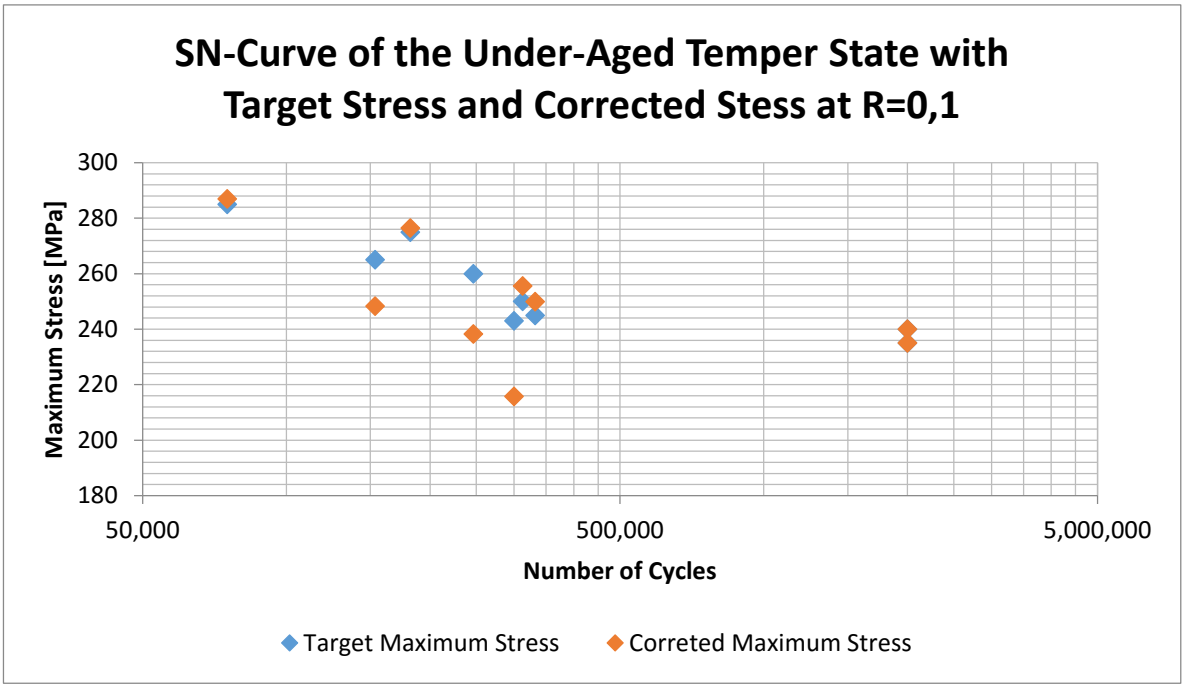

Figure 5.5: The targeted maximum stress and the corrected maximum stress calculated from the cross section area of the fracture for the UA temper state.

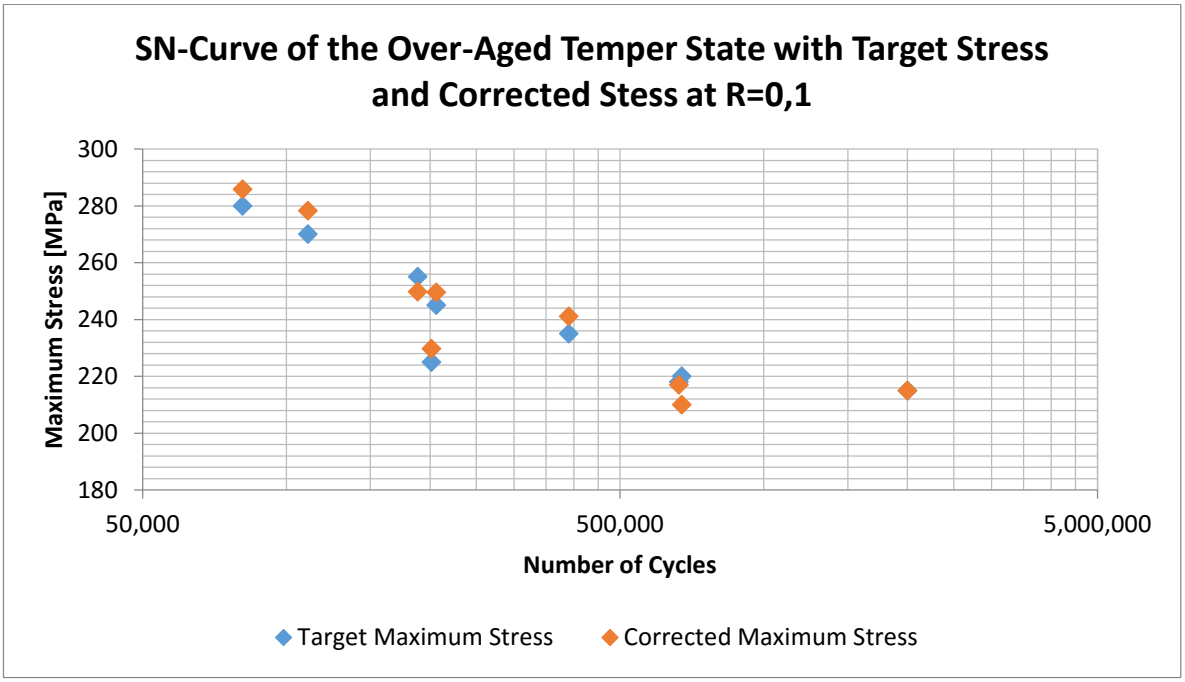

Figure 5.6: The targeted maximum stress and the corrected maximum stress calculated from the cross section area of the fracture for the OA temper state.

5.2.2 Hardness

The T1 temper state underwent cyclic hardening, with reduced impact from work hardening with decreasing with increased fatigue life. According to K. Pedersen cyclic hardening is caused by the formation of high density dislocation loops [13].

In the same work of K. Pedersen [13] cyclic softening is due to the formation of slip bands when the material is aged to peak hardness. Both the under-aged and over-aged temper states experienced cyclic softening. The OA temper state showed a fairly constant softening effect, and is supported by the work of K. Pedersen. The UA temper state experienced an increase of cyclic softening with prolonged fatigue life. This indicates that cyclic softening could occur before reaching peak hardness.

5.2.3 Electrical Conductivity

No substantial change in electric conductivity was found after fatigue hardening. Only the T1 temper state showed signs of change with a small trend towards a reduction. If this is the case and Matthiessen's law is applied it could suggest a slight decrease in the fraction of impurities or solid solution. As no impurities were introduced, the likely source would be a reduction in solid solution. This would indicate precipitation or growth of particles, both deemed to be unlikely.

6 Conclusions

- Naturally aged, long time stored, AA6005 exhibits very good fatigue properties as it needs to exceed the yield stress to fracture.
- Under-aged AA6005 had large deviations in results and might not always be consistent, but further investigation is required to verify this.
- The UA temper state showed the best fatigue resistance with regard to applied stress level, with the T1 temper state slightly worse.
- Increased fatigue life reduces the effect of cyclic hardening in the T1 temper state, and increases the effect of cyclic hardening in the UA temper state. The OA temper state has a constant cyclic softening influence.

7 Further Work

Point analyses of the chemical composition of the primary particles as the matrix was also included in the scans.

TEM investigation of the grain boundaries to determine the presents of precipitate free zones.

Investigations into the stability of the under-aged temper state.

8 References

1. Solberg, J.K., *Teknologiske metaller og legeringer*. 2010, NTNU: Department of Materials Science and Engineering.

2. Hydro. *Aluminiumens kvaliteter*. Available from: http://www.hydro.com/no/Hydro-i-Norge/Om-aluminium/Hvorfor-aluminium/Fysiske-egenskaper/.

3. Reiso, O., *Extrusion of AlMgSi Alloys.* Materials Forum, 2004. **28**.

4. Dieter, G.E., *Mechanical Metallurgy*. 1988: McGraw-Hill Book Company (UK) Limited.

5. Askeland, D.R. and P.P. Phulé, *The Science and Engineering of Materials (International Student Ediition)*. 2004: Nelson.

6. Tunestam, F., *Fatigue of Long Time Stored Naturally Aged Aluminium Profiles*. 2015, NTNU: Trondheim.

7. Hjelen, J. 1989, NTNU: Department of Materials Science and Engineering.

8. Furu, T., *Personal communication*. 2015.

9. Yu, Y., *Personal communication during training*. 2015.

10. ATSM, *Standard Practice for Conducting Force Controlled Constant Amplitude Axial Fatigue Tests of Metallic Materials*. 2007.

11. Aruga, Y., et al., *Formation and reversion of clusters during natural aging and subsequent artificial aging in an Al–Mg–Si alloy.* Materials Science and Engineering: A, 2015. **631**: p. 86-96.

12. Pedersen, K., O. Helgeland, and O. Lohne, *THE EFFECT OF GRAIN STRUCTURE ON FATIGUE LIFE OF AGE HARDENING ALUMINIUM ALLOYS*, in *E.C.F.* 1982.

13. Pedersen, K., *CYCLIC DEFORMATION OF AN EXTRUDED ALMGSI ALLOY*. 1987, Virginia Univ.

Appendix A – Artificial Ageing Data

Data from the artificial ageing experiments are presented below.

Hardness

Table A.1: Hardness data after solution heat treatment.

Ageing time	0 min	10 min	30 min	60 min	5 hours	48 hours
Hardness [HV1]	79.2	81.1	103.7	116	118.4	93.9
Hardness [HV1]	78.5	76.4	104.2	108.6	119	95.9
Hardness [HV1]	78.6	86.6	107.8	116.8	116.7	87.8
Hardness [HV1]	79.2	81.9	106.8	116.7	113.3	86
Hardness [HV1]	77.6	79.2	108.6	113.4	119.8	93.1
Mean Hardness [HV1]	78.6	81.0	106.2	114.3	117.4	91.3
Standard Deviation	0.6	3.4	1.9	3.1	2.3	3.8

Electrical Conductivity

Table A.2: Electrical conductivity data after solution heat treatment.

Ageing time	0 min	10 min	30 min	60 min	5 hours	48 hours
Electrical conductivity [MS/m]	24.33	24.9	26.42	27.1	27.6	28.56
Electrical conductivity [MS/m]	24.19	24.78	26.47	27.12	27.52	28.52
Electrical conductivity [MS/m]	24.16	24.75	26.37	27.02	27.47	28.54
Electrical conductivity [MS/m]	24.16	24.68	26.42	27.03	27.48	28.46
Electrical conductivity [MS/m]	24.12	24.73	26.35	27	27.38	28.48
Mean Electrical conductivity [MS/m]	24.19	24.77	26.41	27.05	27.49	28.51
Standard Deviation	0.07	0.07	0.04	0.05	0.07	0.04

Measurements to Identify the Under-Aged and Over-Aged temper States

Table A3: Measurements taken to identify the UA and OA temper states.

Measurement number	UA [HV1]	OA [HV1]
1	94.6	96.5
2	93.9	92.6
3	93	90
4	96.8	96.5
5	86.5	96.5
Mean	93	94
Standard Deviation	3	3

Appendix B – Fatigue Data

Fatigue Test Data

Table B.1: Fatigue test data from of the T1 temper state. Specimen 2 was rejected due to appliance error.

Specimen Number	Maximum Stress [MPa]	Area [mm^2]	Cycles to fatigue
1	190	21.7	RO
3	215	21.5	RO
4	250	21.6	201,374
5	240	21.3	204,938
6	230	21.4	RO
7	235	21.3	RO
8	255	21.4	106,301
9	238	21.8	165,081
10	236	21.4	212,725
11	280	21.7	62,625

Table B.2: Fatigue test data from of the UA temper state. Specimen 1 was rejected due to user error.

Specimen Number	Maximum Stress [MPa]	Area [mm^2]	Cycles to fatigue
2	240	21.5	RO
3	250	21.6	312,489
4	245	21.6	331,907
5	260	21.9	246,611
6	275	21.7	181,852
7	285	21.3	75,131
8	265	21.9	153,341
9	243	21.6	299,791
10	235	21.4	RO

Table B.3: Fatigue test data from of the OA temper state.

Specimen Number	Maximum Stress [MPa]	Area [mm^2]	Cycles to fatigue
1	225	21.5	201,363
2	235	21.7	390,622
3	245	21.5	206,000
4	255	21.9	188,233
5	215	21.9	RO
6	270	21.6	110,851
7	220	21.4	672,852
8	280	21.6	81,010
9	218	21.4	663,730

Hardness after Fatigue Testing

Table B.4: The hardness of the T1 temper state after fatigue testing. Specimen 2 was rejected due to appliance error.

Specimen Number	Mean Hardness [HV1]	Standard Deviation	Maximum Stress [MPa]	Cycles to fatigue
1	86.5	1.8	190	RO
3	89.0	2.0	215	RO
4	90.6	2.5	250	201,374
5	92.2	2.3	240	204,938
6	88.8	2.2	230	RO
7	87.8	2.2	235	RO
8	90.3	1.4	255	106,301
9	91.6	3.0	238	165,081
10	89.8	3.3	236	212,725
11	97.6	1.2	280	62,625

Table B.5: The hardness of the UA temper state after fatigue testing. Specimen 1 was rejected due to user error.

Specimen Number	Mean Hardness [HV1]	Standard Deviation	Maximum Stress [MPa]	Cycles to fatigue
2	75.2	1.8	240	RO
3	77.0	1.8	250	312,489
4	89.4	3.6	245	331,907
5	88.6	3.2	260	246,611
6	90.1	1.7	275	181,852
7	91.9	1.6	285	75,131
8	91.6	1.0	265	153,341
9	94.8	4.5	243	299,791
10	94.0	1.5	235	RO

Table B.6: The hardness of the OA temper state after fatigue testing.

Specimen Number	Mean Hardness [HV1]	Standard Deviation	Maximum Stress [MPa]	Cycles to fatigue
1	89.5	2.1	225	201,363
2	90.6	1.0	235	390,622
3	90.2	2.4	245	206,000
4	86.3	2.2	255	188,233
5	88.1	1.3	215	RO
6	91.1	1.5	270	110,851
7	89.5	2.5	220	672,852
8	88.9	1.6	280	81,010
9	90.6	2.9	218	663,730

Electrical Conductivity after Fatigue Testing

Table B.7: The electrical conductivity of the T1 temper state after fatigue testing. Specimen 2 was rejected due to appliance error.

Specimen Number	Electrical Conductivity [MS/m]	Maximum Stress [MPa]	Cycles to fatigue
1	24.3	190	RO
3	24.3	215	RO
4	24.2	250	201,374
5	24.2	240	204,938
6	24.2	230	RO
7	24.3	235	RO
8	24.3	255	106,301
9	24.2	238	165,081
10	24.2	236	212,725
11	24.1	280	62,625

Table B.8: The electrical conductivity of the UA temper state after fatigue testing. Specimen 1 was rejected due to user error.

Specimen Number	Electrical Conductivity [MS/m]	Maximum Stress [MPa]	Cycles to fatigue
2	25.8	240	RO
3	25.8	250	312,489
4	25.6	245	331,907
5	25.6	260	246,611
6	25.4	275	181,852
7	25.6	285	75,131
8	25.6	265	153,341
9	25.5	243	299,791
10	25.5	235	RO

Table B.9: The electrical conductivity of the UA temper state after fatigue testing.

Specimen Number	Electrical Conductivity [MS/m]	Maximum Stress [MPa]	Cycles to fatigue
1	27.9	225	201,363
2	27.9	235	390,622
3	27.9	245	206,000
4	27.9	255	188,233
5	28.0	215	RO
6	28.0	270	110,851
7	27.8	220	672,852
8	27.8	280	81,010
9	27.8	218	663,730